https://ntrs.nasa.gov/search.jsp?R=19670002766 2020-03-16T16:59:26+00:00Z

GPO PRICE $ _____

CFSTI PRICE(S) $ _____

Hard copy (HC) $ 2.50

Microfiche (MF) .75

ff 653 July 65

NASA-CR-72068

HYDRODYNAMIC JOURNAL BEARING PROGRAM

QUARTERLY PROGRESS REPORT NO. 4

For Period : January 29, 1966 Thru April 29, 1966

By

H. E. Nichols, R. J. Rossbach,
W. H. Bennethum, J. C. Amos,
and W. D. C. Richards

prepared for
NATIONAL AERONAUTICS AND SPACE ADMINISTRATION
CONTRACT NAS 3-6479

SPACE POWER AND PROPULSION SECTION
MISSILE AND SPACE DIVISION
GENERAL ELECTRIC
CINCINNATI, OHIO 45215

(THRU) 1
(CODE) 15
(CATEGORY)

N67 12095
(ACCESSION NUMBER) 94
(PAGES) CR-72068
(NASA CR OR TMX OR AD NUMBER)

FACILITY FORM 602

NOTICE

This report was prepared as an account of Government sponsored work. Neither the United States, nor the National Aeronautics and Space Administration (NASA), nor any person acting on behalf of NASA:

A.) Makes any warranty or representation, expressed or implied, with respect to the accuracy, completeness, or usefulness of the information contained in this report, or that the use of any information, apparatus, method, or process disclosed in this report may not infringe privately owned rights; or

B.) Assumes any liabilities with respect to the use of, or for damages resulting from the use of any information, apparatus, method or process disclosed in this report.

As used above, "person acting on behalf of NASA" includes any employee or contractor of NASA, or employee of such contractor, to the extent that such employee or contractor of NASA, or employee of such contractor prepares, disseminates, or provides access to, any information pursuant to his employment or contract with NASA, or his employment with such contractor.

Requests for copies of this report should be referred to:

National Aeronautics and Space Administration
Scientific and Technical Information Division
Attention: USS-A
Washington, D.C. 20546

HYDRODYNAMIC JOURNAL BEARING PROGRAM

QUARTERLY PROGRESS REPORT NO. 4

Covering the Period
January 29, 1966 through April 29, 1966

By
J.C. Amos, W.H. Bennethum,
H.E. Nichols, W.D.C. Richards, and R.J. Rossbach

Approved by

E. Schnetzer, Manager
Development Engineering

Prepared for

NATIONAL AERONAUTICS AND SPACE ADMINISTRATION

Contract NAS 3-6479

TECHNICAL MANAGEMENT

NASA-LEWIS RESEARCH CENTER

NUCLEAR POWER TECHNOLOGY BRANCH

JOSEPH P. JOYCE, TECHNICAL MANAGER

SPACE POWER AND PROPULSION SECTION
MISSILE AND SPACE DIVISION
GENERAL ELECTRIC COMPANY
CINCINNATI, OHIO 45215

ABSTRACT

The Space Power and Propulsion Section has been under contract since April 29, 1965 to the National Aeronautics and Space Administration for the design, fabrication, and testing of journal bearings which possess characteristics required for use in space power systems. Requirements include long term unattended operation under zero "g" conditions using low kinematic viscosity lubricants such as potassium liquid at temperatures up to 1200°F.

The program represents a continuation of work carried out under contract NAS 3-2111, and involves the testing and evaluation of bearings under conditions of angular and transverse linear misalignment, and non-rigid bearing supports. The four-pad pivot-pad and the three-lobed journal bearings shall be tested after the bearing test assembly including instrumentation have demonstrated the ability to obtain the required data.

The program will be a continuation of experimental investigations paralleled by analytical studies. These analytical investigations will compare the physical testing of bearing parameters with results based on theoretical assumptions. The goal of such experiments is to generalize the various bearing parameters thereby extending the usefulness of the results as design tools. The experimental tool of this program is a high speed test assembly comprised of a rotor and two test bearings which permits interchangeability of bearings and rotor. The lubricant will be distilled water, temperature-controlled to simulate the kinematic viscosity of potassium liquid at temperatures up to 600°.

The specific requirements of the system are:

1.	Shaft speed	3600 to 30,000 rpm
2.	Inlet lubricant temperature	70 to 150°F
3.	Inlet lubricant supply pressure	0 to 150 psia
4.	Bearing linear misalignment	0 to 0.004 $\pm$ 0.0005 in.
5.	Bearing angular misalignment	0 to 400 $\pm$ 12 sec.
6.	Nominal bearing diameter	1.25 in.
7.	Bearing L/D ratio	1
8.	Diametral clearance	0.005 in.

The program will be performed in two tasks, the first of which will be the modification of the existing bearing test assembly and instrumentation and a demonstration of the ability to obtain accurate data. Task II will involve testing and analysis of the four-pad pivot-pad and three-lobed bearings.

The present report covers progress during the quarter ending April 29, 1966.

TABLE OF CONTENTS

LIST OF ILLUSTRATIONS

LIST OF ILLUSTRATIONS (continued)

LIST OF TABLES

SUMMARY

During this reporting interim the bearing test rig was transferred from the Research and Development Center in Schenectady, New York to the Space Power and Propulsion Section facilities in Evendale, Ohio. All project purchased hardware was relocated and facility modification to accept the new test rig and its associated equipment was initiated.

The design of a self-aligning pivoted-pad bearing with two values of preloading was completed and manufacturing was begun. Fabrication of a three-lobed bearing and a back-up test shaft was also initiated. A decision to employ optical tooling for the determination of the specified conditions of both angular and transverse misalignment of the test bearings was made, and the required equipment was ordered.

Several pretest feasibility and calibration tests of both force and displacement measurements were accomplished.

A digital data recording system will be employed to record dynamic bearing characteristics. The design of the equipment necessary to accomplish this technique of data acquisition has been essentially completed, and procurement of the necessary components is in process.

An analysis of the preloaded pivoted pad bearing was made to guide test planning. Rotor bearing response data over ranges of speed, side load and unbalance is presented.

The program schedule is shown in Figure 1.

Forecast

During the next quarter, the fabrication of test bearings and the modification of the existing components will be completed. The test facility and associated equipment will be completed and installed. All pretest calibration will be finished and the test rig will be checked out.

In addition, the rotor response program and the data reduction program will be completed and checked. The various test parameters and the test plan will also be completed.

I. MECHANICAL DESIGN

During this quarter, a decision to use optical techniques to set the conditions of bearing misalignment was made and the required components were ordered. The design of the self-aligning pivoted pad bearing was completed and placed on order. Also being fabricated during this interim were the backup test shaft and the two required three (3) lobed bearing assemblies. In addition, several items required for calibration and/or feasibility tests were completed and necessary testing performed.

1. Bearing Alignment

As indicated in the Abstract of this report, the program requirements specify that the bearings be tested under conditions of angular and/or transverse misalignment of 400 $\pm$ 12 seconds and/or 0.004 $\pm$ 0.0005 inch, respectively. The loss of bearing clearance resulting from different combinations of these misalignments are shown in Figure 2, which also indicates that the condition of angular misalignment is the more serious problem. The loss of bearing diametral clearance due to angular misalignment is approximately six times greater than that due solely to the transverse misalignment condition.

Three alignment systems have been evaluated for setting the prescribed misalignment during test rig assembly. The first is the "Proficorder" * (Figure 3) described in reference 1 . It comprises an extremely accurate rotating spindle (less than 3 micro inch run out) with a contact sensing head which electronically records the surface contour on a polar chart. A similar available tracing instrument, the "Talyrond"** (Figure 4) was also investigated. This

* Model - RLF Rotary Piloter, Man.-Micrometrical Corporation

** Model - 50 "Talyrond", Man -Rank Taylor Hobson

instrument has a rotating spindle of the same accuracy as the Proficorder and employs a pivoting extension arm attached to the spindle for sensing the surface contour to be measured.

Both of these alignment methods require removal of the test rig from the support structure and set up on the above tracing instrument. In addition, misalignment must be determined by contour measurement in several planes normal to the bearing axis, with subsequent interpretation and remeasurement to obtain the necessary misalignment setting for the test.

A third alignment method has been investigated which promises greater accuracy regarding angular misalignment and considerable increase in ease of adjustment reading of misalignment. The technique involves use of a micro-alignment telescope in conjunction with very precise targets, capable of measuring squareness of the target's surface to the telescope axis by either auto-reflection or auto-collimation, in addition to determining linear transverse measurements. Much of the accuracy of such an optical measuring system is dependent upon the accuracy to which the targets are fabricated, and the means for locating these targets in or on the item to be inspected. The selected target design contains narrow cross-hairs and concentric circles, the center of which is located within 20 micro-inches of true center. In addition, the reflecting surface of the targets will be square to centerline of the target holder within $\pm$ 1 second of arc. Location of the target holder inside the bore of the various test bearing configurations within 20 micro-inches is accomplished by utilizing a tapered external surface (0.00025 inch per inch of length).

A comparison of the above three methods for measuring the alignment of the test rig was undertaken. The basis for such a comparison was the total possible error resulting from each alignment configuration and the tolerances of the equipment, in addition to the estimated readability of the data resulting from the inspection media.* The comparative conditions were (1) zero alignment, (2) four mils transverse misalignment with zero angular misalignment, and (3) a combination of both four mils transverse and 400 seconds angular misalignment. The results of the investigations are listed in Figure 5 and indicate that all three techniques will resolve transverse linear movement within 46 to 126 micro-inches from true center. However, it can be seen that the optical tooling has the advantage of greater potential accuracy regarding angular settings. Resolution of an angular position using the telescope target assembly is feasible within eight seconds of true position. A distinct advantage of the optical tooling is that one can see the movement of the bearings while establishing a specified position. Both of the tracing techniques yield an envelope pattern from which the center can be determined. The bearing assembly must then be moved and the contour tracing repeated in order to define the new location. To add to the difficulty of making adjustment in location is the fact that the traces for angular settings will be that of an ellipse. Not only is the optical tooling convenient to use, but eliminates transporting of the test rig from the test site. Based on the aforementioned findings, the optical tooling technique appears to best satisfy the requirements of the program and has therefore been selected as the media through which conditions of alignment will be resolved.

* Source material for this comparison was obtained from the respective manufacturers and from detailed discussions with technicians skilled in the operation of each piece of inspection tooling.

The proposed method of establishing bearing alignment is to mount the telescope and its mounting assembly atop the modified instrument housing (Figure 6). A reflecting target assembly will then be assembled into the bore of the upper test bearing. The upper test bearing will serve as a reference position since the upper bearing housings are fixed by pins and a locating diameter. Squareness of the axis of the telescope to the plane of the reflecting target (by using the principle of autocollimation) and coincident centerlines (telescope and target) will then be set.

The principle of autocollimation is depicted in Figure 7 . An image is projected by light rays from the point 'P' onto the reflecting mirror. When the mirror is at 90° to the direction of the image rays, they are reflected exactly to their source, superpose themselves on the projected image. Autocollimation is independent of the distance "L" between the objective and the mirror since it is performed with the focal length "f" being set at infinity.

Figure 7 depicts the condition when the mirror is at angle x/2 to the direction of the image rays. The reflected image returns at angle x, a distance P-P' from the real image at P.

Coincident alignment of the centerlines is obtained by transversely moving the telescope until it is coincident with the target in the top bearing (superposing crosshairs). The target is then transferred to the lower test bearing, and the lower bearing housing is adjusted until it also coincides with the common centerline.

Sketches of the desired target configurations and a suitable mounting arrangement (Figures 8, 9, and 10) along with a complete set of specifications for the micro-alignment telescope were sent to various optical tooling manufacturers for cost quotes. The estimates for the required components have been received and an order was placed. Delivery of all hardware is scheduled for July 1, 1966.

2. Test Equipment Procurement

A. Force Measurement Hardware

A design study was initiated to modify the existing bearing housing assemblies to accept quartz crystal force transducers rather than strain gaged force buttons. Reasons for this change in the force monitoring equipment are discussed in the Instrumentation Section of this report. The piezoelectric load cell selected for incorporation into the rig is the Kistler force transducer - Model #902A, as shown in Figure 11. Completion of both the design effort and the detailed manufacturing prints are expected during the first week in May.

B. Three-Lobed Bearing

The requirements of the present contract specify a three-lobed bearing configuration that when assembled with the test shaft will result in a 5 mil diametral clearance. The previously tested design[1] cannot be utilized because the assembled condition yields only a 3 mil diametral clearance. Therefore, the machining drawing was modified to the required

[1] Reference 3.

configuration with copies submitted to various vendors for cost quotes (Figure 12). The estimates have been received and an order has been placed, with the delivery of two bearing assemblies scheduled for June 30, 1966.

C. Second Test Shaft

The backup test shaft for the high speed test rig was fabricated identical to the first. The integral journal diameters are 1.2500 - 1.2499 inches and when mated with the bearing sleeves will provide a nominal diametral clearance of 5 mils. Results from the 100 percent inspection of the shaft indicated that all drawing requirements were fulfilled. A portion of that inspection record is listed below while Figure 13 shows actual recorded traces of the journal diameters.

Condition	Specification (in)	Actual (in)
Roundness	0.000050 FIR	0.000050
Concentricity	0.000300 FIR	0.000020
Taper	0.000050 FIR	0.000050
Plating Thickness	0.0050 Nominal	0.005 $\pm$ 0.00025
Surface Finish	8AA	5AA

D. Self-Aligning Pivoted Pad Journal Bearing

The detail manufacturing drawings for the self-aligning pivoted-pad journal bearing assemblies, reference 2, (Figure 14) were completed and submitted to several vendors for cost quotes. These estimates included extra pads, pivot pins and contacting disks. Several bids were received, the vendor selected and an order was placed with the delivery of all components scheduled by July 1, 1966.

3. Relocation of Program Test Rig

All test rig equipment procured on NASA Contracts NAS 3-2111 and NAS 3-6479 was relocated from the General Electric Company, Research and Development Center in Schenectady, New York to the Space Power and Propulsion Section's facilities in Evendale, Ohio. A testing area is being prepared in Building 314 to accept the high speed test rig and its associated hardware. The design and procurement of those required items (i.e., heat exchanger, pressure and temperature transmitters, controllers, etc.) required to complete the testing assembly has been initiated.

4. Pre-test Calibration Hardware

A decision was made to record and reduce experimental data using a digital data system. Several feasibility tests were required to verify methods of obtaining the required information within desired tolerances such as measuring the phase angle between shaft displacement and the corresponding bearing forces. To accomplish this, along with calibrating other components, several experimental devices were required.

A set of bench centers has been procured for static calibration of Bently Nevada proximity probes, sensing off a silver plated test shaft (Figure 15). Mounted adjacent to the proximity probe is an Electrojet Cartridge gage (linear variable displacement transformer) which provides resolution of clearance measurements to 10 micro inches. These displacement measuring instruments are mounted in a holding fixture which is fixed to an optical staging table. The staging table provides movement of $\pm$ 1 inch with the traversing measured by a micrometer head which has been subdivided into 0.0001 inch increments. Also depicted in the figure is the readout equipment required for such tests.

To verify the ability to measure phase angle, a high speed test rig (0 to 16,000 rpm) was mounted to the base of the aforementioned set of bench centers. A small stub shaft was fabricated with the circumference containing a 0.005 inch thick band of silver plating. This shaft was then mounted eccentrically to the shaft centerline of the high speed rig by using a locking collet. The optical staging device equipped with distance measurement detectors was subsequently mounted with the detectors sensing off the silver plated stub shaft (Figures 16 and 17). Upon rotating the shaft the angle between the two proximity probes was read out on a phase angle meter. Repeatable data was obtained within the accuracy of the indicating instrument - $3^\circ \pm 1$ percent.

Prior to utilizing the Electrojet Cartridge (contacting probe) in any set-up, it must first be calibrated. This is performed by employing a Sheffield Corporation Linearchek Gage Calibrator (Figure 18). Accuracy of this instrument is $\pm$ 0.000010 inch over a one inch traversing distance being provided by a 4 inch diameter Sheffield Ultra-Precise Micrometer. The circumference of the micrometer has been divided into increments of 0.0001 inch.

II. ROTOR BEARING ANALYSIS

Under the present contract, experimental performance and rotor-bearing response data are to be obtained for three types of bearings, namely, the two-groove cylindrical, the three-lobe and the pivoted-pad bearing with two values of preload. These bearings will be tested with deliberate shaft unbalance on specially designed unbalance disks outboard of each bearing as shown in Figure 19. For the purpose of guiding test planning analytical rotor-bearing response data is useful in establishing the level of unbalance to be used for various test operating conditions. The analysis requires the knowledge of the dynamic characteristics of the bearings.

It is customary, e.g., reference 4, to represent the dynamic characteristics of a bearing by an eight-parameter linear model consisting of four springs and four dashpots. The model is shown schematically in Figure 20 . The fluid film forces are then represented by the following equations

$$\begin{aligned} -F_x &= K_{xx}\, X + \omega\, C_{xx}\, X + K_{xy}\, Y + \omega\, C_{xy}\, Y \\ -F_y &= K_{yx}\, X + \omega\, C_{yx}\, X + K_{yy}\, Y + \omega\, C_{yy}\, Y \end{aligned} \qquad (1)$$

The symbols are defined in the Nomenclature.

The actual bearing stiffnesses and damping coefficients are not linear, but if it is assumed that the rotor motion is confined to small oscillations around the shaft equilibrium position, this error due to non-linearity of the fluid film dynamic coefficients is small.

Equations (1) can also be used to calculate the dynamic characteristics of a bearing from experimental response data. Following the analysis of

reference 3 in which F_x, F_y, x and y are complex functions of the form

$$Z = /Z/e^{iwt} \quad \text{or} \quad /Z/ = Z_c + i\ Z_s, \tag{2}$$

equations (1) can be written as

$$\begin{aligned}
-\left[F_{xc}\right] &= \left(K_{xx}\right)\left[X_c\right] - \omega\left(C_{xx}\right)\left[X_s\right] + \left(K_{xy}\right)\left[Y_c\right] - \omega\left(C_{xy}\right)\left[Y_s\right] \\
-\left[F_{xs}\right] &= \left(K_{xx}\right)\left[X_s\right] - \omega\left(C_{xx}\right)\left[X_c\right] + \left(K_{xy}\right)\left[Y_s\right] - \omega\left(C_{xy}\right)\left[Y_c\right] \\
-\left[F_{yc}\right] &= \left(K_{yx}\right)\left[X_c\right] - \omega\left(C_{yx}\right)\left[X_s\right] + \left(K_{yy}\right)\left[Y_c\right] - \omega\left(C_{yy}\right)\left[Y_s\right] \\
-\left[F_{ys}\right] &= \left(K_{yx}\right)\left[X_s\right] - \omega\left(C_{yx}\right)\left[X_c\right] + \left(K_{yy}\right)\left[Y_s\right] - \omega\left(C_{yy}\right)\left[Y_c\right]
\end{aligned} \tag{3}$$

In equations (3) the terms in square brackets are measured during testing as is ω and the terms in round brackets are the eight parameters of the bearing dynamic characteristics model which are to be found. Obviously equations (3) represent four equations in eight unknowns. Their solution requires two independent sets of experimental data from a test bearing at the same operating condition, defined by a rotational speed, fluid temperature and unidirectional load. This can be accomplished in two ways: one, run the test shaft twice, once with symmetric and once with anti-symmetric unbalances in the unbalance disks (Figure 21); two, run the test shaft once with unequal unbalances in the two unbalance disks (reference 5). In the first instance only one bearing need be instrumented; in the second instance both bearings must be instrumented.

The dynamic characteristics of pivoted-pad bearings are presented in reference (7), but no such data is available for the two-groove cylindrical or the three-lobe bearings. Therefore, the rotor-bearing response analysis was carried out for the pivoted-pad bearing.

The description of the pivoted-pad bearings to be tested is presented in Table II. A drawing of the pivoted-pad bearing is shown in Figure 12. Pivoted-pad bearings having preload values of 0.2 and 0.52 will be tested. Reference to Figure 12 indicates that in the case of the preloaded bearing the center of each pad does not coincide with the bearing center. The preload is given by

$$m = \frac{a}{R_p - R_s} \qquad \text{(Reference Figure 20)} \qquad (4)$$

The purpose of geometrical preloading is to obtain high bearing stiffness even when there is no applied load and to avoid "negative fluid film pressures" (reference 4). The analysis which follows is for a preload of 0.4 since it was carried out prior to the final selection of preload.

A rotor-bearing response computer program was presented in reference 2 in which a symmetric-rotor model was considered. The distributed rotor mass is replaced in the model by two concentrated masses. In reference 9 a rotor-bearing response computer program is presented which is more general than that of reference 4. This latter computer program which is based upon the Prohl-Myklestad method (references 6, 7 and 8) was used in the present analysis. The shaft is represented by lumped masses separated by massless springs of the required length. The bearings are represented by the eight-parameter model discussed previously. In addition, the bearing pedestals can be represented by masses, springs and dashpots in orthogonal planes and springs and dashpots in the misalignment mode of motion. Gyroscopic effects may also be accounted for. The program assumes elliptical orbits about the shaft centerline for the lumped masses and it calculates the displacement orbits and corresponding forces. The forces on the pedestals are also calculated.

1. Input Data

The input data required to carry out the rotor-bearing response analysis are the following:

- Rotor Configuration
- Bearing Static Load Characteristics
- Bearing Dynamic Characteristics
- Pedestal Characteristics

The rotor shaft is shown in Figure 19; twenty-seven mass stations were used to represent this shaft in the calculation.

In order to determine the maximum displacement of the shaft under a given orbiting condition, the equilibrium position of the shaft must be calculated. Shown in Figure 23 is the variation of shaft equilibrium position with speed and unidirectional load. The data for this curve came from Figures 4-6, 8, 9 of reference 4. The eccentricity is reduced as speed increases and increased as the load increases. When the load is zero (vertical shaft), the equilibrium position is at the bearing center (zero eccentricity).

The bearing dynamic coefficients were calculated using Figures 4-18 of reference 4. The stiffness, K, and damping coefficienct, ωB, were plotted against speed with side load, W, as a parameter. At W = 0, the Sommerfeld Number, S, is undefined and Figures 4-6, 8-19 from reference 4 give no values for determining the dynamic coefficients of this case. The zero load dynamic coefficients were determined by plotting K and ωB versus W with rotative speed, N, as a parameter and extrapolating the curves to W = 0.

Shown in Figure 24 is the variation of bearing stiffness with speed and unidirectional load. The stiffness increases as speed and/or load increases. At high speed, the effect of the load is diminished. The stiffness ranges between 10^4 and 10^5 lbs. in.$^{-1}$. In Figure 25 the variation of the damping coefficient with speed and unidirectional load is shown. Damping increases with both speed and load and has a range around 10^5 lbs. in.$^{-1}$.

The stiffness of the pivot, K_p, must be considered in the analysis of the rotor-bearing system. The bearing pivot, shown in Figure 15, is a spherical surface of a hard material in contact with a flat hard surface on the back of the pad. The expression (reference 10 and 11) for force F_p for a given displacement, δ, is differentiated with respect to δ to obtain the following expression for pivot stiffness.

$$K_p = \frac{dF_p}{d\delta} = \frac{3}{2} \frac{\sqrt{\frac{D}{2}}\ \delta^{1/2}}{(0.77)^{3/2} \left(\frac{1}{E_1} + \frac{1}{E_2}\right)} \qquad (5)$$

Shown in Figure 26 is the variation of pivot stiffness with bearing load for a 2-inch diameter 410-stainless steel pivot against a 316-stainless steel pad. The pivot stiffness increases with the 1/3 power of load. In each of the two orthogonal directions the spring representing the pivots has twice the stiffness of a single pivot. The value used in the analysis was 5.46×10^5 lb./in., corresponding to a load of 12 lbs. The pedestal (in this case the pads) is assumed not to resist rotation in the pitch or roll mode and since the damping of the pivots is not known, it was ignored.

2. Rotor Response

Presented herein is rotor-bearing response data for the preloaded pivoted-pad bearing in the form of shaft displacements and fluid-film forces as influenced by rotative speed, deliberate unbalance, and unidirectional load (or side load).

Shown in Figures 27, 28 and 29 is the variation with speed of the rotor displacement from equilibrium position at the upper and lower bearings. The displacement limit line reflects the clearance lift after the static displacement shown in Figure 22 is made equal to the static displacement in Figure 23. If the displacement exceeds this limit, the shaft will rub the bearing. The deliberate unbalance in the rotor for which the response curves in Figure 27 were calculated is 0.5 gram inch per bearing. The orbit radius is insensitive to speed below 20,000 rpm and the response at both bearings are nearly equal. However, at speeds above 20,000 rpm the two bearings have different responses. The upper bearing curves has a resonance peak at 25,000 rpm and indications are that the shaft will rub at this speed. The displacement variation of the lower bearing indicates the critical speed at 26,000 rpm. The displacement of the lower bearing has a greater magnitude than that at the upper bearing. Since there is an extra mass at the upper end of the shaft (see Figure 20), the mass distribution along the length of the shaft is not quite symmetrical with the shaft midpoint. This extra mass is one of the disks used to measure torque. The non-symmetry of the shaft could account for the difference in critical speed and displacement magnitude between the upper and lower bearings. Reference to Figure 20 indicates that the dynamic response of the upper bearing may

be affected by the presence of the quill shaft which is used to drive the test shaft and measure the torque absorbed. The effect is minimized by using a small-diameter quill shaft. The effect of the presence of the quill shaft and the alignment of the motor with the test shaft was not taken into account in the rotor response data presented herein.

Halving the unbalances reduces the displacement magnitudes by approximately one-half over the whole speed range and has no effect on the speeds at which the criticals occur. This is shown in Figure 28. When the unbalances are unequal, the displacements in the low speed range are unequal as shown in Figure 29. However, the critical speeds remain the same for each bearing. Thus in the speed range below 20,000 rpm, unequal unbalances are required to get two independent sets of test data at one operating condition. However, unequal unbalances are not necessary above 20,000 rpm.

Maximum fluid film force on the bearings versus speed is shown in Figures 30, 31 and 32. The forces for the 0.5 gram inch per bearing case (Figure 30) are, as in the case of the displacements, nearly constant in the low speed range. Corresponding to the displacements, the force magnitude is greater at the lower bearing critical speed (26,000 rpm) than at the upper bearing critical (25,000 rpm). In the high speed range (above 20,000 rpm) the forces like the displacements are different for the upper and lower bearings, even though the unbalances are equal. For this

reason, the two bearings will give independent sets of force data when forces are measured at both bearings during a test run with equal unbalances. Halving the unbalances reduces the force component due to the unbalance. The maximum values still occur at the same speeds. Significant inequality of forces can be seen at low speeds in Figure 31 when the unbalances are unequal at the upper and lower bearings. This inequality in the low-speed range is evident in both force and displacement when the unbalances are different. Larger differences are to be expected as the difference in unbalance increases. Thus, the requirement that the sets of force and displacement data for the upper and lower bearings will be independent is met in the low-speed range when unequal unbalances are used.

Shown in Figure 33 is the total shaft center displacement at the lower bearing versus unidirectional side load at 24,000 rpm. The displacement due only to the side load is represented by a solid line. The displacement due to both side load and unbalance force is represented by dotted lines. Different unbalance combinations are shown. Above a side load of 10 lbs., the major part of the displacement is due to the unidirectional load. In Figure 34 is shown the total force on the lower bearing versus side load at 24,000 rpm. The undirectional force is represented by a solid line, the sum of side load and unbalance force is represented by a dotted line for each unbalance combination. When the side load has a magnitude greater than 20 lbs., it is the larger part of the total force even for the largest unbalance shown. The total displacement at the lower bearing versus side load at 26,000 rpm is shown in Figure 35. At this speed, the

orbit radii are larger than the displacement due to side load. The orbit radii for two of the unbalance combinations, 0.5 gram inch per bearing and 0.25 gram inch at the upper and 0.5 gram inch at the lower bearing, are large enough that the shaft will rub the bearing. This occurs where the dotted lines intersect the bearing surface line. The total force on the lower bearing versus side load at 26,000 rpm is shown in Figure 36. At this speed, the unbalance forces are the major part of the total force. Figures 33, 34, 35 and 36 illustrate the comparison between displacement and force amplitudes at and away from critical speeds.

In order to obtain accurate measurements of force and displacement it is necessary that the measurements be a large portion of the full scale range of the instrument. Thus, since side load affects these measurements more than unbalance, the unbalance used should be scheduled with load instead of speed below 20,000 rpm. Above 20,000 rpm lower load schedules must be used because of the large amplitudes.

3. Concluding Remarks

The rotor-bearing response analysis has led to the following conclusions:

1. System resonances at the bearings occur at rotational speeds of 25,000 and 26,000 rpm for the upper and lower bearings, respectively.

2. The upper and lower bearing resonances occur at different speeds due to non-symmetry of the shaft.
3. At the resonances, the unbalance is predominant in the determination of shaft center displacement and fluid film force.
4. The response in the resonant speed range is different for the upper and lower bearings even though the unbalances are the same.
5. The unidirectional load is responsible for the greater part of the shaft displacement and forces in the speed range below 20,000 rpm.
6. In the speed range below 20,000 rpm, the response is nearly the same for both upper and lower bearing if the unbalances are equal at each bearing.
7. If the unbalances for the upper and lower bearing are different, the response of the bearings in the low-speed range differs with the ratio of the unbalances. Thus, the forces and displacements can be made to differ significantly between the upper and lower bearings.

Since the side load contributes most to shaft displacement, except near critical speeds, the unbalance must be scheduled with side load rather than speed so the force and displacement measurements can be made in a range approaching full scale of the instruments. However, at constant side load, the same unbalances can be used over the non-resonant speed range, up to 20,000 rpm. If, in this speed range, the unbalances at the upper and lower bearings are sufficiently different, two independent sets of measurements required by the eight simultaneous equations can be obtained by measuring

the forces and displacements at each bearing. In the resonant speed range, the unbalance must be reduced to prevent the shaft from rubbing the bearing. As the resonant speeds for the upper and lower bearings are different, an independent set of data can be obtained from each bearing in the resonant speed range when the unbalances are equal at each bearing.

III. INSTRUMENTATION

During the reporting period the instrumentation approach has been improved. These improvements include the use of a digital data acquisition system for quickly and accurately recording test data, the instrumentation of two bearings instead of one, and the replacement of the strain-gauged force buttons by piezoelectric load cells.

Several advantages accrue because of the selection of the digital data acquisition system. The digital data acquisition system has a high-accuracy digital voltmeter (about 0.05 percent of full scale) contributing greatly to the accuracy of the data to be taken. In addition, the data can be scanned in about 60 seconds, minimizing test point drift during data taking and the amount of time to get a test point. The digital data acquisition system produces printed-tape output for checking immediately after data acquisition and punched-tape output for automatic data reduction. Thus, no tedious manual reading of photographs or strip charts is required. This reduces the time duration and effort needed for data reduction. Using the digital acquisition system reduced data should be available within days after a particular test. Photographs of oscilloscope traces showing the locus of the shaft center shall be taken as a visual record of the test condition.

This technique, however, places additional requirements on the measuring system since it is necessary to convert the signals into meaningful parameters and to sequentially switch each such converted signal into the digital recording system.

The instrumentation of both bearings permits acquiring all data required for the eight dynamic coefficients of the bearing mentioned in the previous section at one operating condition with one digital scan. Previously it has been planned to instrument but one bearing and run the shaft at the same operating condition twice, each with a different unbalance configuration, in order to obtain the requisite experimental information for the dynamic performance of the bearing at a given operating condition.

Shown in Figure 37 is the test assembly; test bearings, load cells and inductance-gage distance detectors are shown. The force and displacement measurements are made in four planes perpendicular to the shaft center line. Shown in Figure 38 are the displacement sensors and load cells for any one of the four instrumentation planes. The displacement sensors are seen to be in pairs which are in line with and at right angles to the direction of the side load. The load cells are in pairs and are equidistant between the displacement sensors. The displacement sensors are adjacent to the shaft and the load cells measure the forces exerted by the inner bearing housing on the outer bearing housing.

Shown in Figure 38 is a schematic diagram of the instrumentation to be read on the digital data acquisition system. Only one pair of displacement probes and one pair of load cells are shown. The outputs from each displacement

probe in a pair are combined so as to give one signal for the pair. To do this the individual signals of each pair will be conditioned so that slopes of displacement versus output signal curves are identical. Summing of the individual signals will provide cancellation of symmetrical differential thermal expansion of the bearing housing and will double the sensitivity of the displacement measuring system. Only one load cell in a pair is connected to the read out. The stiffness of each load cell will be determined experimentally before installation. From these data multipliers can be established for the output of each active load cell to give the correct force reading. After passing through switching circuits, the dynamic measurements are directed to a peak-to-peak level detector, an average level detector, or a phase meter. The output of these detectors is scanned by the digital data acquisition system. The peak-to-peak detector yields double amplitude for force and displacement. The average-level detector yields the equilibrium position of the shaft. The unidirectional load, corresponding to the equilibrium position of the shaft, is read on pressure transducers connected to the loader bearing actuation cylinders.

The phase angles to be measured are shown in Table III. Eight each displacements and forces and eight phase angles between displacements and forces are required for each test condition to provide data for the bearing dynamic coefficients.*

Oscilloscopes will be available for surveillance of bearing behavior during testing. One oscilloscope will be connected to two perpendicular

*See Section II. Rotor Bearing Analysis.

pairs of displacement sensors for each bearing. The signal on this oscilloscope will be reinforced once each revolution. Thus synchronous whirl will be identified by one blip on each orbital trace and fractional-frequency whirl will be identified by two. The second oscilloscope will be used to monitor any dynamic measurements of interest during testing. A camera for the oscilloscopes will be available to make permanent records as required.

For all runs in which the oscilloscope indicates fractional-frequency whirl, the synchronous tracking filter can be put on manual control. Then by noting peak output at some hand-set frequency near one-half of the shaft speed the whirl ratio can be obtained.

1. Force Measurement

To facilitate force measurement the inner bearing housing for the test bearings was to be supported in two mutually perpendicular planes by a total of eight strain-gaged force buttons fixed to the outer bearing housing at two axial locations, as shown in Figure 39. In a radial-axial plane the vibrating system can be represented by the diagram shown in Figure 39.

It can be seen that the mass of the inner bearing housing plus attachments is between the fluid film where the force measurement is required and the strain-gaged force buttons represented by springs in Figure 40. Thus the measured force on the strain-gaged force buttons is given by the sum of the fluid film force and the mass times acceleration of the inner bearing housing. At forcing frequencies far below the natural frequency of the vibrating system consisting of the strain-gaged force buttons and the inner bearing housing, the measured force and the fluid film force will be essentially equal. Near the natural frequency, but below it, the two forces will not be equal because of the mass times acceleration of the inner bearing housing will

become larger. Beyond the natural frequency, in addition to being different, the two forces will be out of phase.

Recent experiments have indicated that typically the strain-gaged force buttons have a spring constant of approximately 50,000 lb./in., and the actual weight of the sprung mass consisting of the inner bearing housing, the bearing and the eight displacement gauge holders is 16 lbs. Shown in Figure 40 is a plot of the ratio of the measured to the actual fluid film force, and the phase angle between the forces. It can be seen that the natural frequency of the system shown in Figure 40 corresponds to a rotative speed of 21,000 rpm (350 cps). Since this speed is within the speed range specified for the test program, namely, 3600 to 30,000 rpm, larger errors in measured force can be expected as shown in Figure 41 over an inportant part of the test speed range. It is also seen from the figure that the measured and actual fluid-film force are 180° out of phase beyond the critical speed. Actual tests of a force button in a vibrating system indicate that the force-button signal is plagued by excessive noise. This is due to the large amplification needed for the force button because of its low output per unit load, about 0.05 mv/lb.

Primarily because of the low natural frequency of the force button-inner bearing housing system and to eliminate the noise problem, piezoelectric load cells have been selected to measure force by placing eight of them on the outer bearing housing in a manner similar to that contemplated for the strain gaged force buttons. The piezoelectric load cells chosen (Kistler, Model 902A) each have a spring constant of about 1.67×10^7 lb./in., resulting in a natural frequency of the inner bearing housing system in Figure 40 of

383,000 rpm (6400 cps). Shown in Figure 41 also is the ratio of measured to actual fluid film force for the load cells. The use of the piezoelectric load cells will assure a flat response well beyond the maximum test speed of 30,000 rpm as shown in the figure. The highly stiff load cells will not, however, eliminate possible errors due to casing natural frequencies. The piezoelectric load cells have a substantially larger output per unit force measured, about 100 mv/lb.

Only one charge amplifier is required to read the eight active load cells because they will be read one at a time. Switching circuits driven by the digital data acquisition system will connect the proper load cell to the digital voltmeter prior to scanning that particular reading. Actually two amplifiers will be purchased because two are needed for the original adjustment of the load cells in the outer bearing housing.

2. Displacement Measurement

Major problem areas associated with the proximity sensors have included sensitivity to water spray, zero shift, sensitivity to shaft surface irregularities and conductivity inhomogeneity. An examination of some of these problems was undertaken in order to determine the ultimate system measurement capabilities. Included in these tests were measurement of effects of water spray in the probe tip-to-shaft gap and measurement of long term stability. Pairs of Bently (Model H1084) probes with teflon end caps were mounted in a fixed position relative to a fixed silver plated shaft segment. Probe tip-to-shaft gap was adjusted to 10 mils, approximately that which will

exist during operation in the test rig. Figure 41 is a picture of the assembly. The nominal sensitivity for the probe pairs was 800 mv/mil. In each pair of probes a D152 and a D252R detector were used. The probes were excited at 12.75 volts using a Harrison Laboratory Model 802B D.C. power supply. The probe output signals were combined and connected to a sensitive (Fluke Model 801B) differential voltmeter. Measurements of the net change in output caused by squirting water into the gap were made for all 16 probe assemblies and the results are tabulated in Table IV. Although the values were slightly different for each probe, all behaved effectively the same way in that the presence of water caused an instantaneous change in output. Removal of the water caused the output signal to return to its original value. The maximum change in output was equivalent to a shaft movement of 19 micro inches. This appears to be an acceptable level and indicates that the displacement probe teflon cap sealed with silicone rubber configuration has substantially reduced the sensitivity of the probe output signal to water.

Although the preliminary tests, just described, had indicated the sealing of the probes with teflon caps and General Electric RTV sealant was satisfactory for short-time durations, there existed doubt concerning the leak tightness of the probes under testing conditions in which the probe would be submerged and subjected to high fluid velocities caused by rotating parts. Therefore a pair of probes was subjected to complete submersion in water bath for approximately 110 hours. For approximately 20 hours the water was agitated. After the removal of the water the test continued for about another 45 hours. The zero was reset when agitation was initiated and after removal of the water. The results are presented in Table V. During non-

agitated submersion the maximum zero shift was 25 mv, corresponding to an error of 20 micro inches. During agitation the maximum zero shift was an additional 18 mv, corresponding to 14.4 micro inches. Within an hour of water removal the zero shift reached a maximum of -30 mv (-24 micro inches) and 33 hours later the zero shift was zero which is essentially where it stayed for the remainder of the test. Thus the zero shift due to the presence of water is less than the zero shift permitted by the contract work statement (namely, 25 micro inches).

Additional tests were conducted with the probe detector circuits immersed in an isothermal bath which was maintained at 32 $\pm$ 1°F. The data are presented in Table VI. The maximum change in output over a 24-hour period was equivalent to approximately 9 micro inches displacement.

Tests using the same apparatus were also conducted to determine the long term stability characteristics of the displacement measuring system. In this test the same pair of probe assemblies was used mounted as before. The results are presented in Table VI. The combined output signals were recorded on a potentiometric strip chart instrument. No movement between probes and shaft was induced. The test was conducted in an air conditioned area maintained at 77 $\pm$ 5°F so differential thermal expansion effects would be insignificant. The maximum change in output of the probe pair was equivalent to 29 micro inches displacement during a test period of one week.

These tests were conducted under nearly ideal conditions and provide an indication of the ultimate accuracy of the displacement measuring system. In addition to effects of water and zero shift, the measuring system accuracy tolerance must include effects of shifts in output versus deflection curves, signal combining circuit stability and temperature sensitivity, peak-to-peak and average level detector accuracy and digital recording system accuracy.

3. Phase Angle Measurement

The apparatus shown in Figure 17 was set up to test the feasibility of measuring phase angle between two typical waveforms generated by two Bently detectors mounted perpendicular to each other adjacent to a silver-plated shaft segment which was mounted in a collet attached to the spindle of a modified tool post grinder. Initial tests were conducted using a Technology Instrument Corp. phase meter (Type 320-AB) without any input filters. This instrument measures the time interval between zero crossings of the two waves and is a.c. coupled to the signal sources to eliminate any d.c. components. The signals produced by the two Bently detectors were proportional to the runout of the shaft. Shaft runout during initial tests was approximately 4 mils. Tests were conducted over a speed range of 2500-7160 rpm and are shown in Table VII. The results indicated that phase angle measurements were not appreciably affected by shaft speed. Measured phase angle varied from 86.5 to 91 degrees over all test conditions. The actual angle between the probes was estimated to be 90 $\pm$ 1 degrees and was determined by alignment of the probe centers with the high point on the shaft using a spring loaded linear variable differential transformer sensor (Electrojet) mounted beside the Bently probe as an indicator. This method of alignment provided accuracy within the limits of phase meter capability which is 3 degrees plus or minus 1 percent of full scale (90 degrees).

The results of the tests proved the feasibility of making the desired measurements by measuring phase angle directly instead of using an oscilloscope. However, the requirements of the test program are somewhat

more difficult to meet than those established during the feasibility tests. Signal levels will be considerably lower and phase angle between force and displacement signals will be required rather than between two signals from the same type of source. Under certain test conditions the presence of fractional-frequency whirl will complicate the phase measuring problem. For these reasons, a more sophisticated system consisting of a dual channel tracking filter with a band pass center frequency, automatically adjusted to shaft speed will be used in conjunction with a phase meter during operation of the test rig. Overall system accuracy tolerances will be $\pm$ 0.5 degrees. The same system will be used to determine the whirl frequency by connecting the filter tracking signal to an audio oscillator and manually adjusting the audio frequency to obtain maximum voltage output at the filter output.

IV. TEST FACILITY PREPARATION

The Hydrodynamic Journal Bearing Test Rig and supporting equipment will be set up in the control room of Building 314. This available location is especially suited because of the air-conditioned environment. Plans are underway to locate the major portion of the apparatus in the assigned area although the high frequency power supply along with the digital data recorder will remain in an adjacent building.

Overhaul operations are scheduled for an available Ward-Leonard M.G. high frequency power supply. While the power supply apparatus is being reconditioned, the 15 horsepower test rig drive motor will be checked and the two units will be matched for optimum performance. A remotely operated control panel will be fabricated and installed in the test area for operation of the M.G. set located in another building (309). Elevated power cables will be constructed to connect the two facilities.

An additional cable link will be required between Buildings 314 and 309 to connect the test rig instruments with the 600 channel digital data recorder that exists in the latter location. This link will provide digital recording of all the required journal bearing test data.

The design of the test rigs distilled water loop will be similar to the arrangement used in the previous bearing test program (NAS 3-2111). However, a new 80 gallon glass-lined electric water heater, a new water cooled heat exchanger, and a new piping will be provided to maintain the high purity of the distilled water lubricant. Additional instrumentation will be inserted in the loop piping for use with the digital data recording system in addition to that required for operational purposes.

Building utilities such as cooling water, instrument air, electrical power, drains, etc., are being extended to fulfill the requirements of the test rig and its auxiliary equipment. In addition, a new set of control panels are being designed to house and consolidate all required controls and instrumentation.

REFERENCES

1. J.D. McHugh, H.E. Nichols, W.D.C. Richards, and H.C. Lee: "Hydrodynamic Journal Bearing Program - Quarterly Progress Report No. 1", Contract NAS 3-6479, NASA-CR-54792.

2. J.D. McHugh, H.E. Nichols, and W.D.C. Richards: "Hydrodynamic Journal Bearing Program - Quarterly Progress Report No. 3", Contract NAS 3-6479, NASA-CR-72034.

3. "Low Viscosity Bearing Stability Investigation", NASA Report NASA-CR-54039.

4. F.K. Orcutt, C.W. Ng, J.H. Vohr and E.B. Arwas: "Lubrication Analysis in Turbulent Regime - First Quarterly Report", NAS w-1021, NASA-CR-54195.

5. J.D. McHugh, H.E. Nichols, W.D.C. Richards, and H.C. Lee: "Hydrodynamic Journal Bearing Program - Quarterly Progress Report No. 2", Contract NAS 3-6479, NASA-CR-72033.

6. M.A. Prohl: "A General Method For Calculating Critical Speeds of Flexible Rotors", Journal of Applied Mechanics, Volume 12, 1945, pp. 142-148.

7. N.O. Myklastad, Journal of Aeronautical Sciences, Volume 11, 1944, p. 153.

8. S. Timoshenko: "Vibration Problems in Engineering", D. VanNostrand Company, Third Edition, 1955.

REFERENCES (Continued)

9. J.W. Lund, "Rotor-Bearing Dynamics Design Technology", Mechanical Technology Incorporated, Technical Report AFAPL-TR-64-45, Part V, May, 1965.

10. S. Timoshenko: Strength Of Materials, Part II, Advanced Theory and Problems, D. VanNostrand Co., Inc., N.Y., 1941, p. 356.

11. H.A. Rothbart, Editor-in-Chief, Mechanical Design and Systems Handbook, McGraw-Hill Book Company, New York, 1964, Section 15.15.

TABLE I

INSTRUMENTATION AND EQUIPMENT LIST

	Name	Model No.	Manufacturer
1.	Differential Voltmeter	801	John Fluke Co.
2.	Single Channel Recorder	19301-01-01	Honeywell Corp.
3.	Proximity Probe	H-1-084-3	Bently Nevada
4.	Proximity Detector	D152 D252R	Bently Nevada
5.	Power Supply	802B	Harrison Lab. Inc.
6.	Dial-A-Volt	DAV46D	General Resistance Inc.
7.	Accutron Transistor Amplifier	51	Sheffield Corp.
8.	Electrojet Cartridges	59230108 59230119	Sheffield Corp.
9.	Linearchek Gage Calibrator		Sheffield Corp.
10.	Sundstrand Bench Centers	BC 6"x36"	Sundstrand Machine Tool
11.	Leitz Optical Stage	1"x1"	Opto-Metric Tools Inc.
12.	Oscilloscope	RM561A	Tektronix Corp.
13.	Oscilloscope	RM535	Tektronix Corp.
14.	Oscilloscope	8151R	Beckman
15.	Phase Meter	320-AB	Technology Inst. Corp.
16.	Differential Comparator	3A7	Tektronix Corp.
17.	Scope Camera		Dumont
18.	Balance Machine	MU-6	Micro Balancing Inc.

TABLE II

DESCRIPTION OF BEARINGS FOR WHICH DYNAMIC FORCE COEFFICIENTS WERE CALCULATED

Type of Bearing	Pivoted Pad
L/D	1.0
Number of Pads	4
Pad Arc, β , Degrees	80
Pivot Location, θ_p , Degrees Behind Leading Edge of Pad	44
Geometric Preload, m	0.4
Machined Pad Radial Clearance, C_p, mils	2.5
Minimum Clearance, C_B, mils	1.5

TABLE III

BEARING DYNAMIC CHARACTERISTICS - MEASUREMENTS

UPPER BEARING

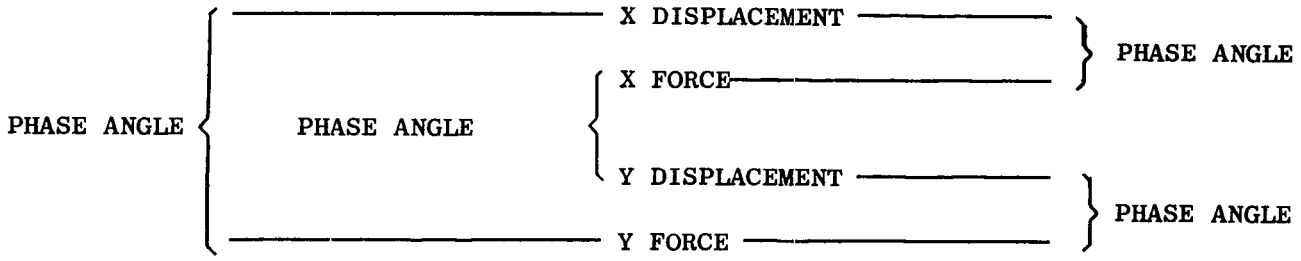

LOWER BEARING

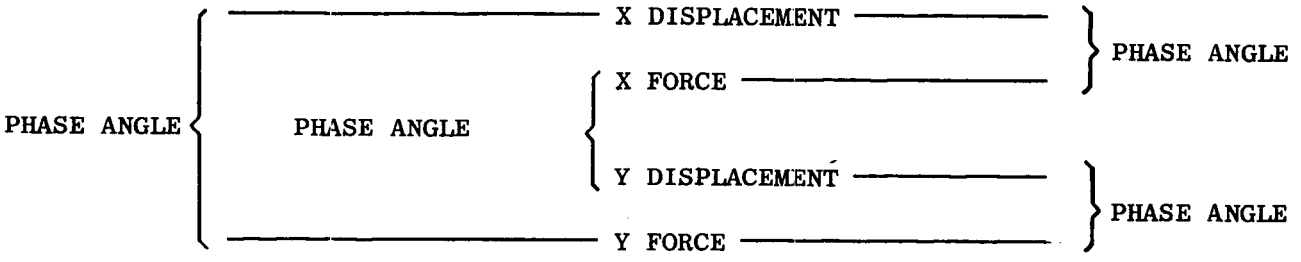

TABLE IV

BENTLY (MODEL H 1084) DISPLACEMENT PROBE

WATER SENSITIVITY TEST RESULT SUMMARY

Probe Pair Designation	Output Change Due to Water, mv	Equivalent Change,* Microinches
1	-15	-19
2	+10	+13
3	+15	+19
4	+ 2	+ 3
5	0	0
6	- 4	- 5
7	- 5	- 6
8	+ 5	+ 6

*Based on nominal sensitivity 800 mv/mil.

1 Probes were set up in apparatus shown in Figure 40 with a nominal probe to shaft gap of 0.010 inch.

2 All probes were Bently type H1084 with teflon end cap mounted in special holder.

3 Probes 1-8 were used with Bently type D152 detectors (slope of sensitivity curve is negative.)

4 Probes 1R - 8R were used with Bently Type D252R detectors (slope of sensitivity curve is positive.)

5 All detectors excited at 12.75 volts with Harrison Lab Model 802B power supply.

6 All measurements made with J. Fluke Model 801B differential voltmeter.

7 Tests were conducted by setting probes at a nominal gap of 0.010 from a silver plated shaft segment. Change in output level was noted as water was sprayed in the probe to shaft gap. In all cases, the output signal returned to its initial value when the water was removed from the probe to shaft gap.

TABLE V

EFFECT OF COMPLETE SUBMERGENCE ON DISPLACEMENT PROBE ZERO SHIFT

Nominal Sensitivity: 800 mv/mil

Date	Time, hrs.	Zero Reading, mv	Remarks
4-22-66	1500	0	Probes submerged
	1600	+10	
	1700	+ 8	
	1800	0	
	1900	- 4	
	2000	0	
	2100	- 4	
	2200	- 2	
	2300	- 8	
	2400	+ 4	
4-23-66	0100	+10	Saturday
	0200	+10	
	0300	+10	
	0400	+ 9	
	0500	+ 9	
	0600	+11	
	0700	+11	
	0800	+14	
	0900	+16	
	1000	+15	
	1100	+10	
	1200	+15	
	1300	+13	
	1400	+18	
	1500	+20	
	1600	+25	
	1700	+25	
	1800	+22	
	1900	+22	
	2000	+20	
	2100	+25	
	2200	+22	
	2300	+21	
	2400	+20	
4-25-66	0800	+24	Monday
	1422	0	Zero reset and water agitated
	1500	+18	
	1600	+ 2	
	1700	+ 4	
	1800	- 1	
	1900	- 5	
	2000	- 7	

TABLE V

EFFECT OF COMPLETE SUBMERGENCE ON DISPLACEMENT PROBE ZERO SHIFT

(Continued)

Date	Time, hrs.	Zero Reading, mv	Remarks
4-25-66	2100	-11	
	2200	11	
	2300	-11	
	2400	-11	
4-26-66	0100	-10	
	0200	- 6	
	0300	- 3	
	0400	- 2	
	0500	- 3	
	0600	- 2	
	0700	- 1	
	0730	- 1	
	0900	0	Water removed and zero reset.
	0950	-30	
	1030	-30	
	1100	-14	
	1200	-14	
	1300	-10	
	1400	- 3	
	1500	0	
	1600	- 2	
	1700	- 7	
	1800	-10	
	1900	-11	
	2000	-12	
	2100	-15	
	2200	-15	
	2300	-15	
	2400	-16	
4-27-66	0100	-13	
	0200	-12	
	0300	-14	
	0400	-12	
	0500	-10	
	0600	-10	
	0700	-10	
	0730	- 9	
	1440	+ 4	
	1540	+ 4	
	1640	+ 6	
	1740	+ 2	
	1840	0	

TABLE V

EFFECT OF COMPLETE SUBMERGENCE ON DISPLACEMENT PROBE ZERO SHIFT

(Continued)

Date	Time, hrs.	Zero Reading, mv	Remarks
4-27-66	1940	+ 2	
	2040	0	
	2140	+ 1	
	2240	- 2	
	2340	- 1	
4-28-66	0040	0	
	0140	0	
	0240	0	
	0340	- 2	
	0440	0	
	0540	- 3	
	0640	- 2	
	0715	- 2	
	1520	0	
	1620	+15	
	1720	+ 5	
	1820	+ 2	
	1920	0	
	2020	0	
	2120	+ 1	
	2220	+ 4	
	2320	+ 5	
4-29-66	0020	+ 6	
	0120	+ 6	
	0220	+ 6	
	0320	+ 6	
	0420	+ 5	
	0520	+ 7	
	0620	+10	
	0730	+11	Test terminated

TABLE VI

TEMPERATURE SENSITIVITY OF DISPLACEMENT PROBE DETECTORS

Date	Time, hrs.	Zero Drift, mv	Remarks
3-22-66	1350	0	Zero set with detectors in ice bath
	1450	+ 3.0	
	1600	+ 3.0	
	1700	+ 5.0	
	1800	+ 3.0	
	1900	+ 4.0	
	2000	+ 5.5	
	2100	+ 7.5	
	2250	+11.0	
3-23-66	0815	+ 7.0	
	1120	- 2.0	
	1220	+ 2.0	
	1300	- 2.0	
			Removed detector from ice bath
	1635	+ 5.0	
	1735	+ 1.0	
	1835	- 3.0	
	2035	- 4.0	
	2235	- 6.0	
3-24-66	0035	- 3.0	
	0235	- 2.5	
	0435	- 2.5	
	0635	- 4.0	
	0835	- 5.0	
	1035	- 1.0	
	1235	+ 1.0	
	1435	+ 2.0	
	1635	+ 3.0	
	1835	+ 1.0	
	2035	- 7.0	
	2235	-11.0	
3-25-66	0035	-12.0	
	0235	-12.0	
	0435	-12.0	
	0635	-13.0	
	0835	-11.0	
	1035	-11.0	
	1235	- 6.0	
	1345	0	
	1545	- 1.0	
	1745	- 2.0	
	1945	+ 1.0	
	2145	- 7.0	
	2345	-10.0	

TABLE VI

TEMPERATURE SENSITIVITY OF DISPLACEMENT PROBE DETECTORS
(Continued)

Date	Time, hrs.	Zero Drift, mv	Remarks
3-26-66	0145	-16.0	
	0345	-17.0	
	0545	-17.0	
	1745	-12.0	
	0945	-12.0	
	1145	-11.0	
	1345	-12.0	
	1545	-12.0	
	1745	-12.0	
	1945	-12.0	
	2145	-14.0	
	2345	-15.0	
3-27-66	0145	-16.0	
	0345	-15.0	
	0545	-13.0	
	0745	-15.0	
	0900	-16.0	Equipment turned off
3-28-66	0810	-30.0	Equipment turned on
	1030	-25.0	
	1230	-20.0	
	1630	0	
3-30-66	0825	-25.0	Equipment turned on
	1030	-20.0	
	1640	- 8.0	Equipment turned off
4-1-66	0630	-36.0	Equipment turned on
	1330	-20.0	Equipment turned off

TABLE VII

PHASE ANGLE MEASUREMENT DATA

Signal From Bently Probe	Phase Shift Degrees	Meter Connection	Speed, rpm 2500	4500	6260	7160
			Phase Angle, Degrees			
2	0	Normal	88.5	87.0	88.5	89.0
7	0					
2	0	Reversed	88.0	88.0	86.5	91.0
7	180					
2	180	Normal	91.0	91.0	91.0	91.0
7	180					

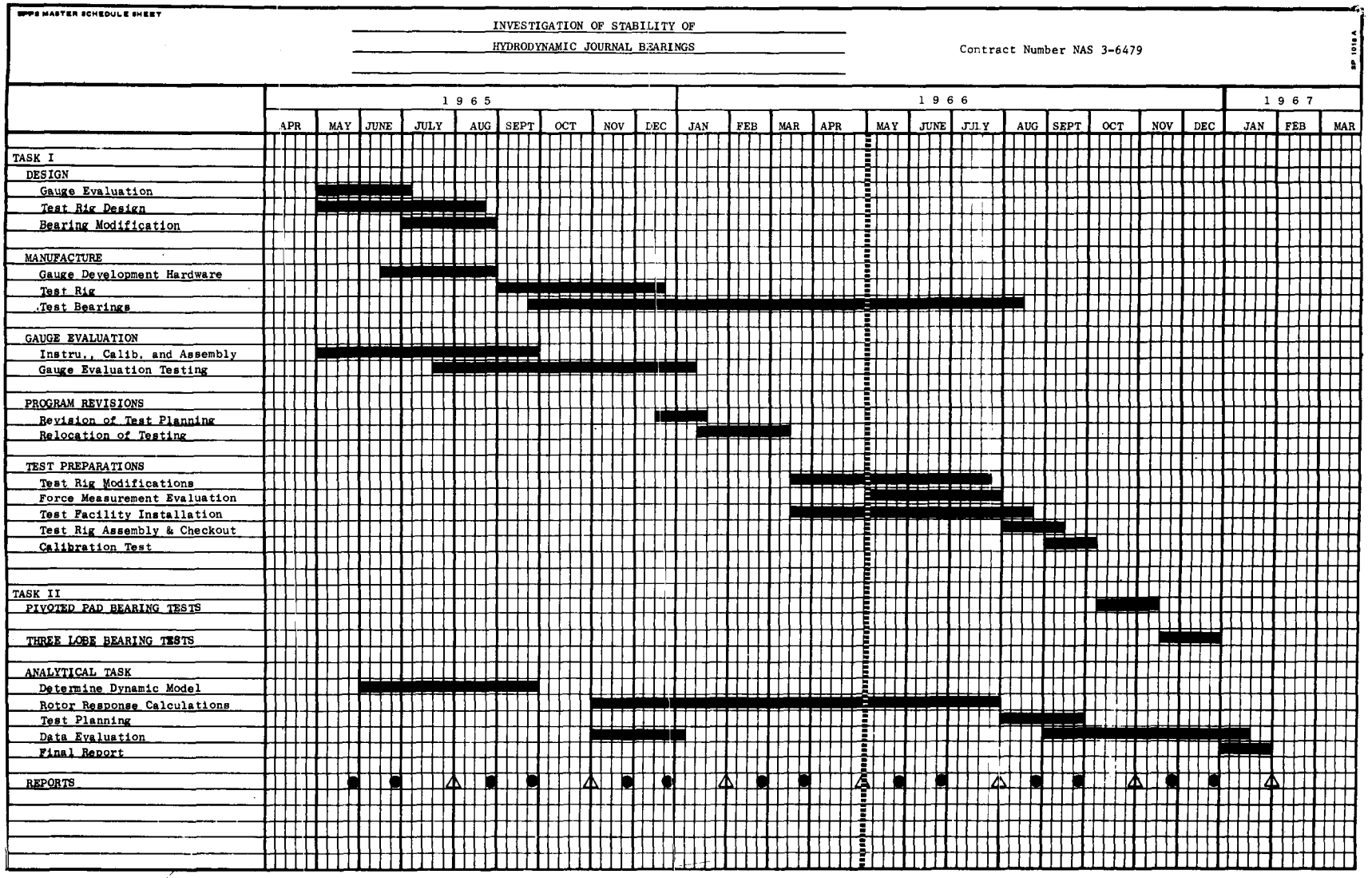

Figure 1. Program Schedule.

		Loss in Diametral Clearance (mils)	Shaft-Bearing Slope
I.	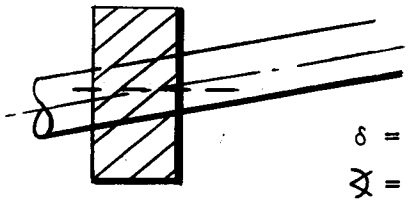 $\delta = 0.004"$ $\measuredangle = 0$	0.404	$\frac{1}{3100}$
II.	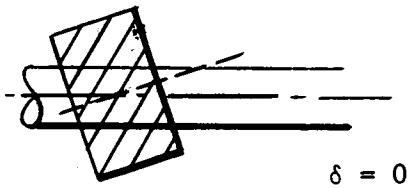 $\delta = 0$ $\measuredangle = 400$ sec	2.376	$\frac{1}{527}$
III.	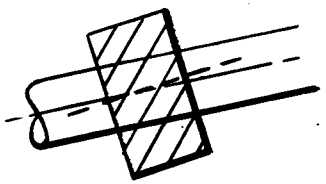 $\delta = 0.004"$ $\measuredangle = 400$ sec	1.972	$\frac{1}{634}$
IV.	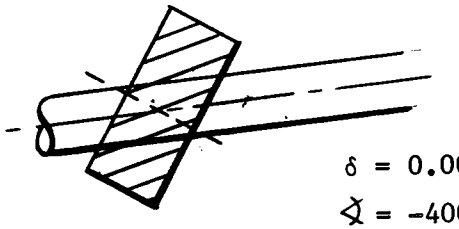 $\delta = 0.004"$ $\measuredangle = -400$ sec	2.780	$\frac{1}{450}$

J1077-6

Figure 2. Loss of Bearing Clearance as Result of Misalignment.

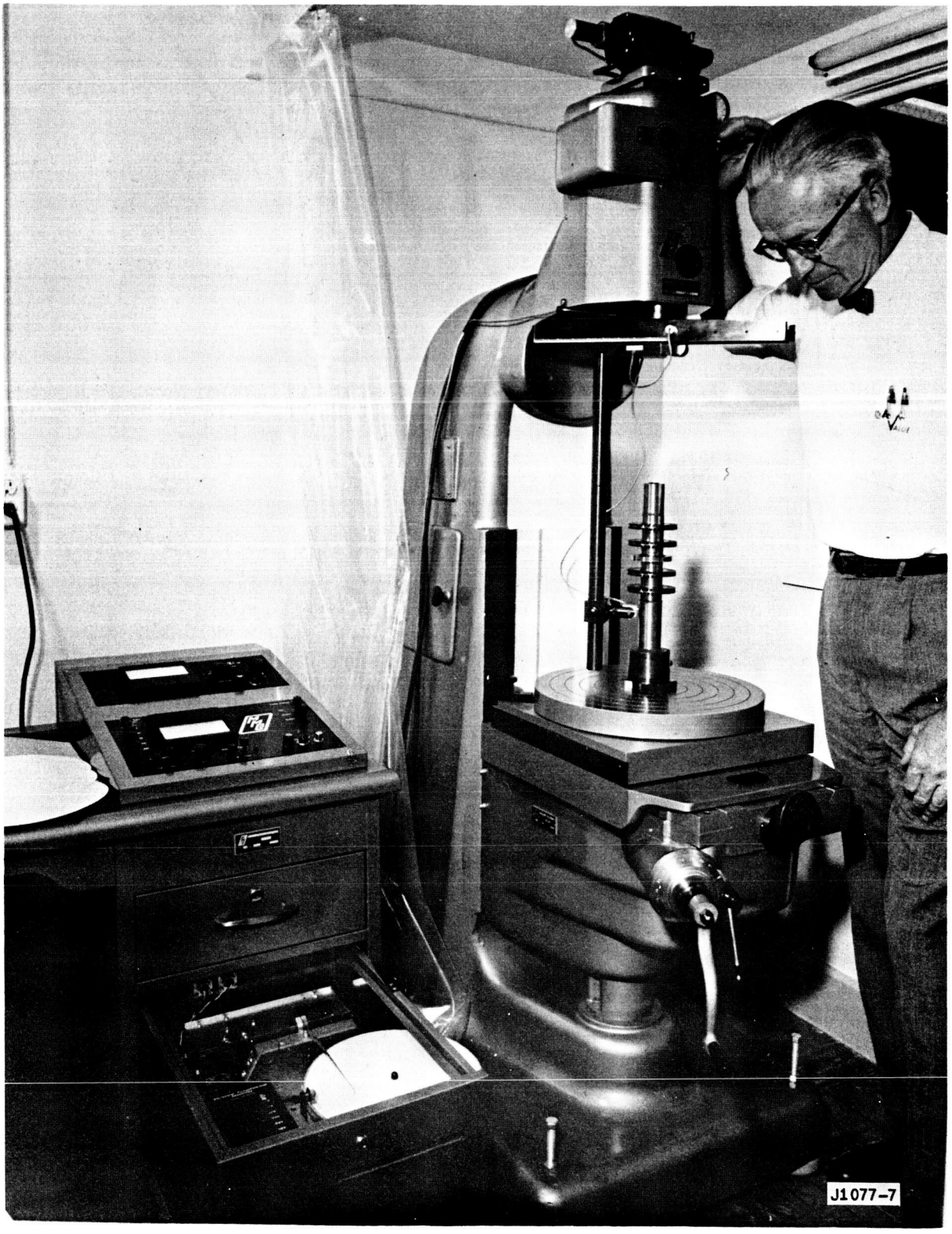

Figure 3. Proficorder.

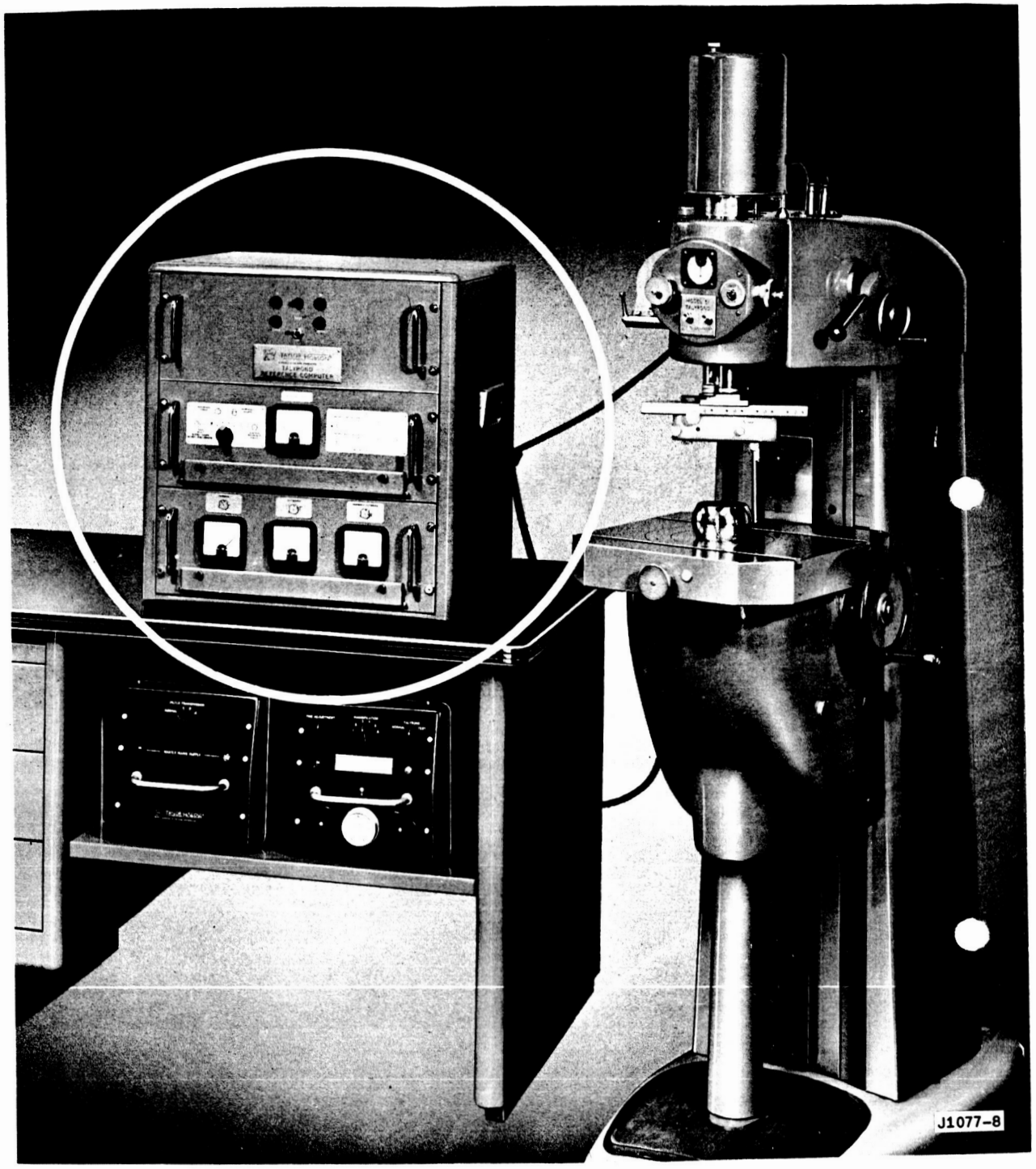

Figure 4. Talyrond.

Displacement Between Bearing Centerlines

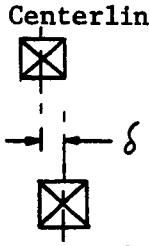

	Zero Alignment Error	0.004" Transverse Misalignment Error	400 Second Misalignment Error
Optical	0.000080	0.000090	0.000090
Proficorder	0.000103	0.000126	0.000077
Talyrond	0.000073	0.000097	0.000046

Angle Between Bearing Centerlines

	Zero Alignment Error	0.004" Transverse Misalignment Error	400 Second Misalignment Error
Optical	8 Seconds	8 Seconds	10 Seconds
Proficorder	30 Seconds	36 Seconds	36 Seconds
Talyrond	21 Seconds	29 Seconds	28 Seconds

J1077-10

Figure 5. Estimated Alignment Accuracy For Various Alignment Techniques.

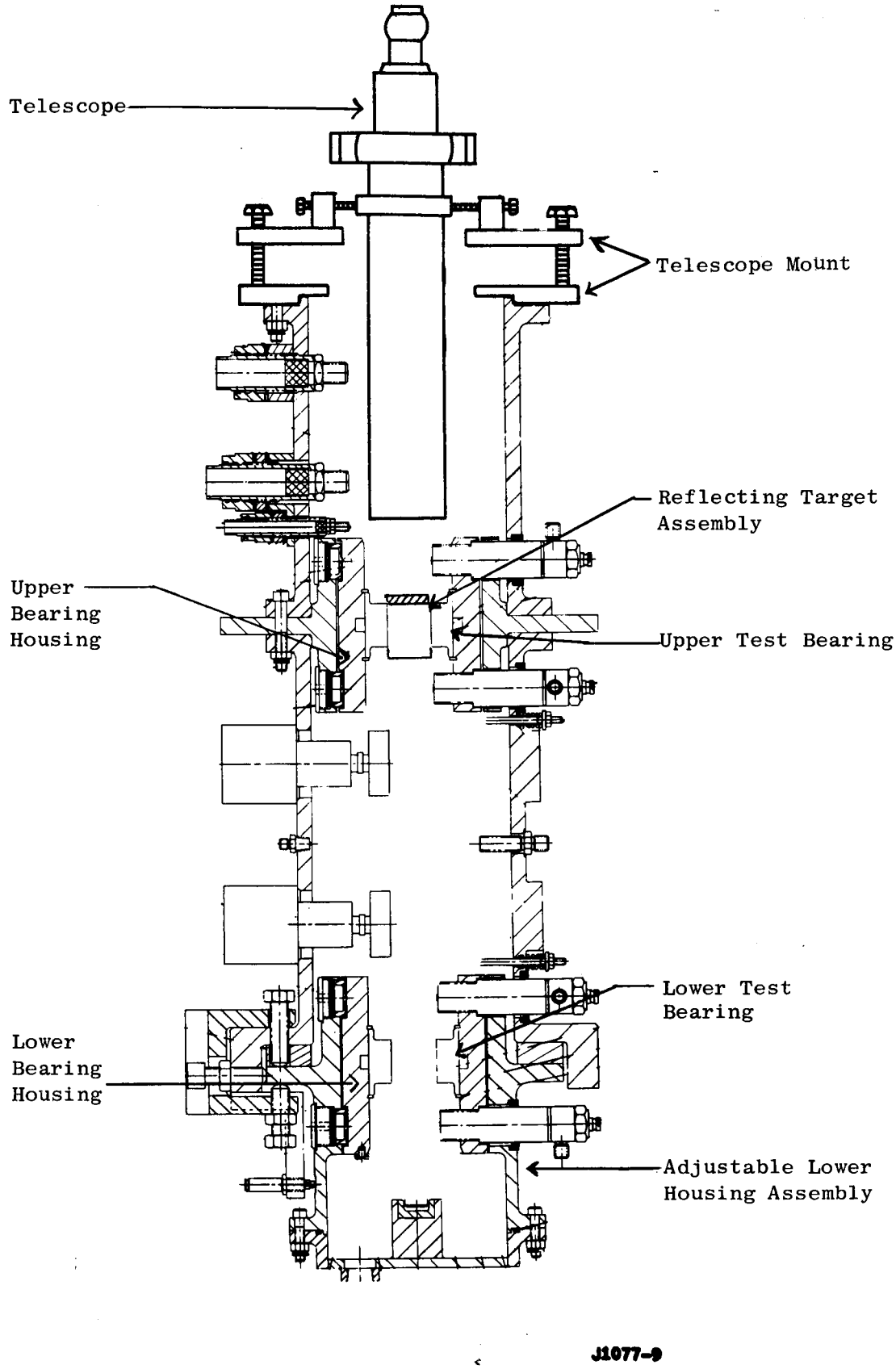

Figure 6. Bearing Alignment Using Telescope.

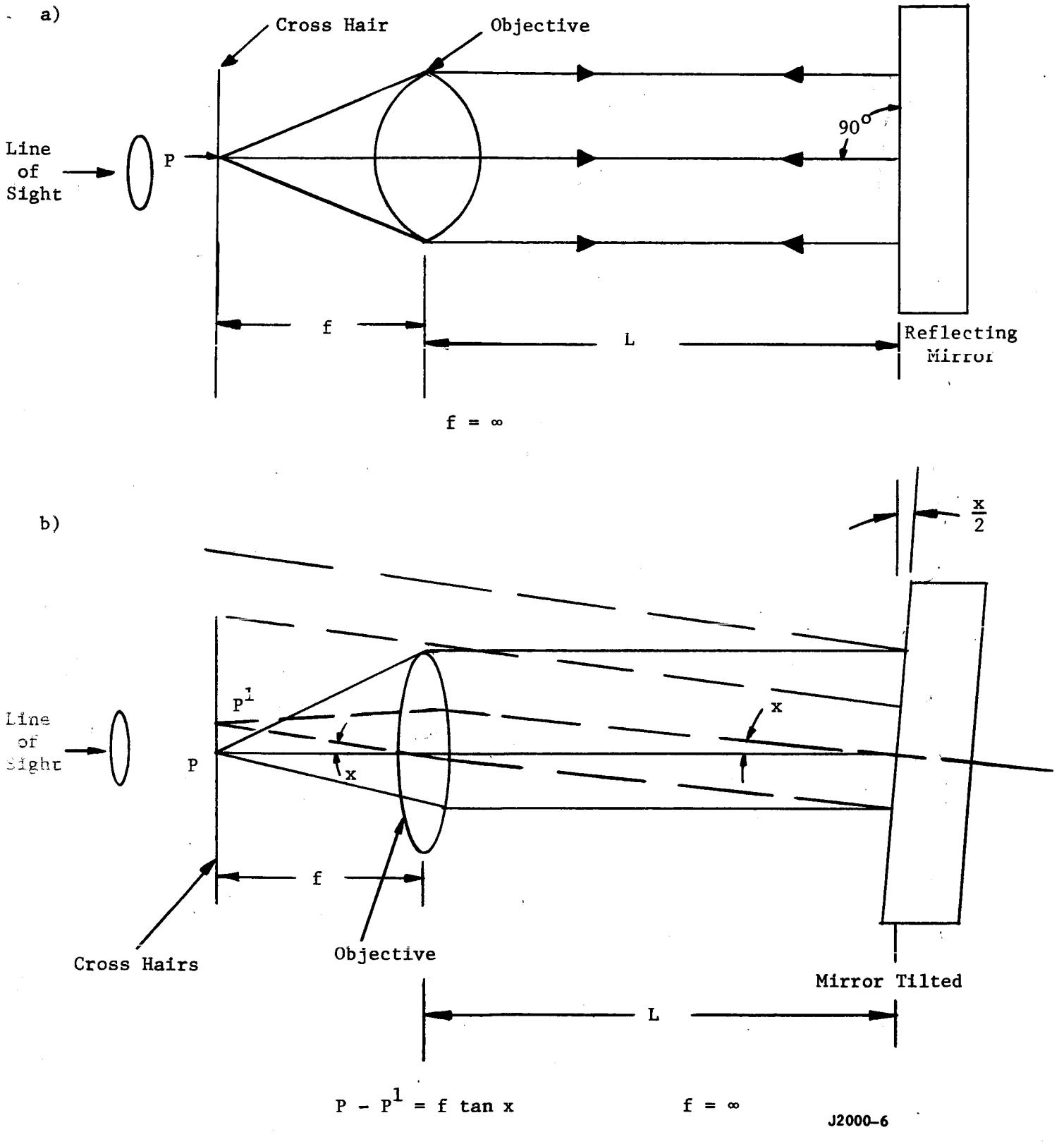

Figure 7. Principle of Autocollimation.

Part No.	Dia. A	Dia. B	Length
P1	1.2545 1.2544	1.2553 1.2552	3.260 3.240
P2	1.2525 1.2524	1.2533 1.2532	3.260 3.240

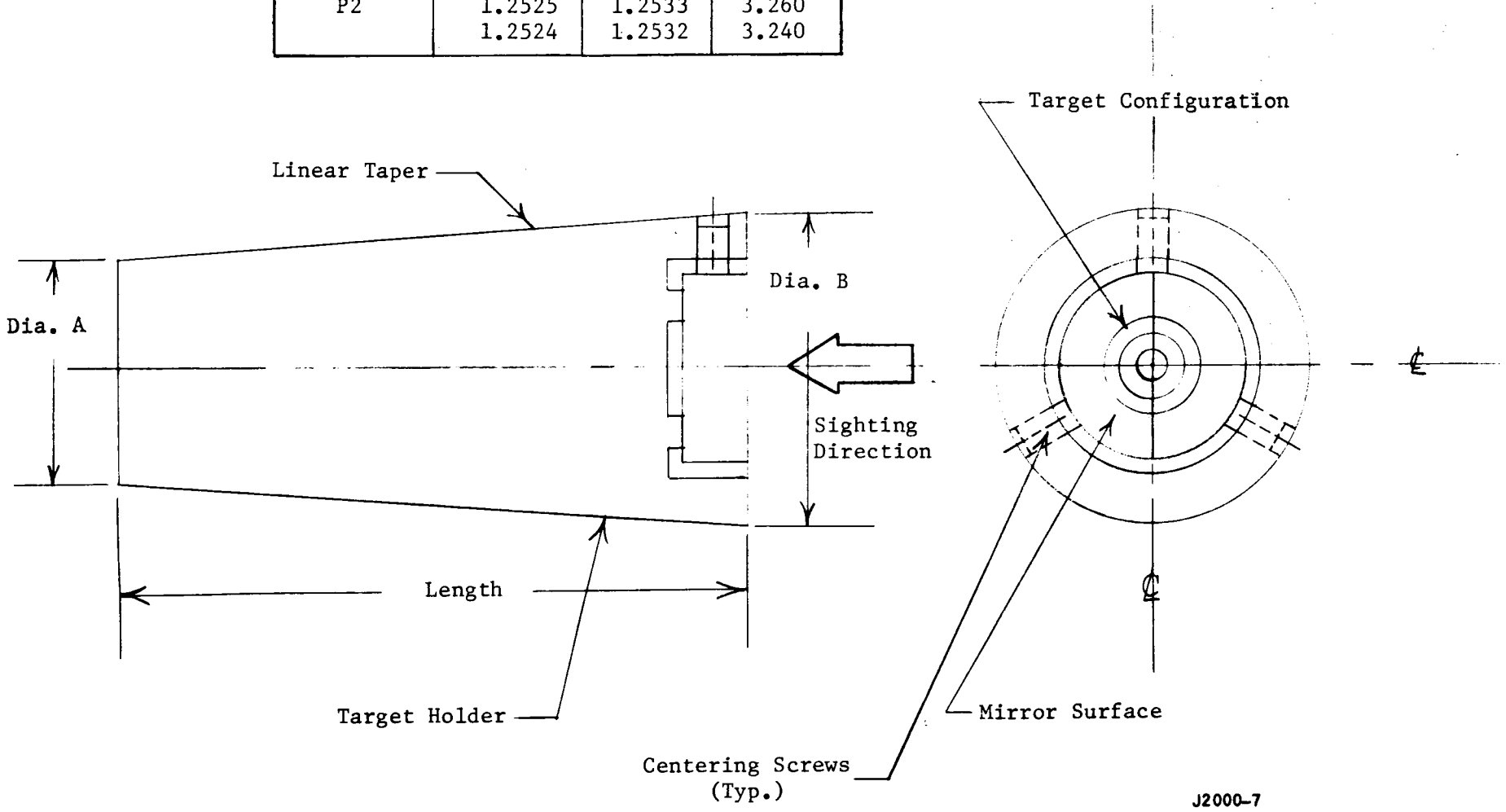

Figure 8. Reflecting Target Assembly.

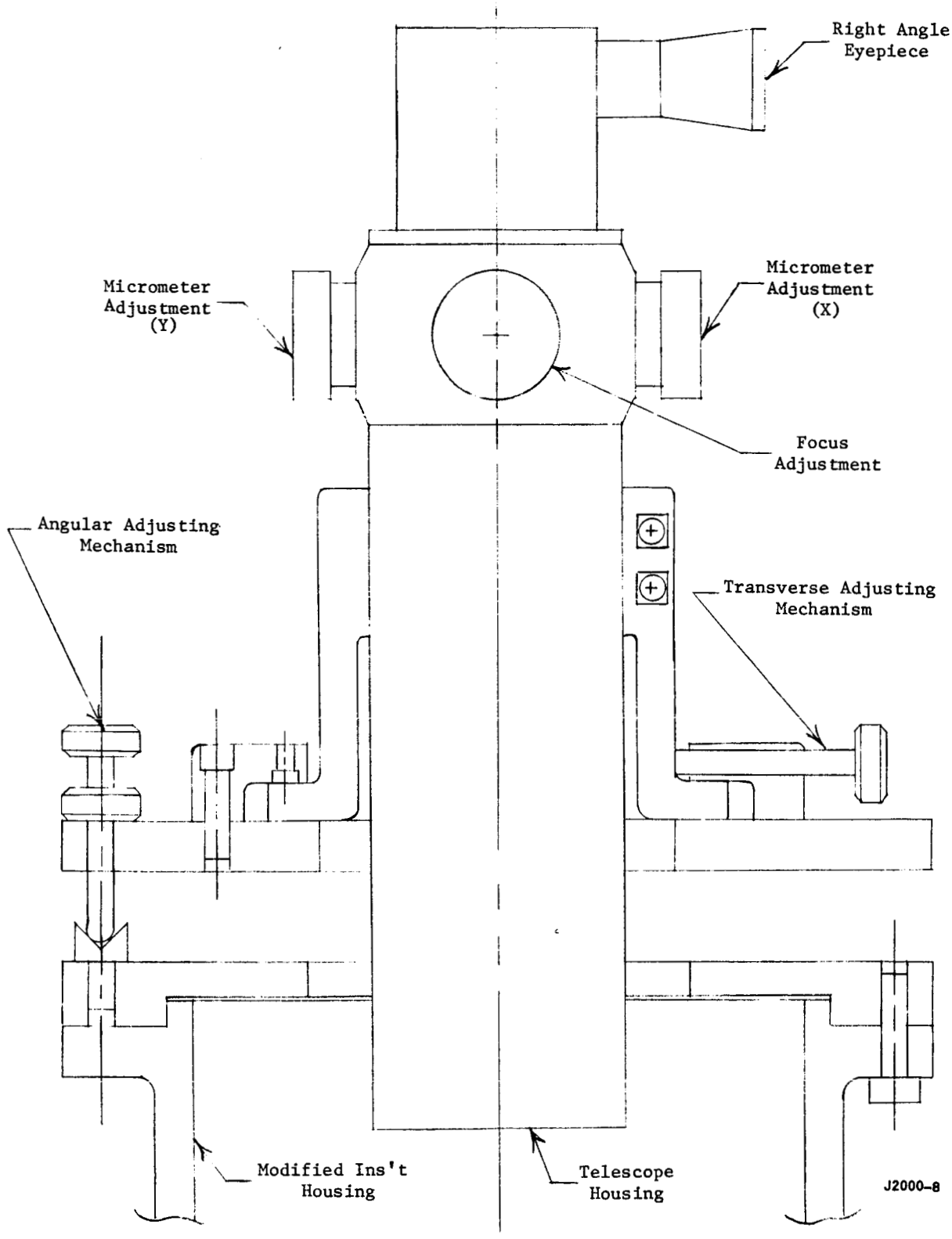

Figure 9. Telescope Mounting Assembly.

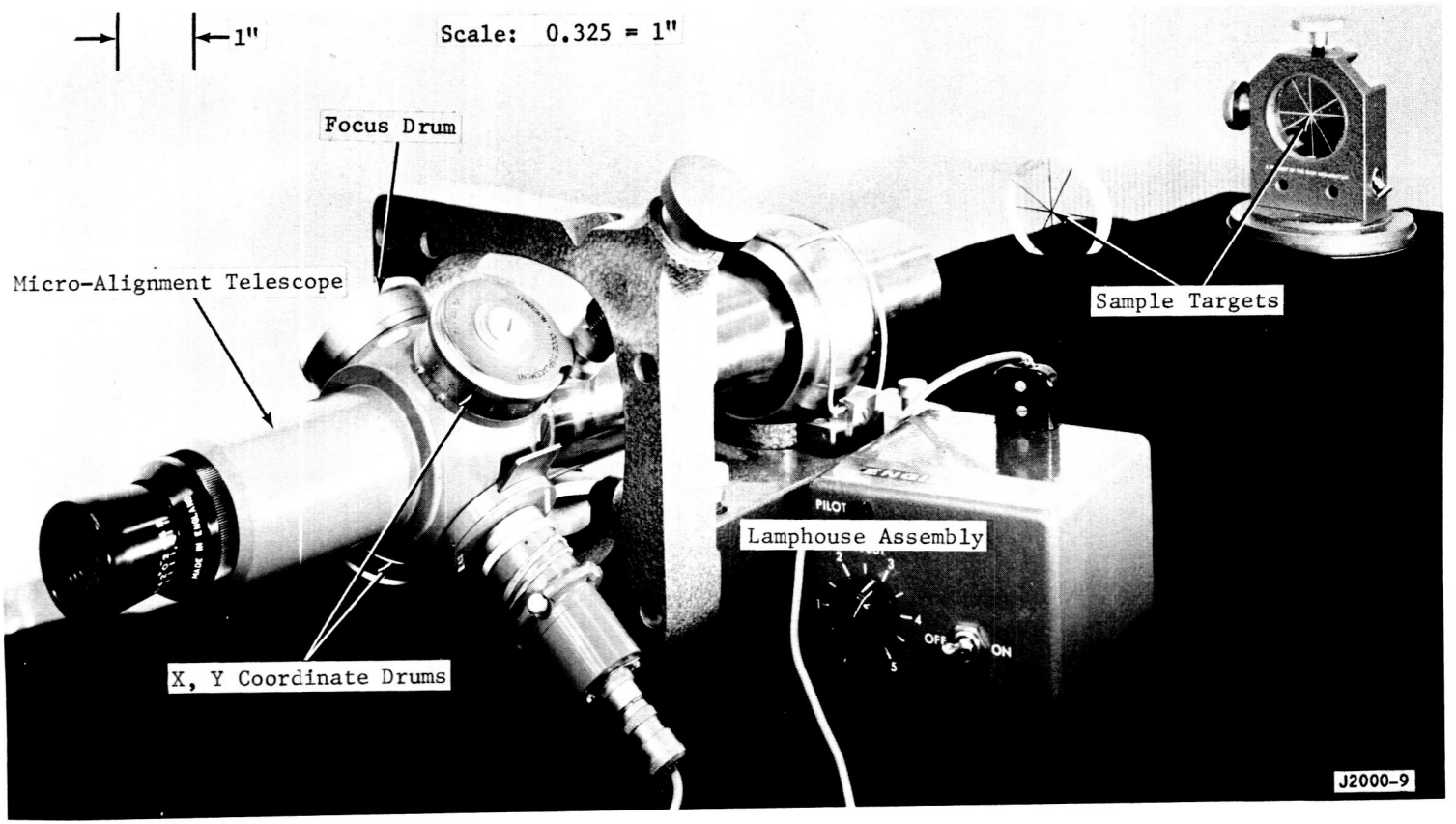

Figure 10. Demonstration of Optical Alignment Setup. (C66031451)

MODELS 901A Through 907A

QUARTZ LOAD WASHERS

Section I

DESCRIPTION

A. INTRODUCTION

Kistler Model 900A Series Load Washers are compact, fast-response transducers for measuring transient force phenomena and short term static loads in tension or compression. These piezoelectric force transducers have inherent rigidity equivalent to a stainless steel washer having the same over-all dimensions.

B. SPECIFICATIONS

Model Number	901A	902A	903A	904A	905A	906A	907A
Size (nominal) See Figure 1. . in.	1/4	3/8	1/2	5/8	3/4	1	1-1/2
Outer diameter (OD) . . . . . in.	0.55	0.87	1.10	1.34	1.58	2.05	2.96
Inner diameter (ID) . . . . . in.	0.26	0.41	0.51	0.67	0.83	1.04	1.60
Height (H) . . . . . in.	0.31	0.39	0.43	0.47	0.51	0.59	0.67
Weight (approximate) . . . . . oz	0.3	0.7	1.3	2	3	6	12
Range, F.S. compression . . lb	3500	8000	12 000	20 000	30 000	45 000	90 000
Sensitivity (nominal) . . . . . pCb/lb	20	20	20	10	10	10	10
Resolution . . . . . lb	.01	0.01	0.01	0.05	0.05	0.1	0.1
Overload capacity . . . . . %	10	10	10	10	10	10	10
Rigidity . . . . . 10^{-8} in./lb	15	6	4	2.5	1.5	1	.5
Capacitance (nominal) . . . . . pf	20	40	70	200	300	500	1000

Common Specifications, all models:

Resonant frequency (minimum)	50 000 cps
Linearity	1 percent
Insulation resistance (minimum)	10^{12} ohms
Temperature sensitivity	0.01 percent/°F
Temperature range	-400 to +500°F
Shock and vibration	10 000 g(s)

J2000-10

Figure 11. Kistler Force Buttons - Model #902A.

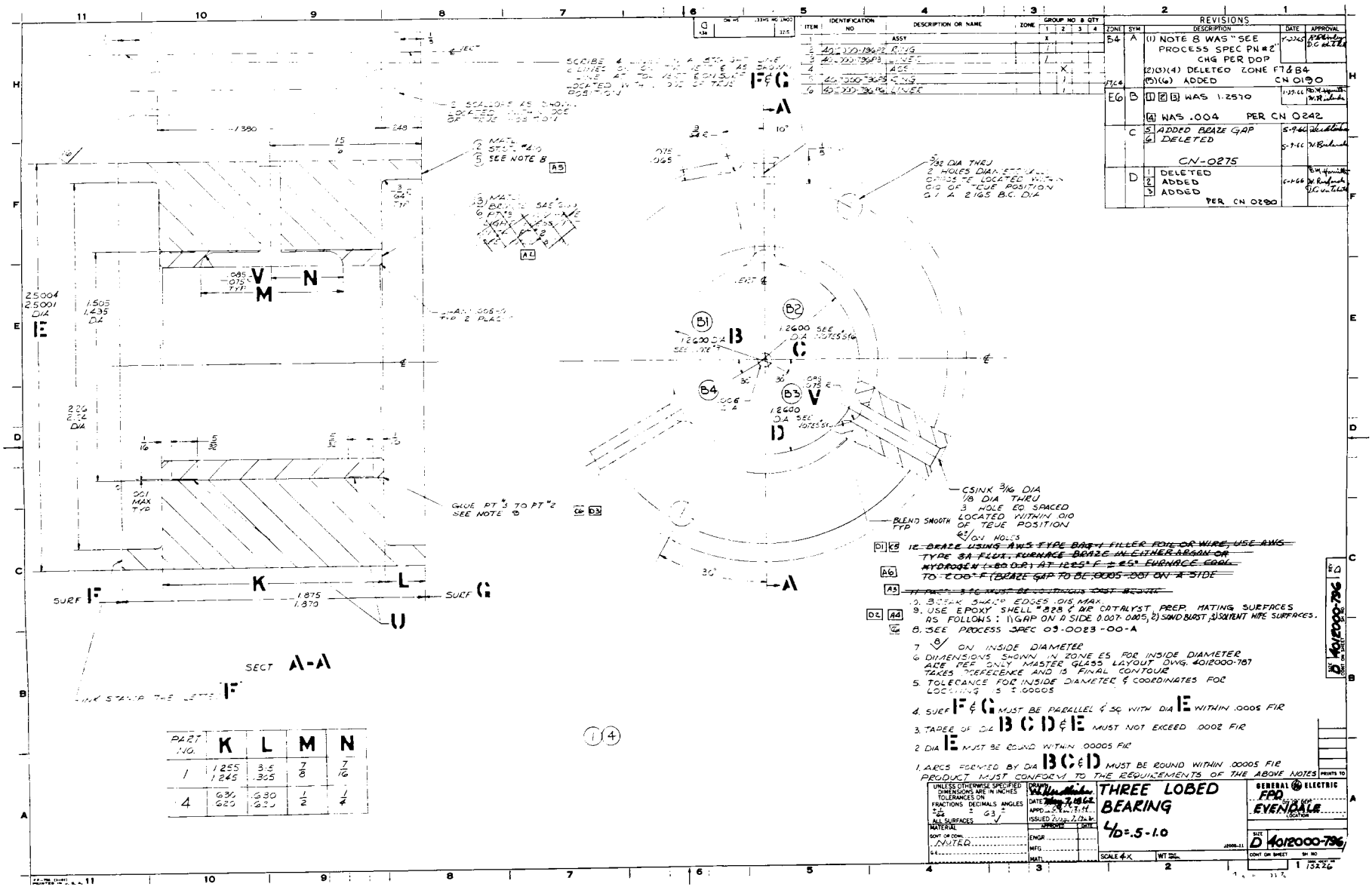

Figure 12. Three-Lobed Bearing (4012000-796 Rev. D)

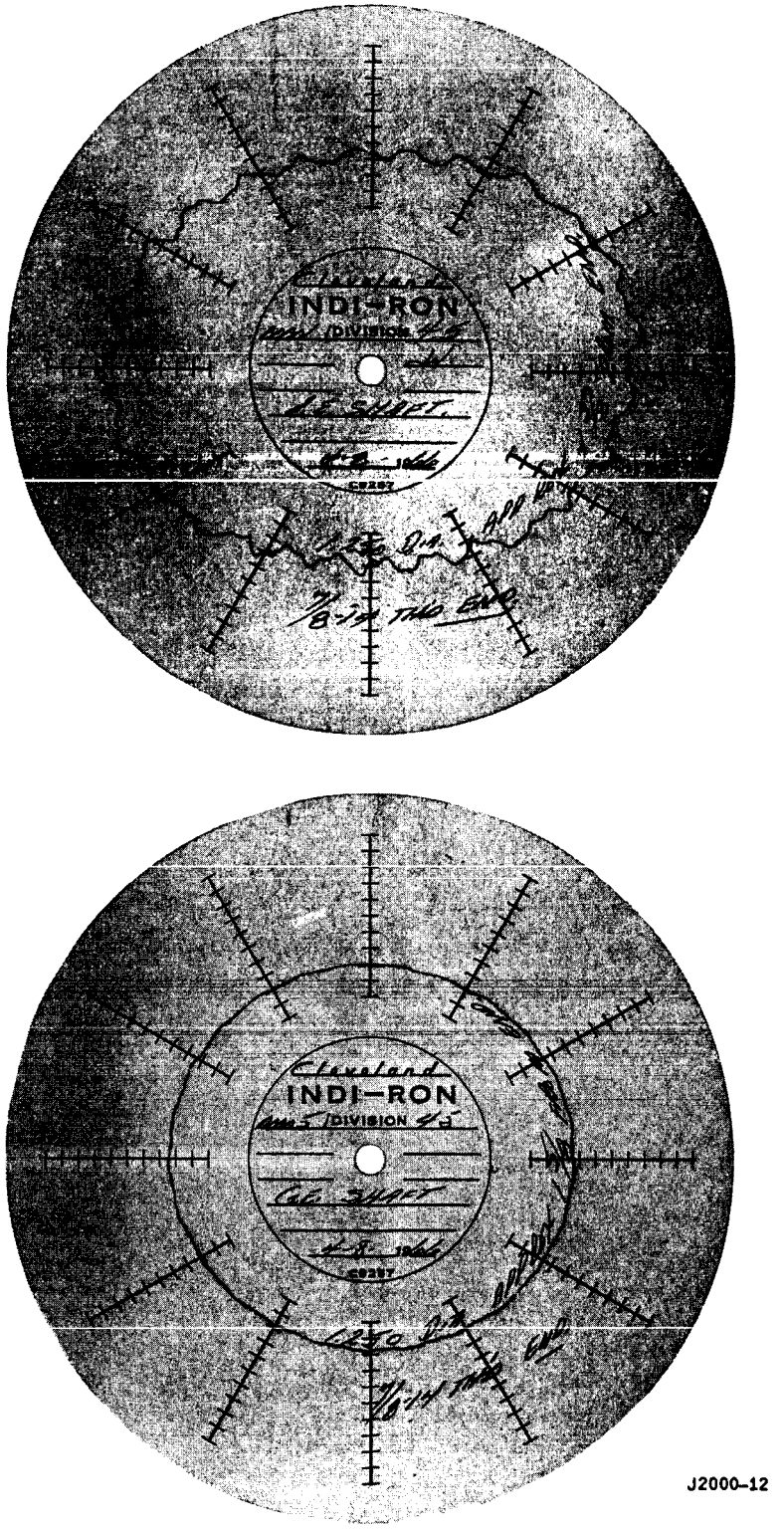

Figure 13. Indi-Ron Traces of Shaft Diameters.

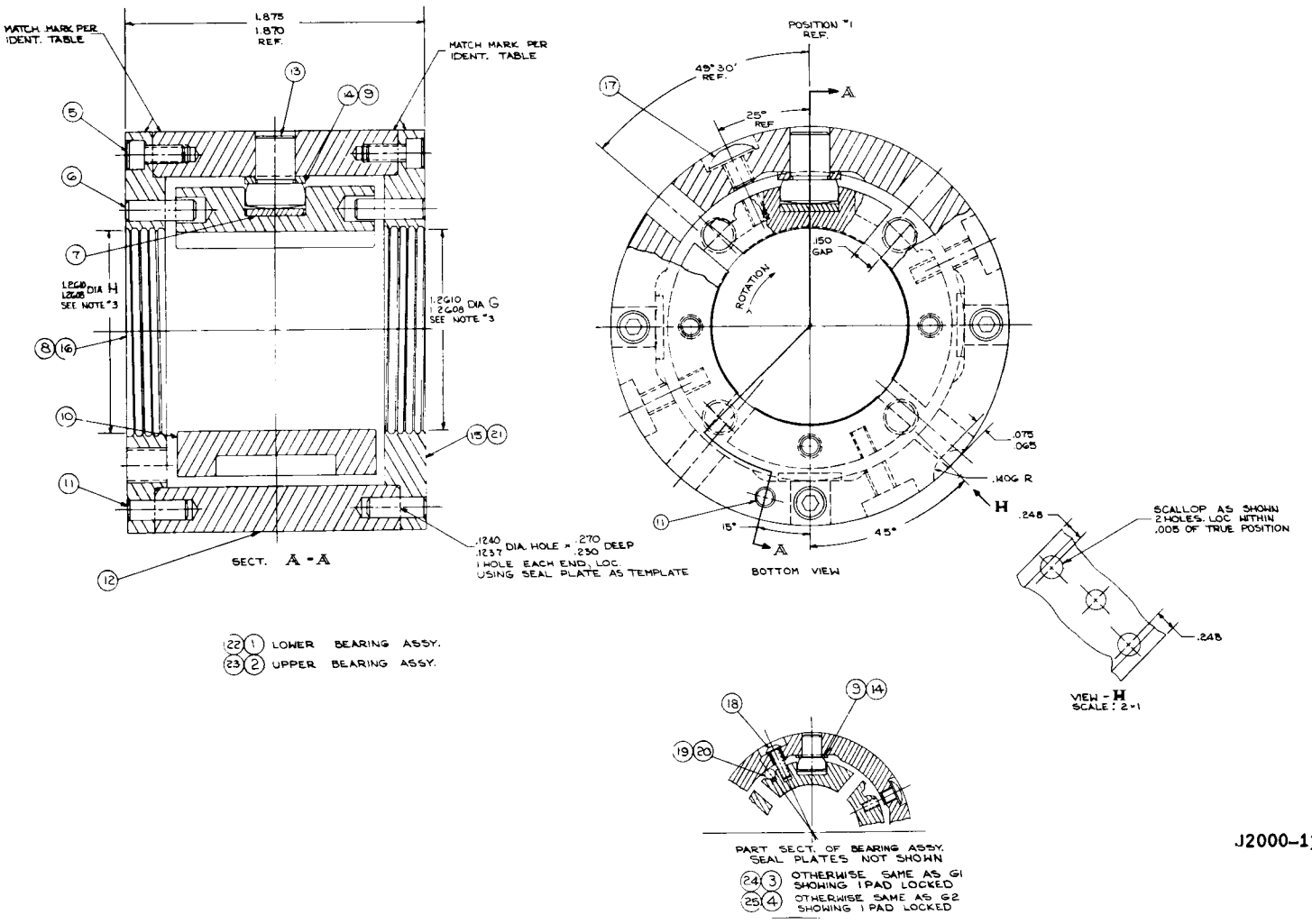

ITEM	IDENTIFICATION NO.	DESCRIPTION OR NAME	ZONE	GROUP NO. & QTY 1	2	3	4	5	6	7	8
1	2GSE838	ASSY		1							
2		ASSY			X						
3		ASSY				X					
4		ASSY					X				
(A) 5	COML	SCREW - "4-40NC - "1/4 LG	G13	8	8	8	8	8	8	8	8
6	1428 1403-P2	PIN - DOWEL	G13	8	8	8	8	8	8	8	8
7	1428 1406	DISC - CONTACT	G12	4	4	4	4	4	4	4	4
8	941D 1032 P1	PLATE - SEAL	E13		1		1		1		1
9	1428 1998-P2	WASHER	C8					4	4	4	4
10	941D 114	PAD - BEARING	E13	4	4	4	4	4	4	4	4
11	1425 1403-P2	PIN - DOWEL	E13	2	2	2	2	2	2	2	2
12	941D 886-P1	RING - RETAINER	D12	1	1	1	1	1	1	1	1
13	1425 1956	PIN - PIVOT	G12	4	4	4	4	4	4	4	4
14	142 B 1932M	WASHER	G12	4	4	4	4				
15	941D103 P1	PLATE - SEAL	E11	1			1		1		1
16	941D102P2	PLATE - SEAL					1				1
(A) 17	COML	SCREW - "8-32NC - 3/16 LG.	C8	8	8	8	8	8	8	8	8
(A) 18	COML	SCREW - "4-40NC - 3/16 LG.	C8				2	2			2
(B) 19	A1-12	PIN - ROLL	C8				1	1			
20	1428 1409	PIN - ROLL	C8							1	1
21	941D103P2	PLATE - SEAL			1		1			1	1
22	2GSE838	ASSY.						X			
23									X		
24										X	
25											X

Figure 14. Self-Aligning Pivoted-Pad Bearing.

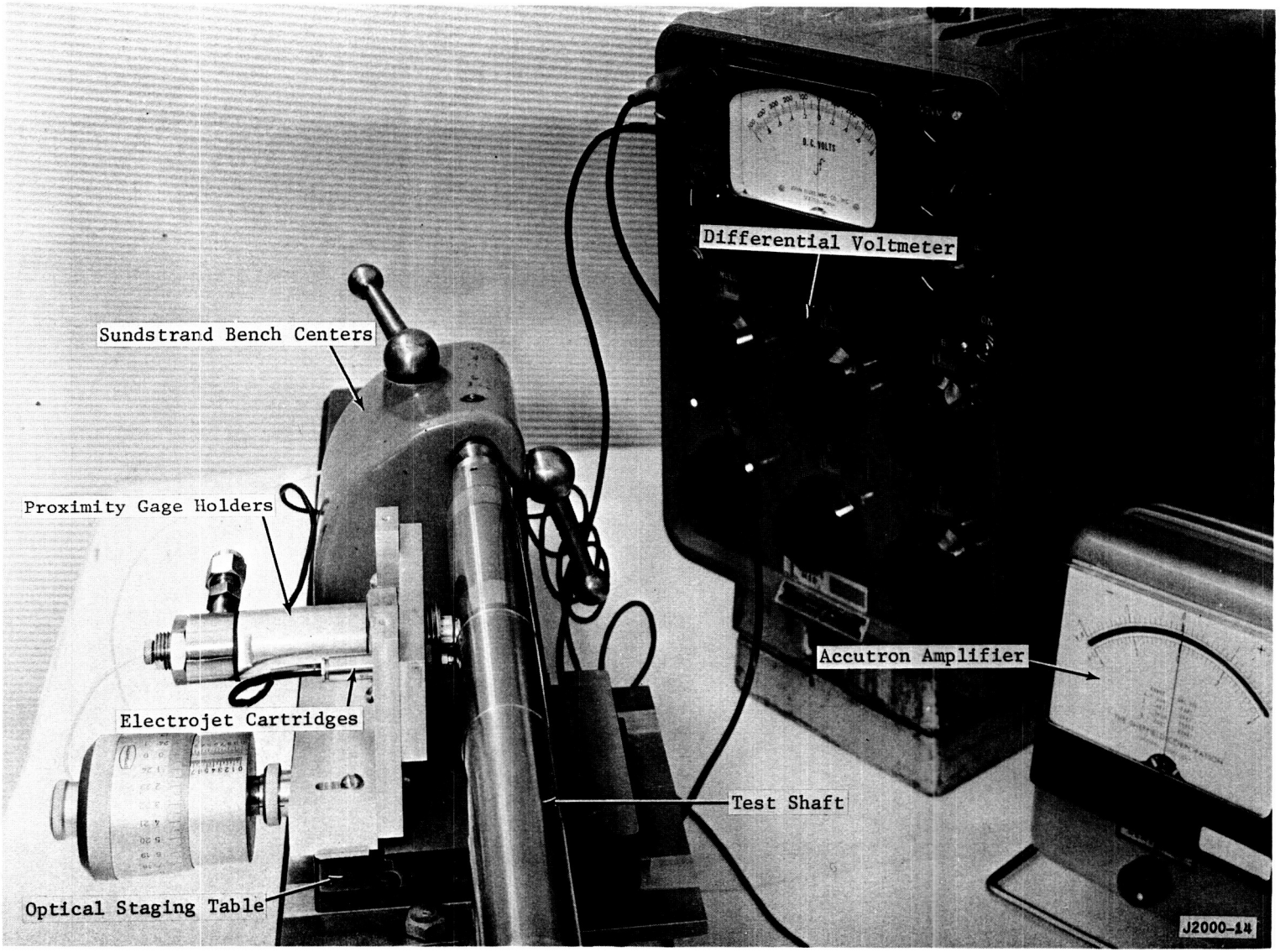

Figure 15. Bently Probe to Electrojet Cartridge Calibration Setup. (C66041412)

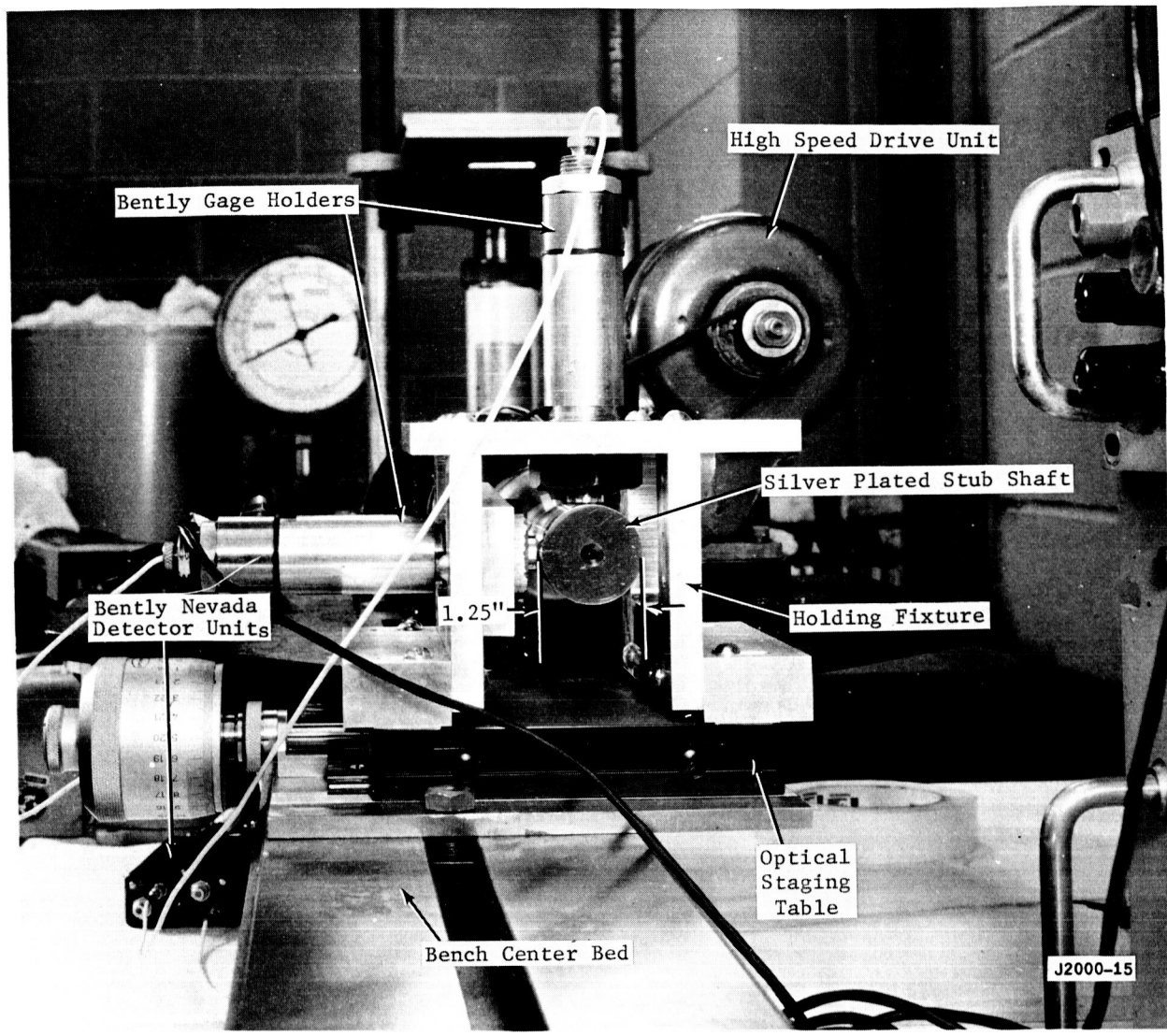

Figure 16. Phase Angle Test Setup. (C66042709)

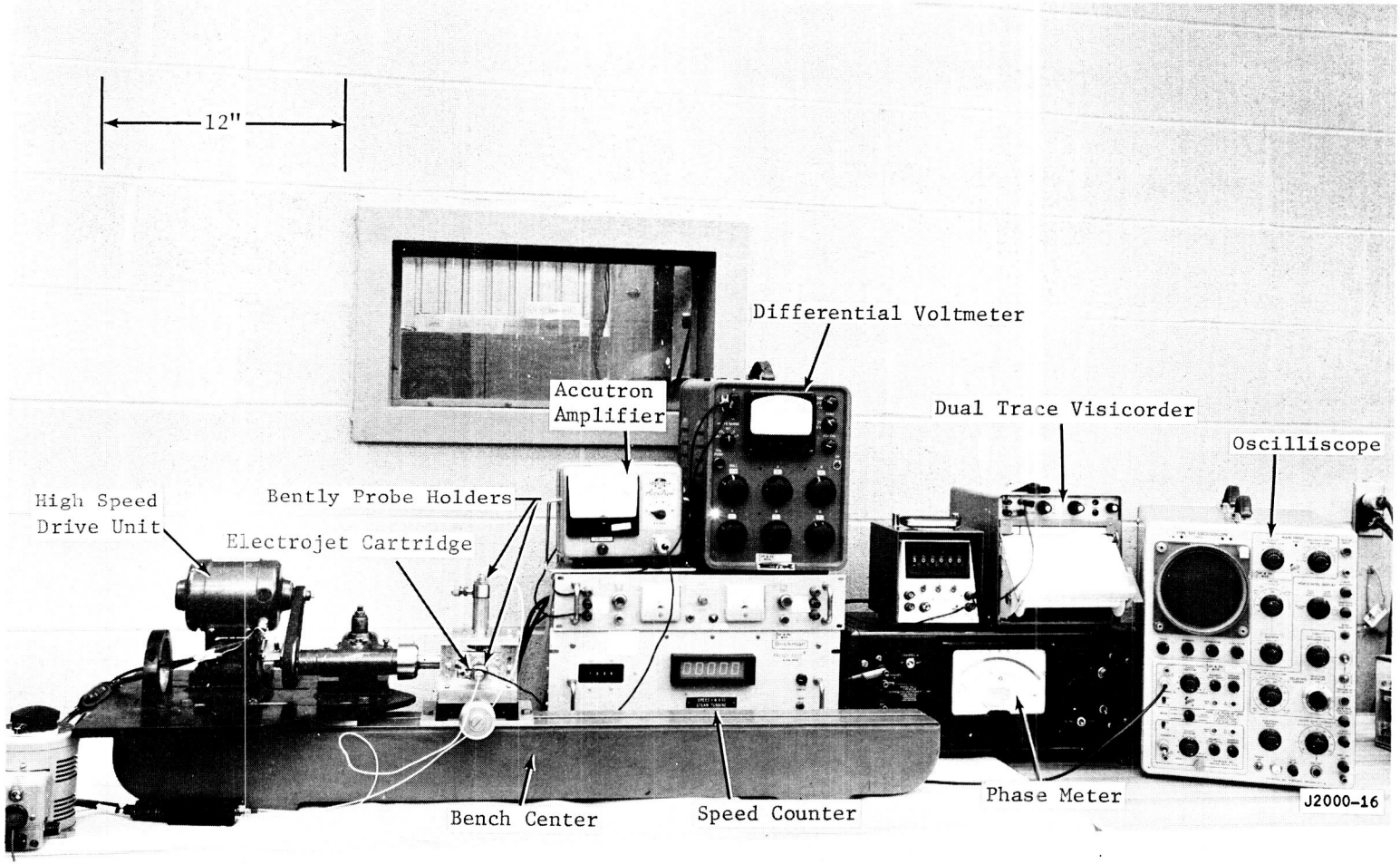

Figure 17. Phase Angle Test Setup. (C66042710)

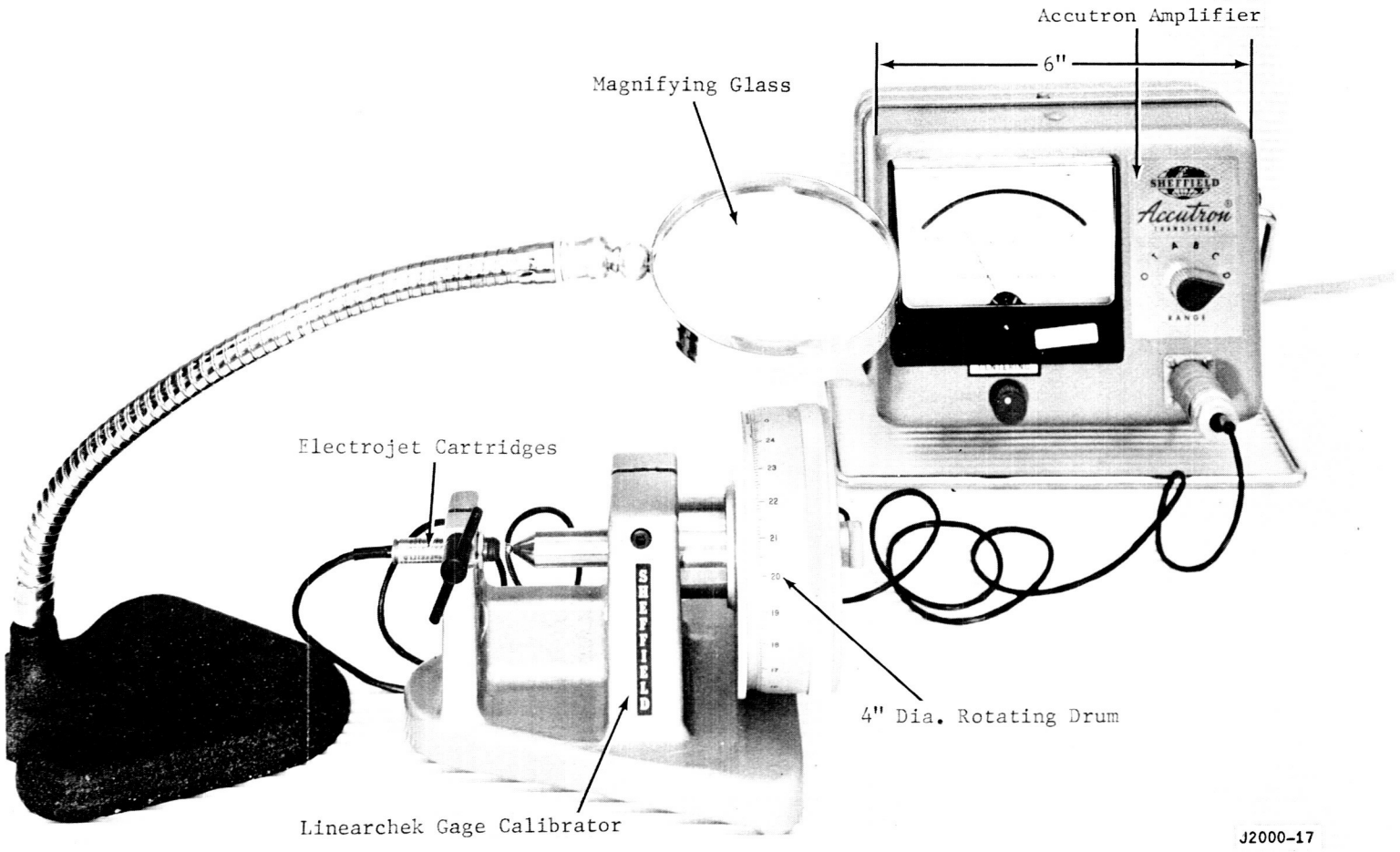

Figure 18. Electrojet Cartridge Calibration Setup. (C66041411)

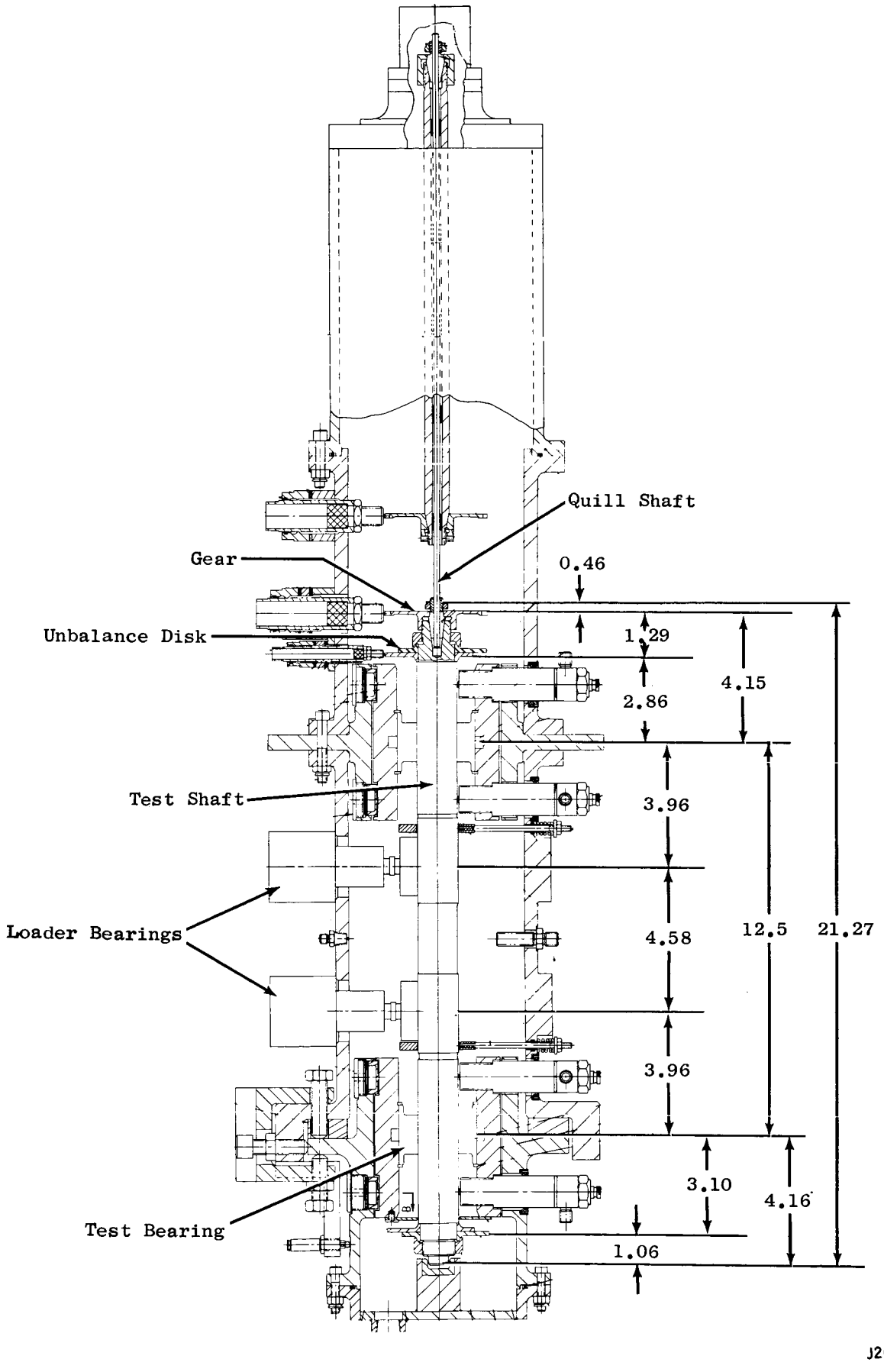

Figure 19. Hydrodynamic Journal Bearing Test Assembly.

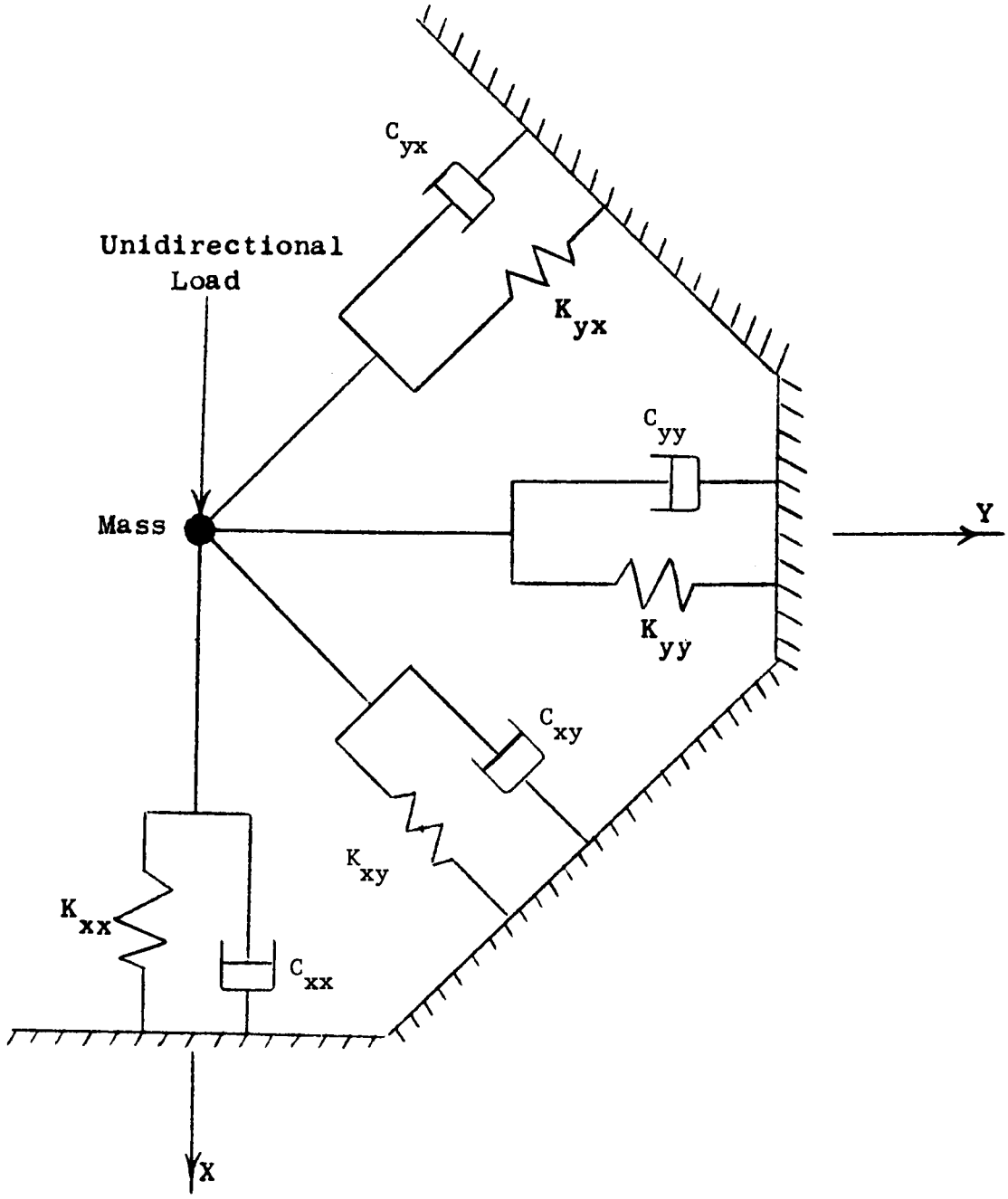

$$-F_x = K_{xx} X + C_{xx} \dot{X} + K_{xy} Y + C_{xy} \dot{Y}$$

$$-F_y = K_{yx} X + C_{xy} \dot{X} + K_{yy} Y + C_{yy} \dot{Y}$$

J2000-19

Figure 20. Schematic Representation of Dynamic Characteristics of Bearing.

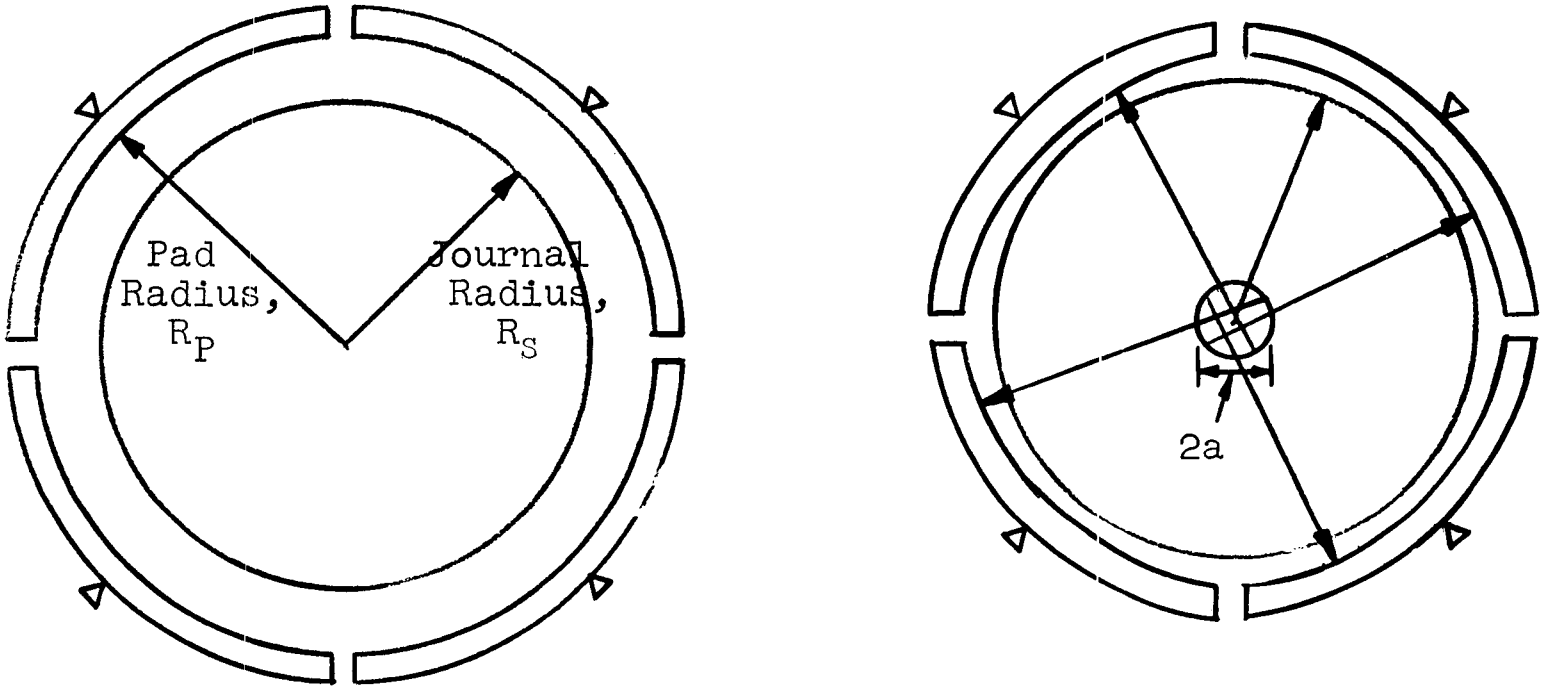

(a) No Preload

(b) Preload

$$\left(\text{Preload Coefficient} = \frac{a}{R_P - R_S}\right) \qquad \text{J2000-20}$$

Figure 21. Geometrical Arrangement of Four-Pad Bearing.

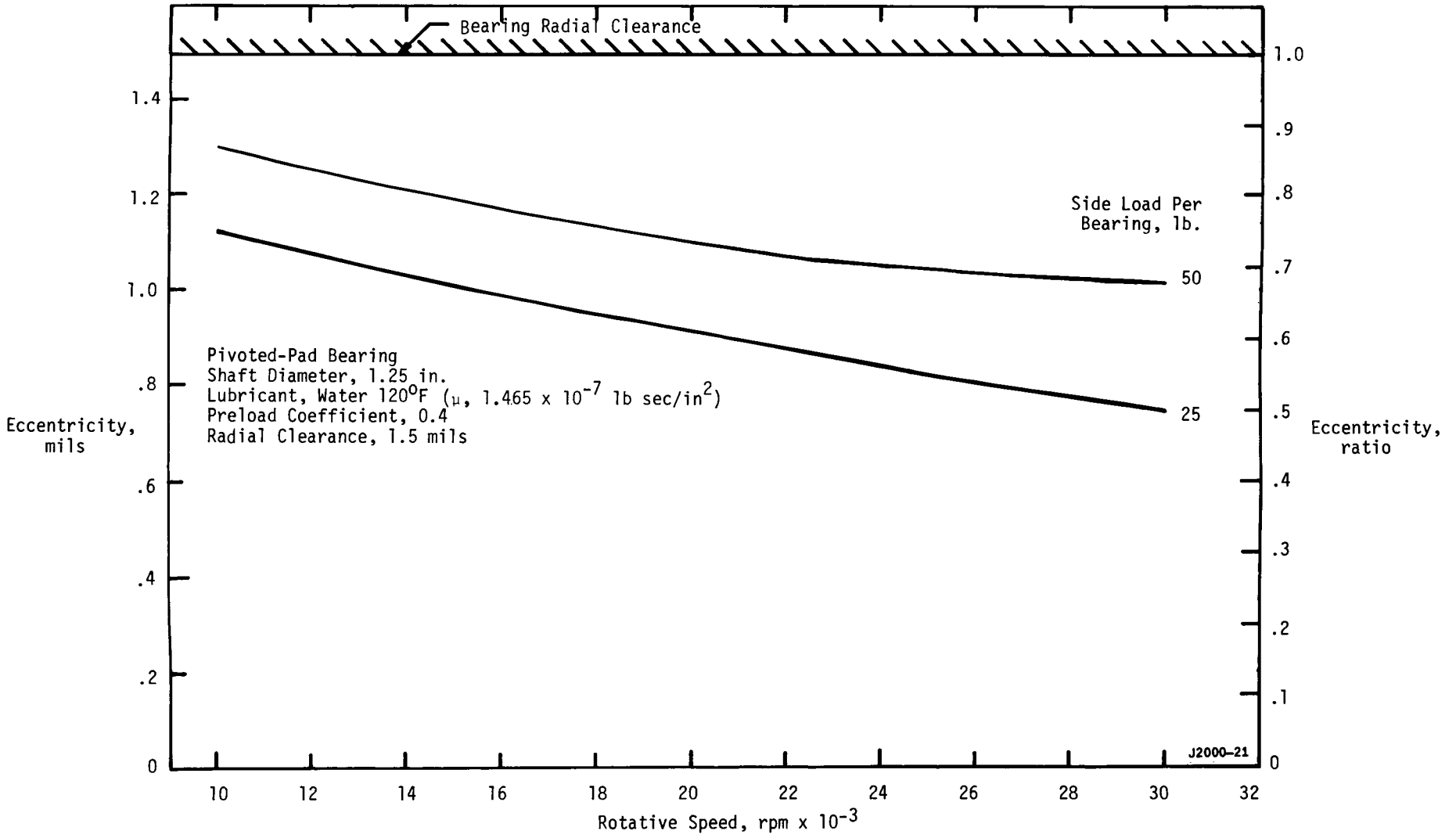

Figure 22. Shaft Eccentricity Due to Applied Unidirectional Force Versus Rotative Speed.

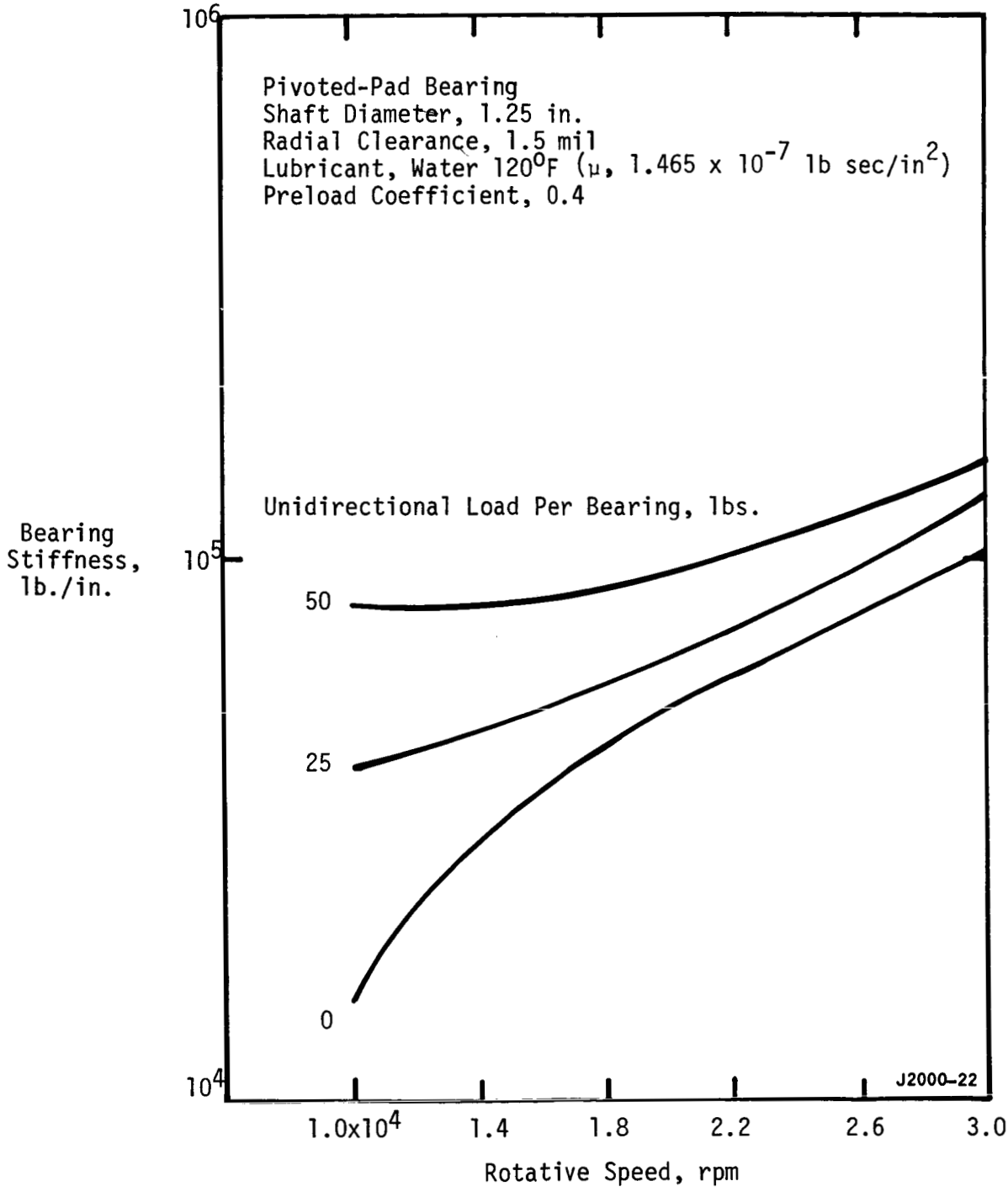

Figure 23. Variation of Bearing Stiffness with Speed and Side Load.

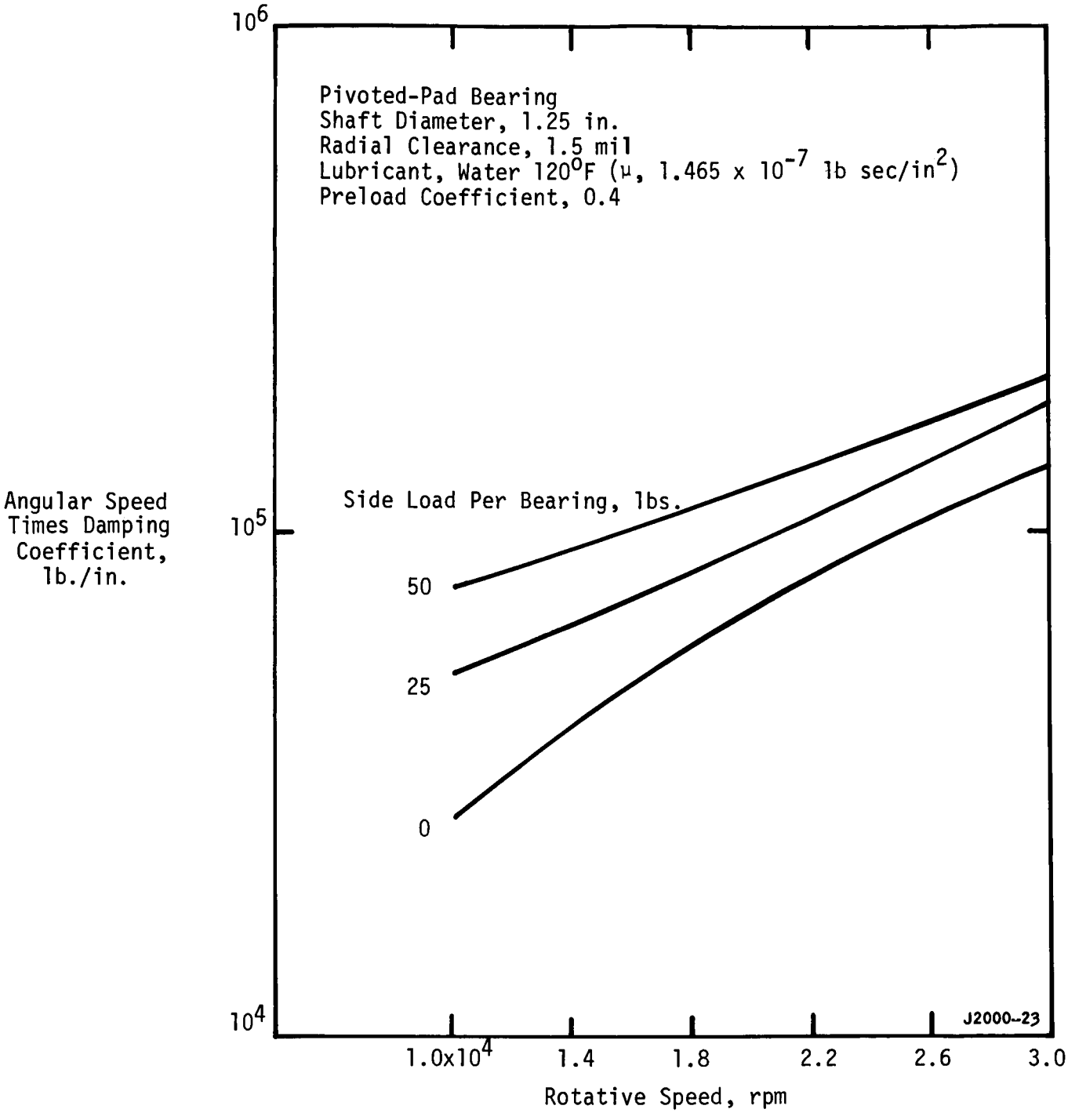

Figure 24. Variation of Bearing Damping Coefficient with Speed and Side Load.

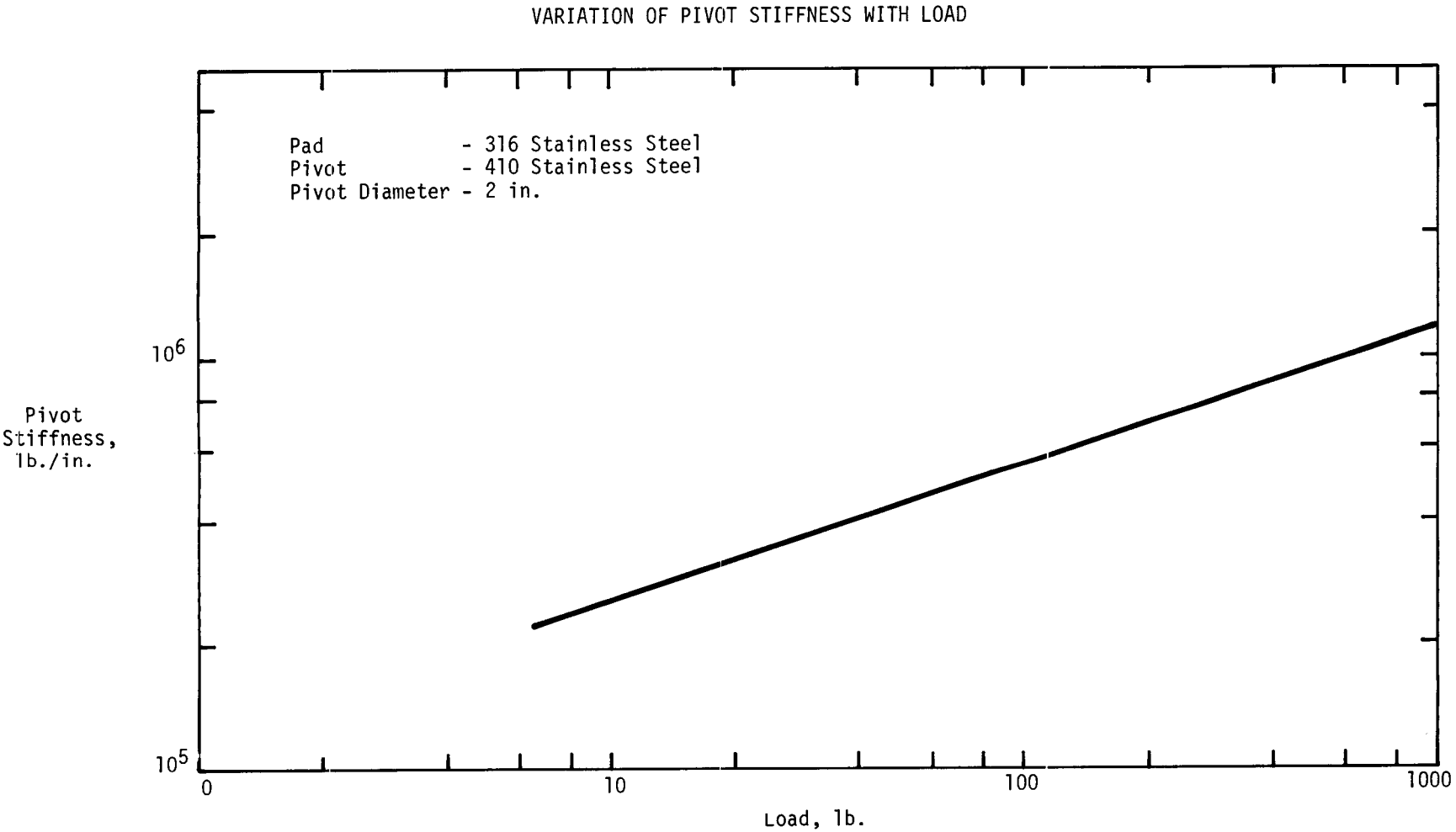

Figure 25. Variation of Pivot Stiffness with Load.

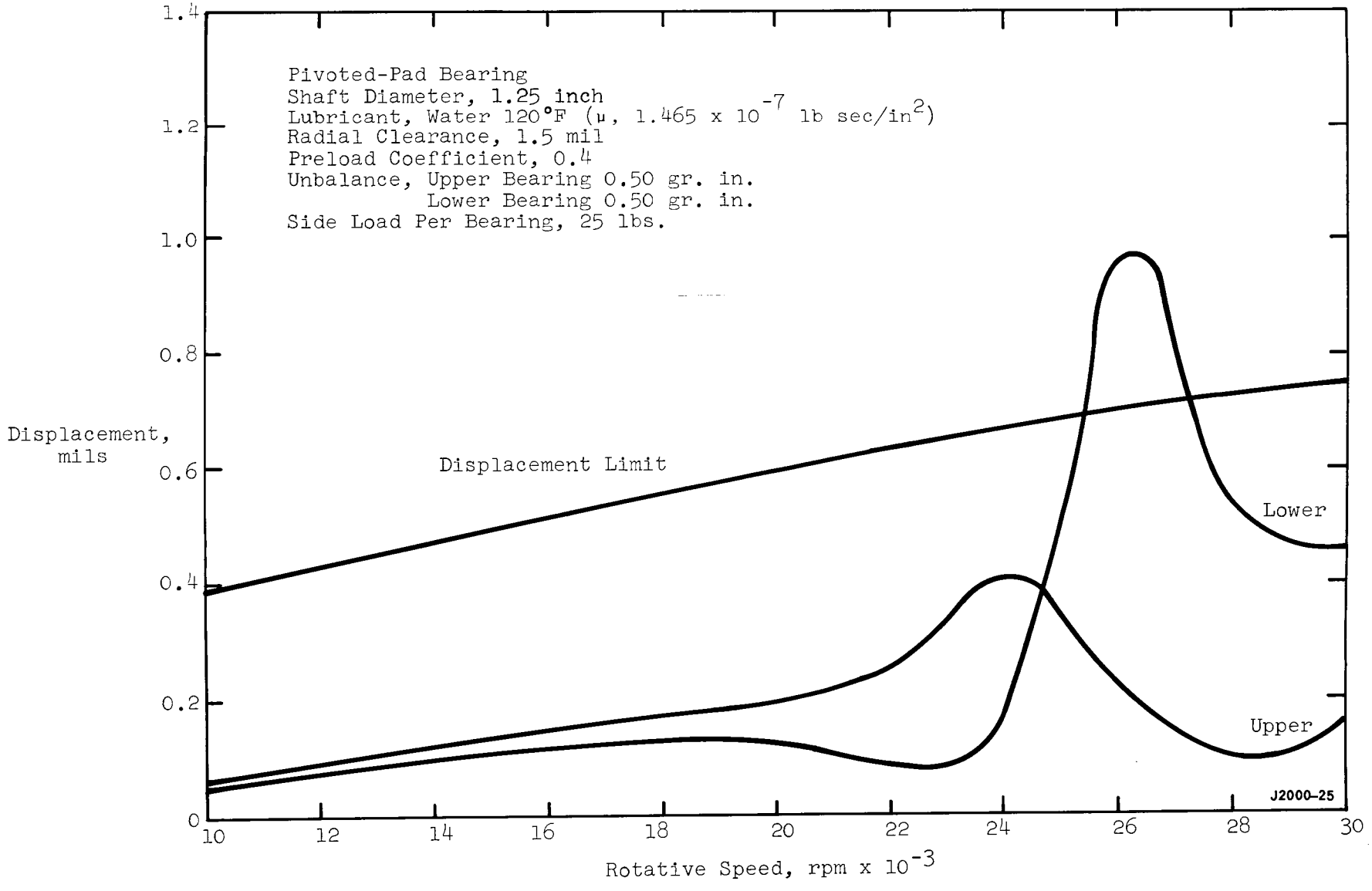

Figure 26. Shaft Displacement from Equilibrium Position Versus Rotative Speed.

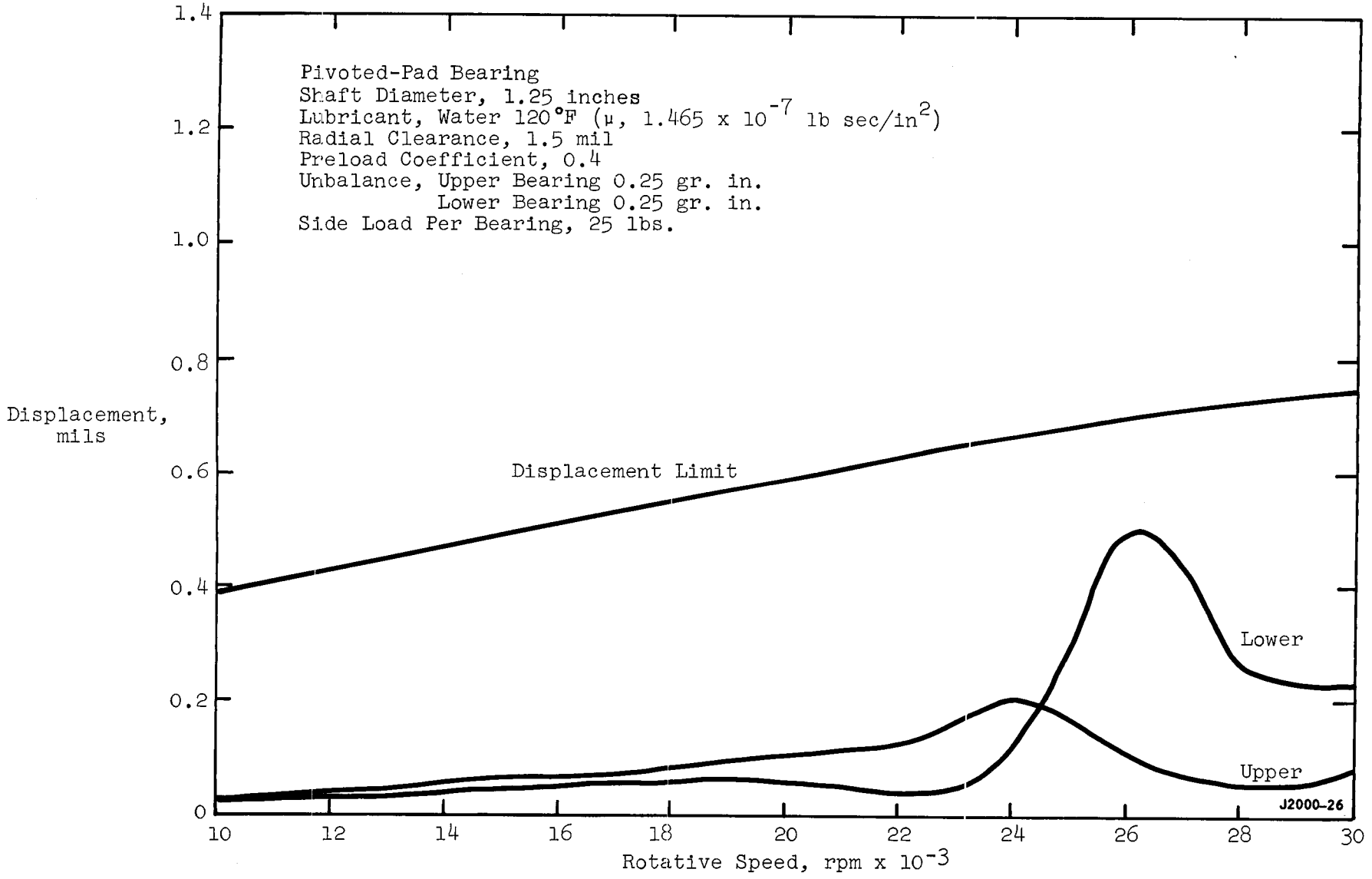

Figure 27. Shaft Displacement from Equilibrium Position Versus Rotative Speed.

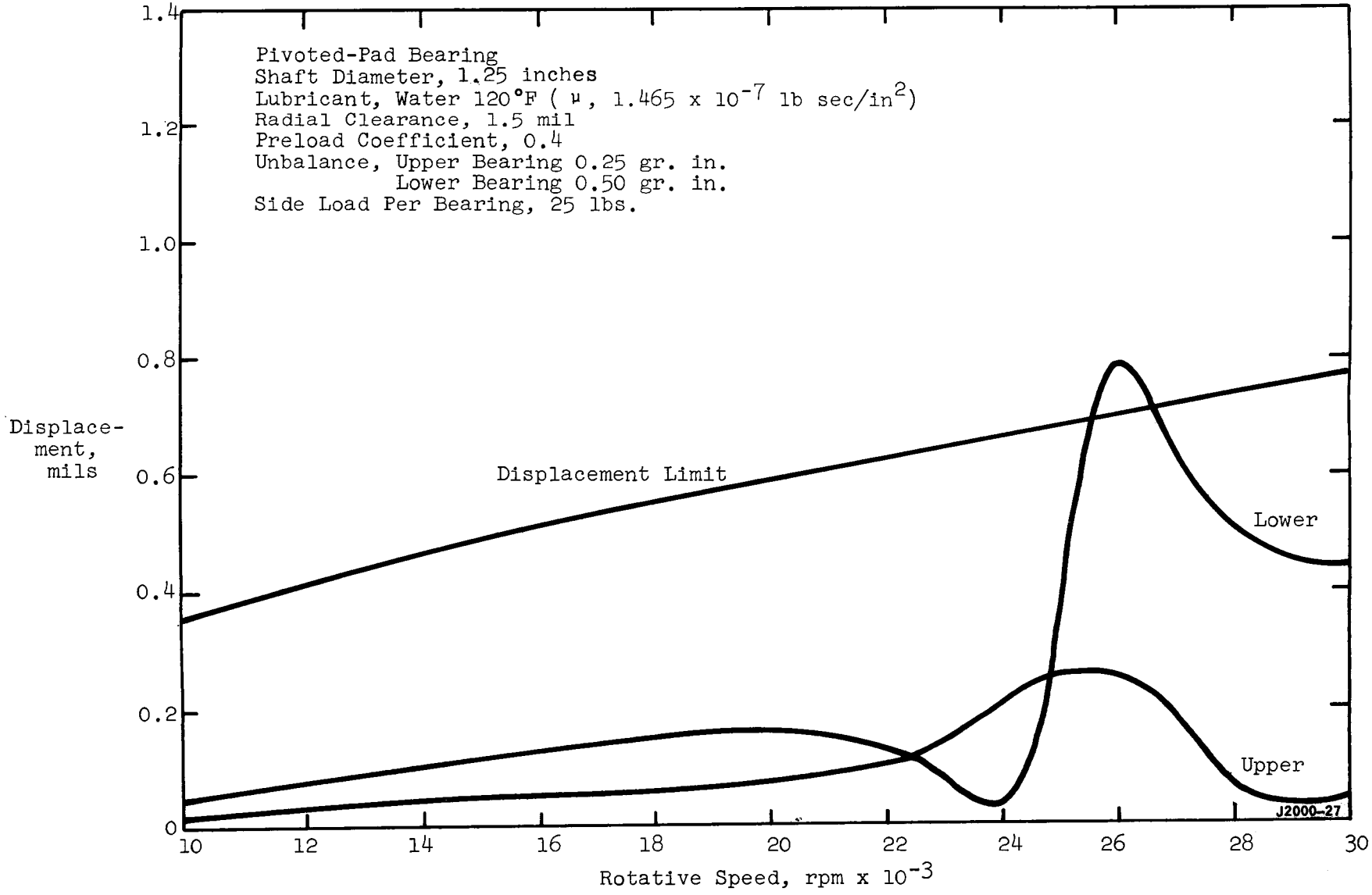

Figure 28. Shaft Displacement from Equilibrium Position Versus Rotative Speed.

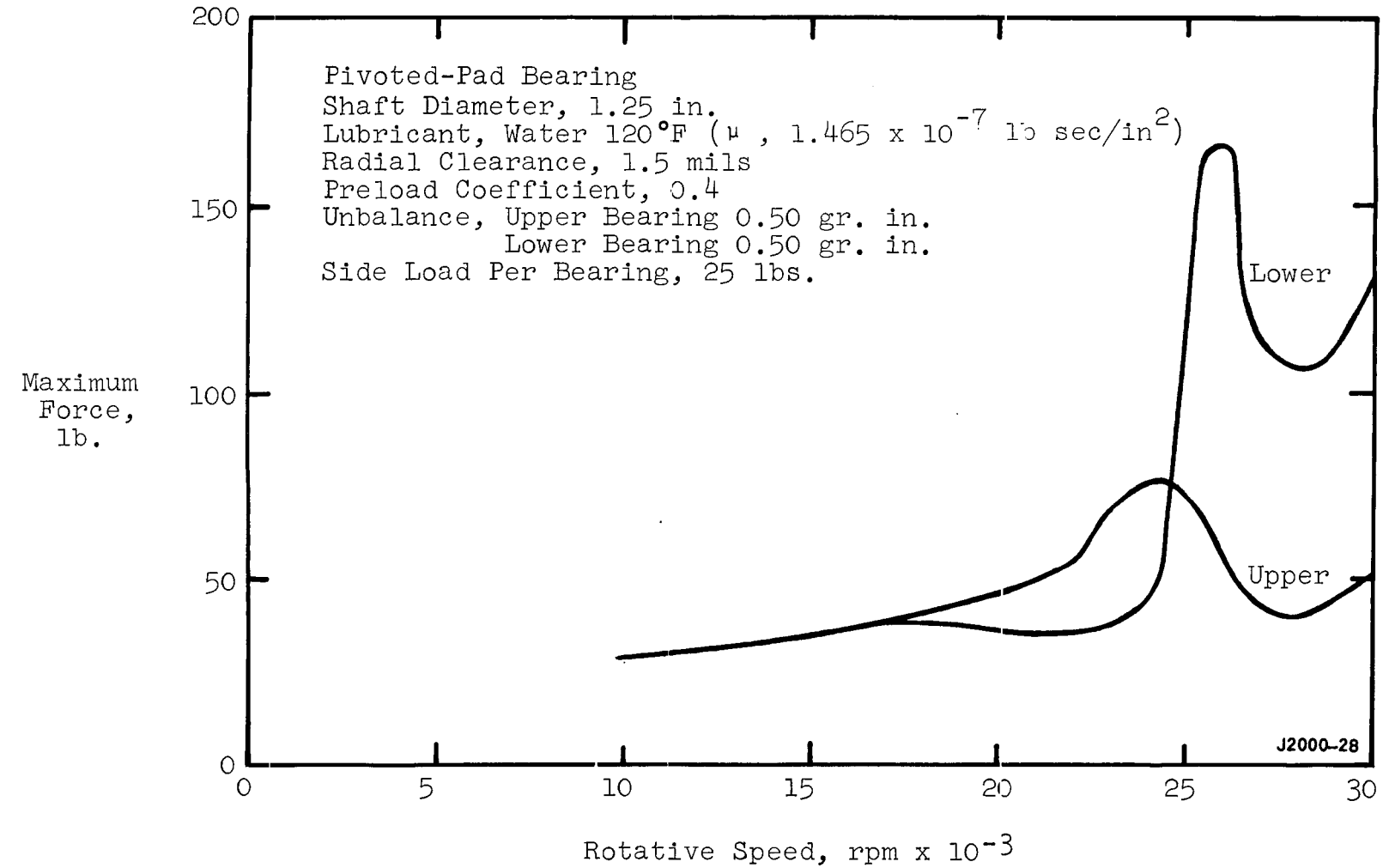

Figure 29. Total Maximum Force on Bearings Versus Rotative Speed.

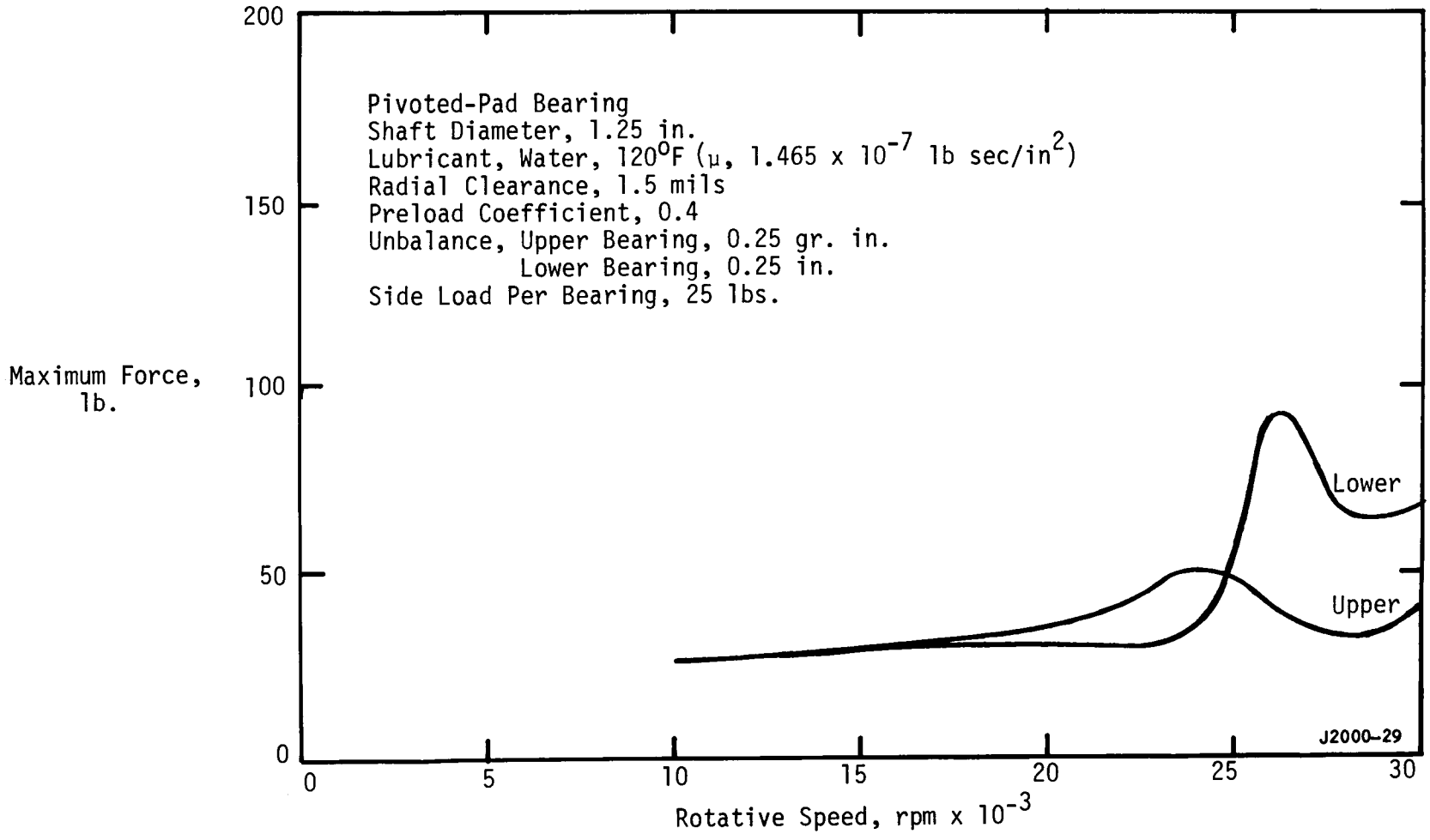

Figure 30. Total Maximum Force on Bearings Versus Rotative Speed.

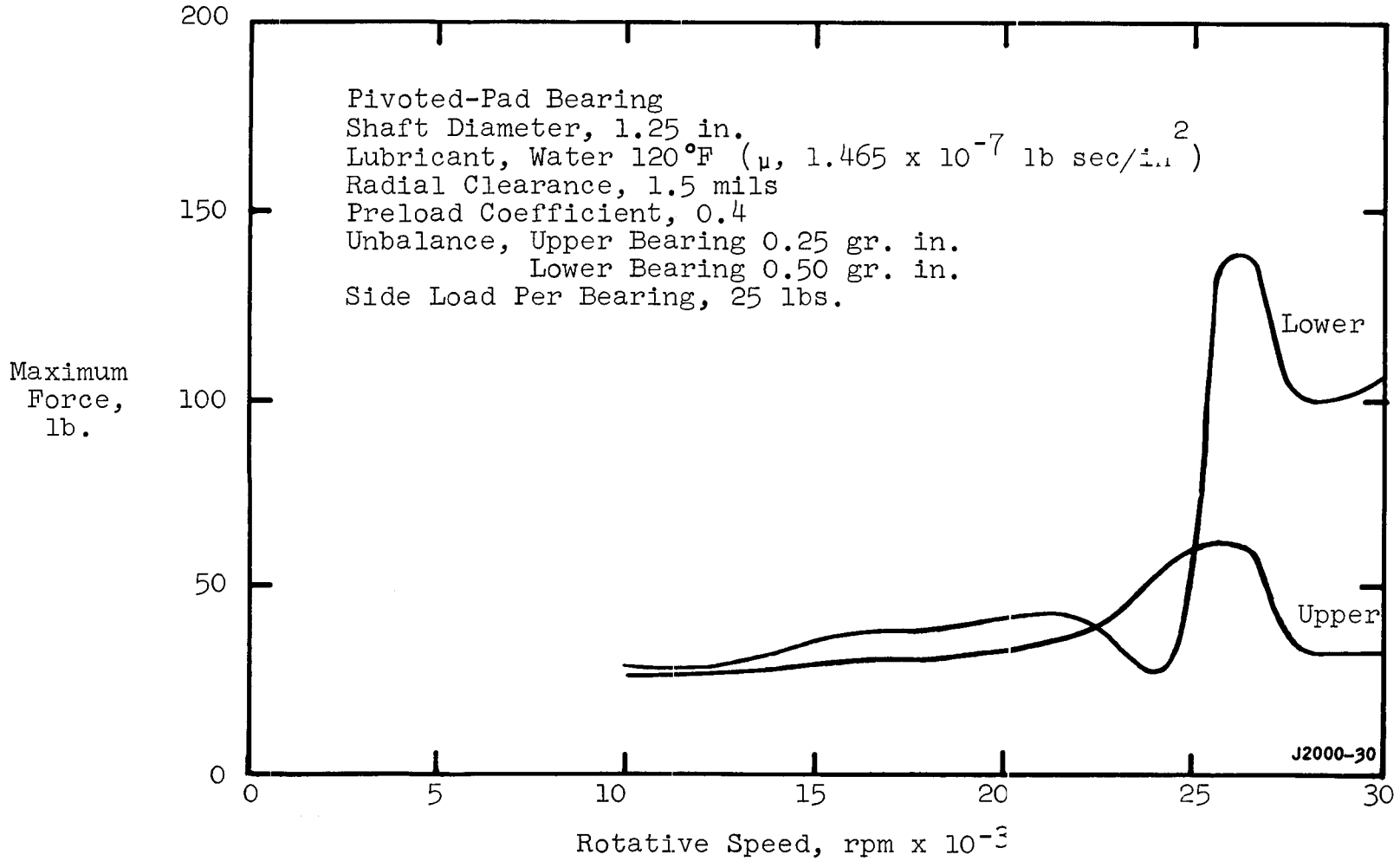

Figure 31. Total Maximum Force on Bearings Versus Rotative Speed.

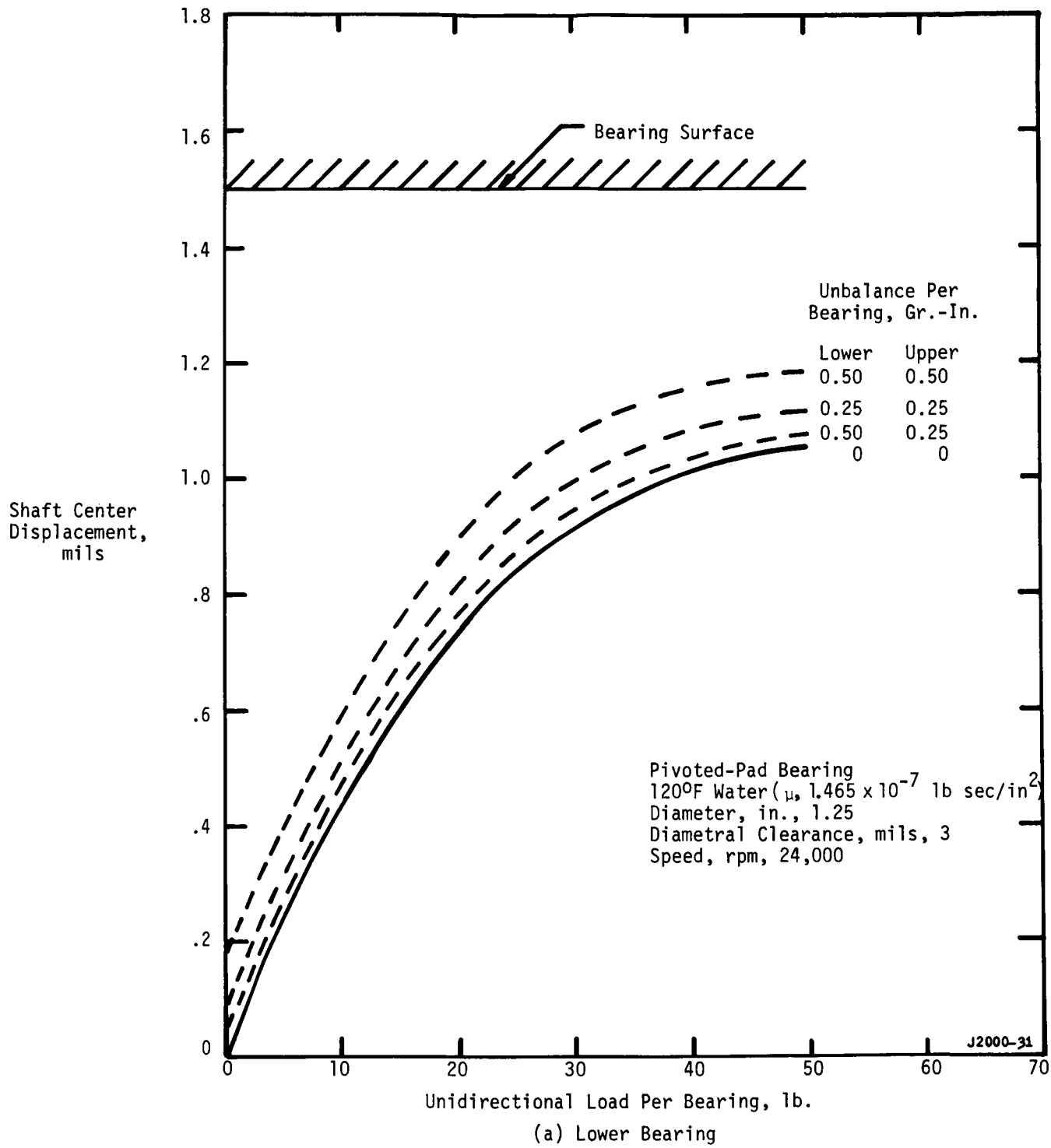

Figure 32. Variation of Shaft Center Displacement with Side Load and Unbalance.

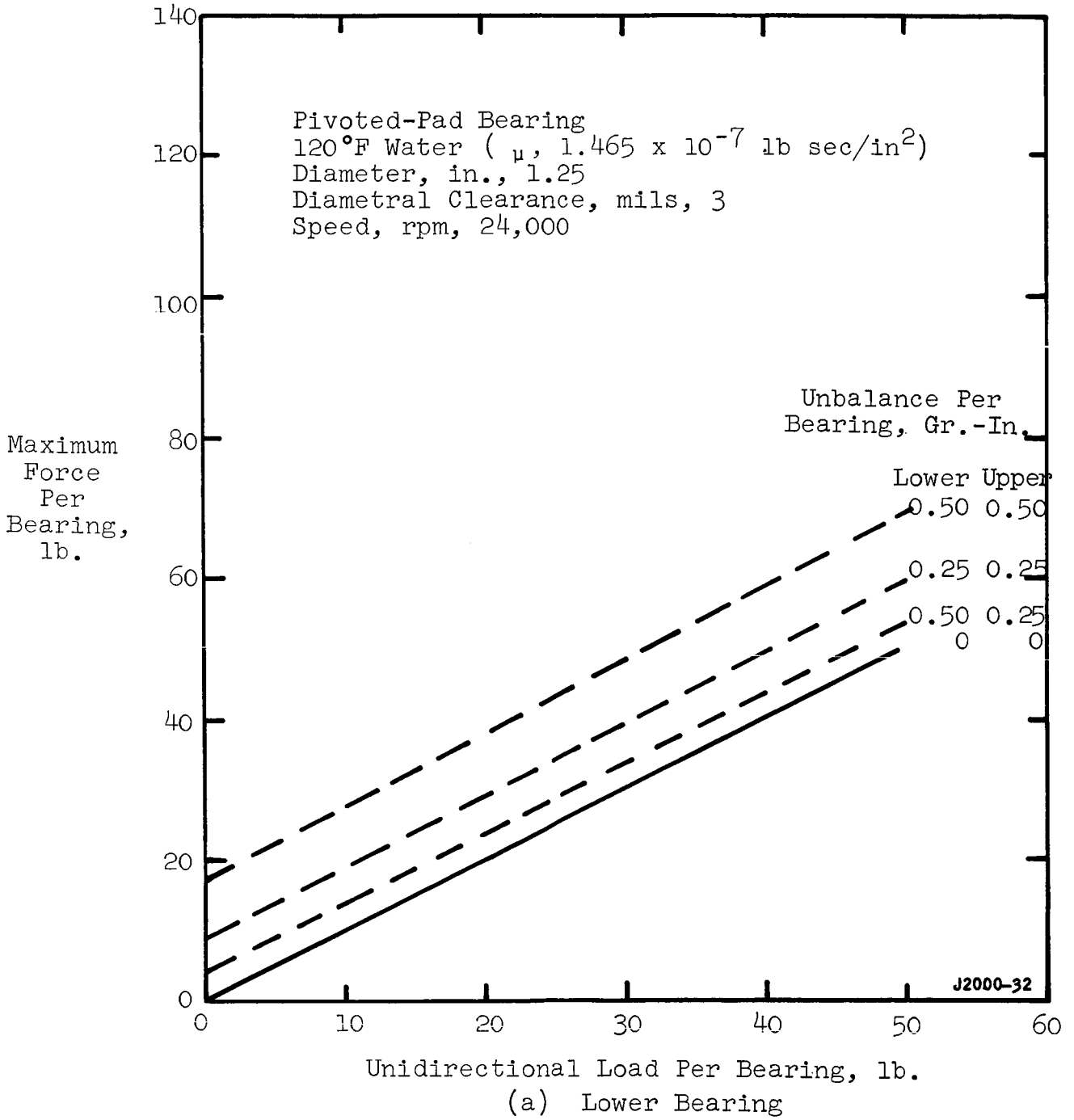

Figure 33. Variation of Maximum Bearing Force with Side Load and Unbalance.

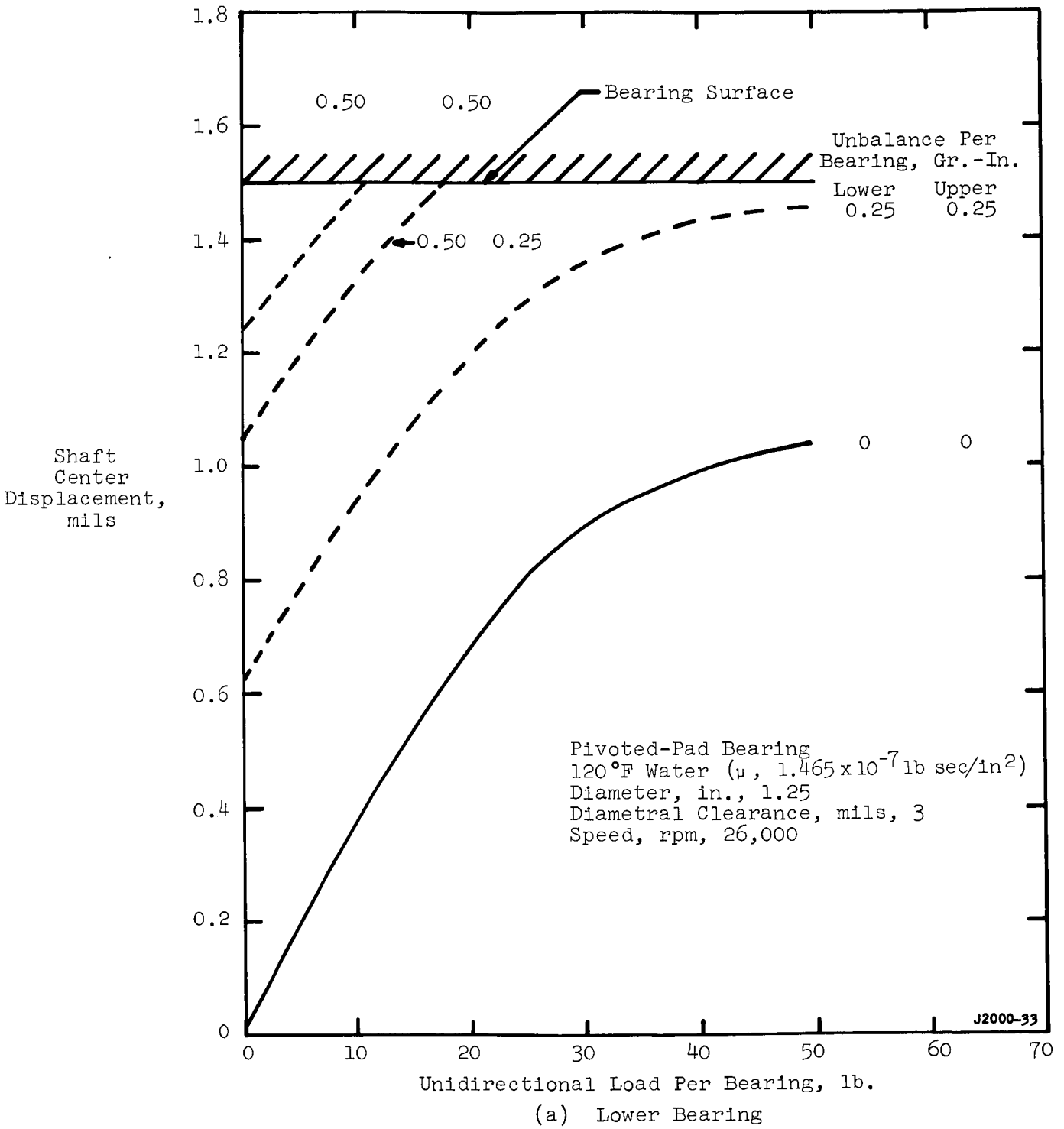

Figure 34. Variation of Shaft Center Displacement with Side Load and Unbalance.

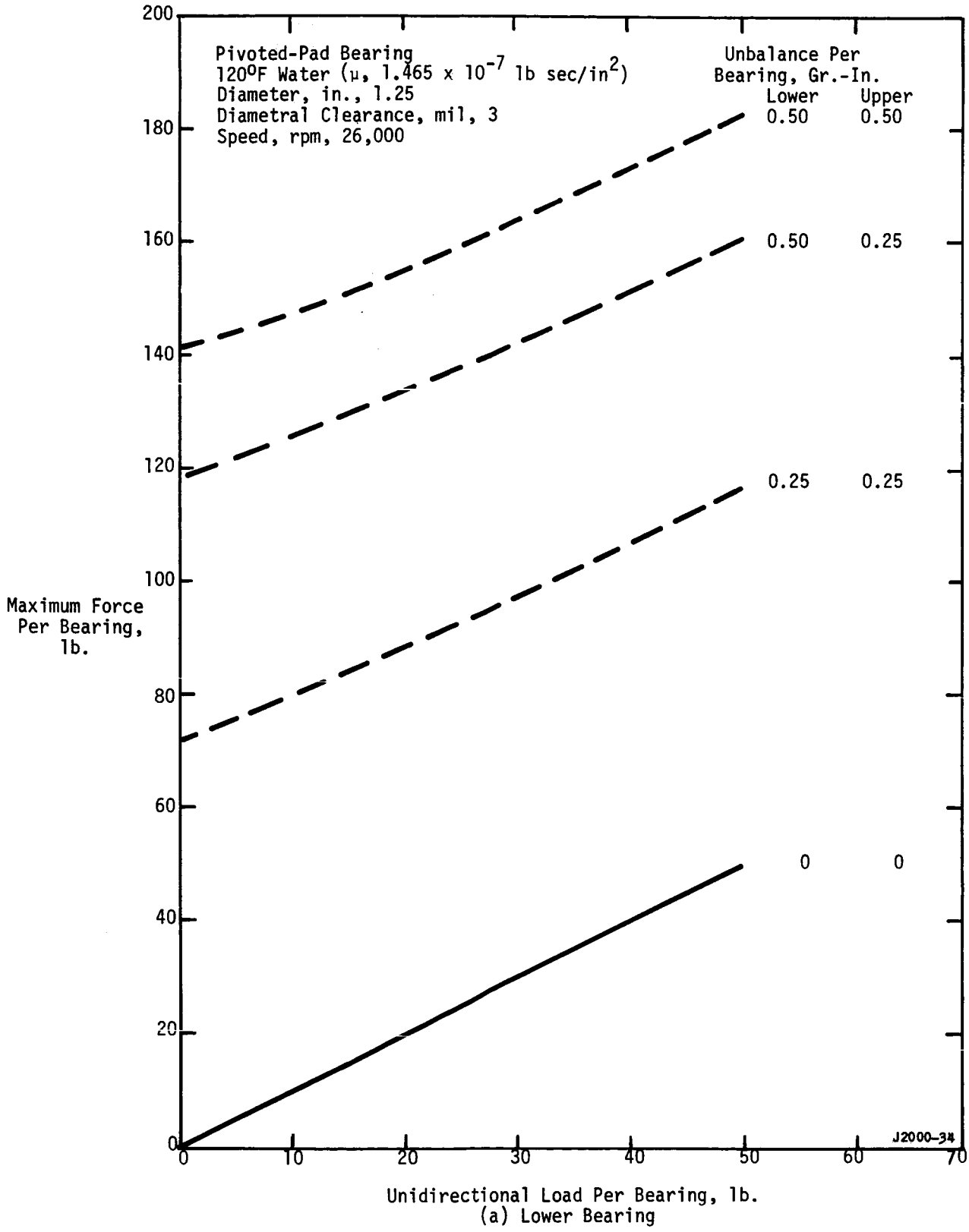

Figure 35. Variation of Maximum Bearing Force with Side Load and Unbalance.

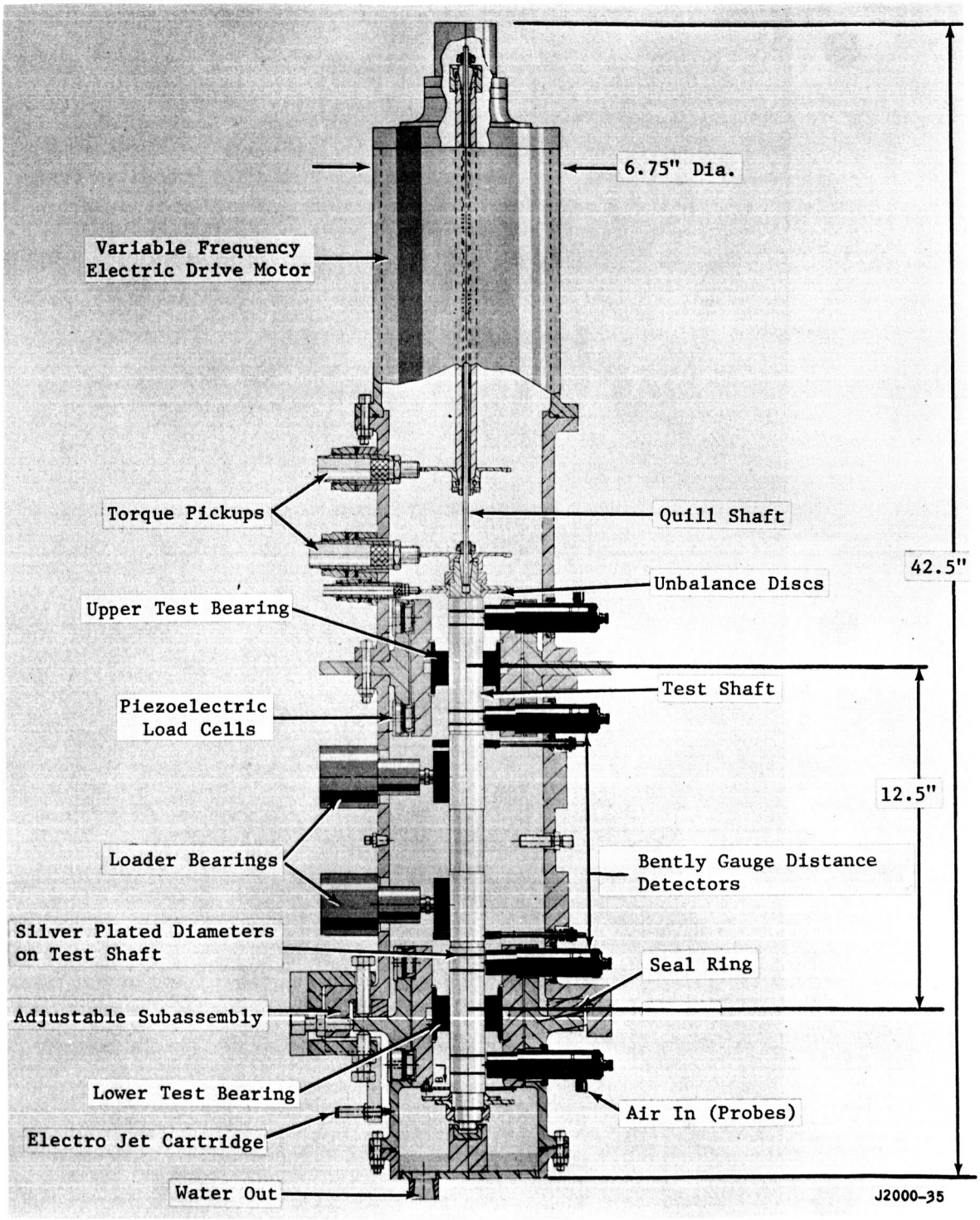

Figure 36. Bearing Stability Test Rig.

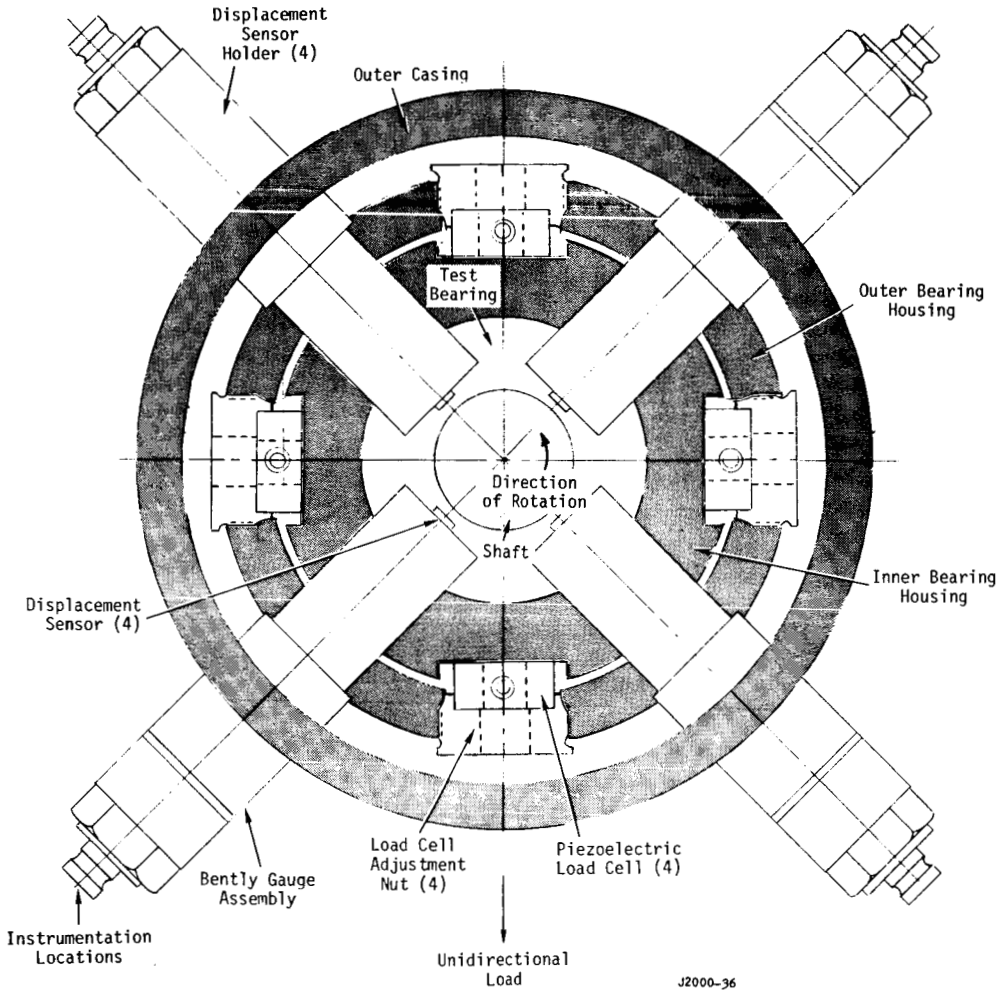

Figure 37. Load Cell and Proximity Gage Installation. (Shaft diameter, 1.25 Inch)

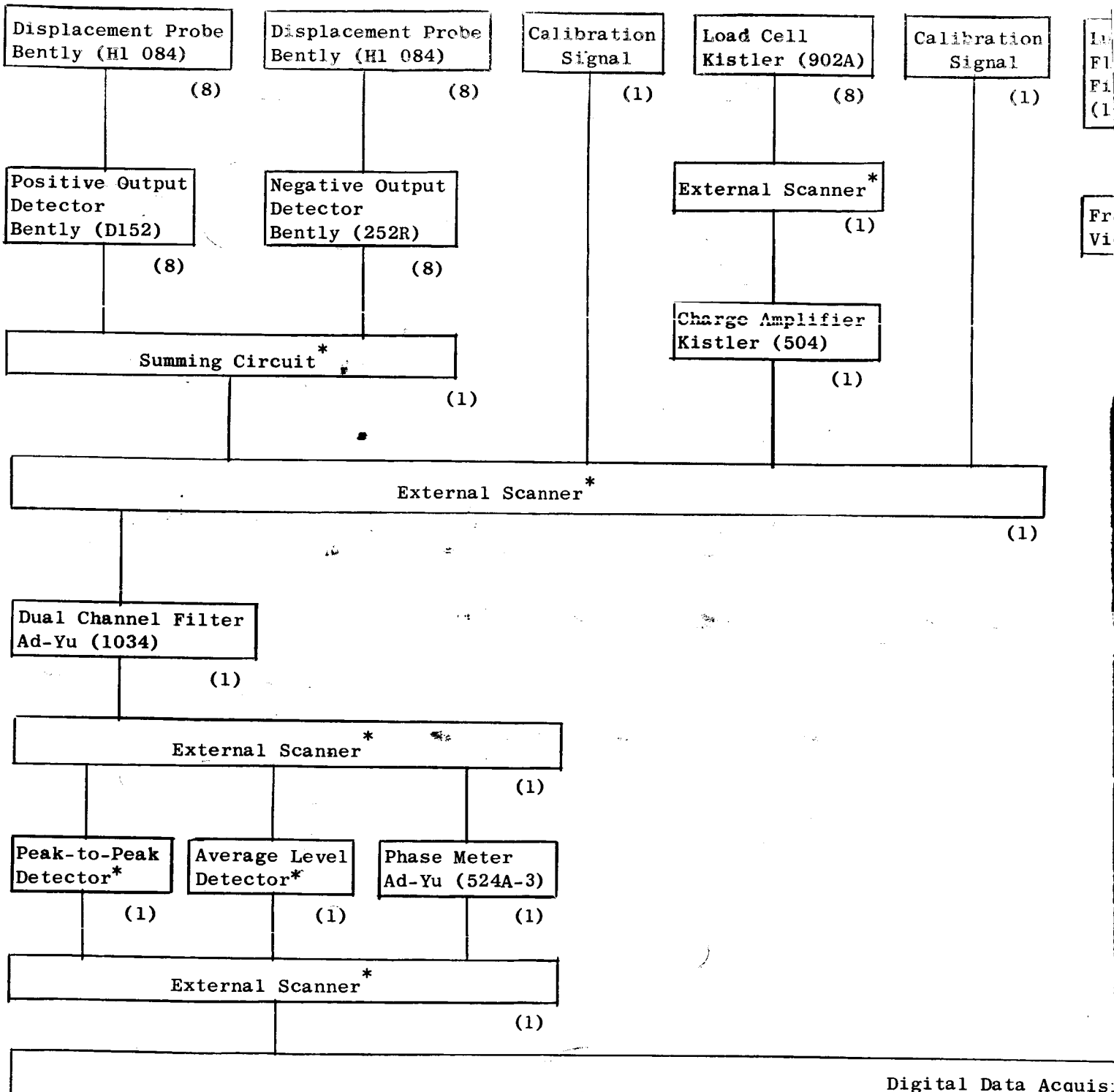

*Specially designed and built.
( ) Number of items.

Figure 38. Dynamic Instrumentation Schematic.
(Schematic Diagram of Instrumentation to be

...ECEDING PAGE BLANK NOT FILMED.

ARING PROGRAM INSTRUMENTATION

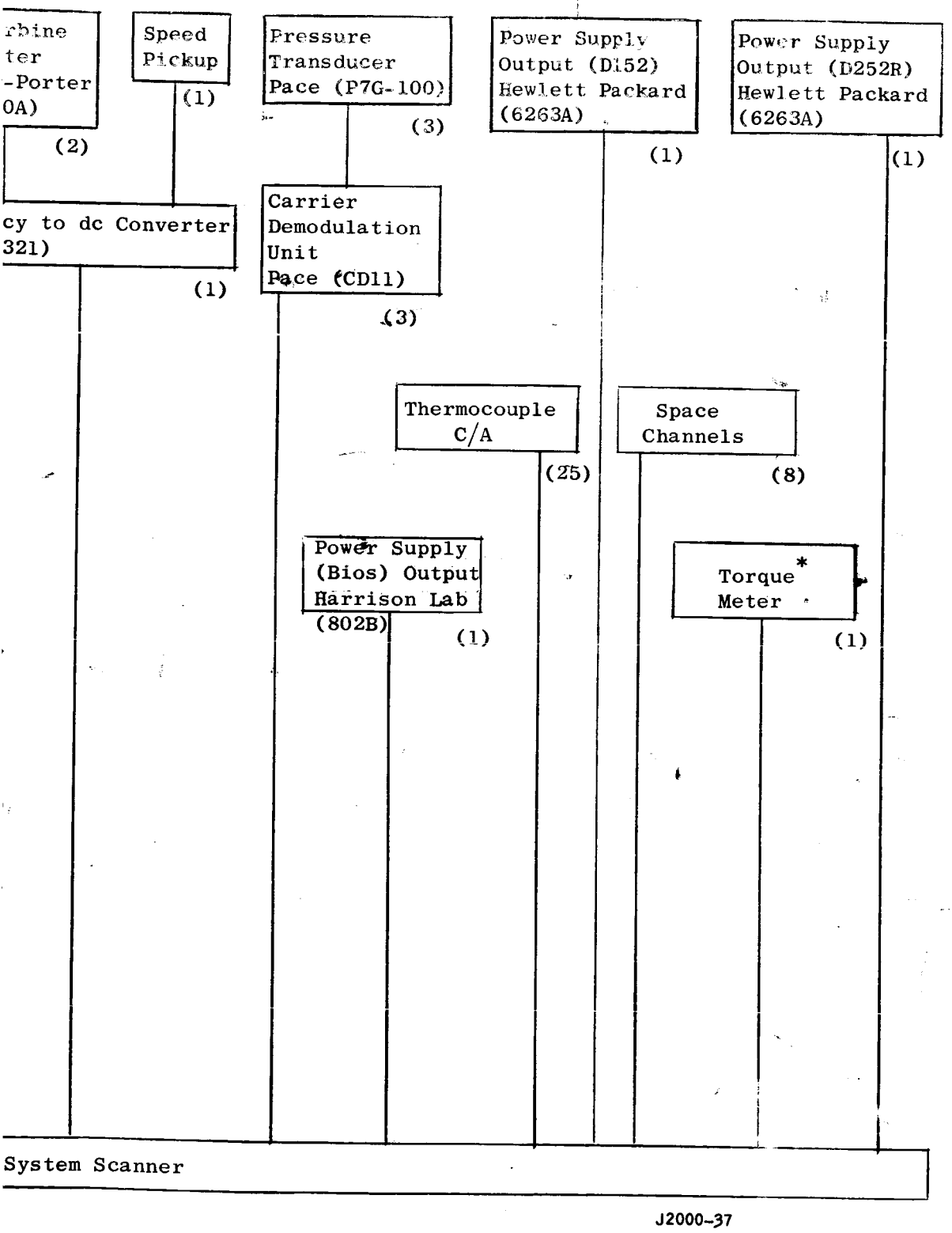

J2000-37

on the Digital Data Acquisition System.)

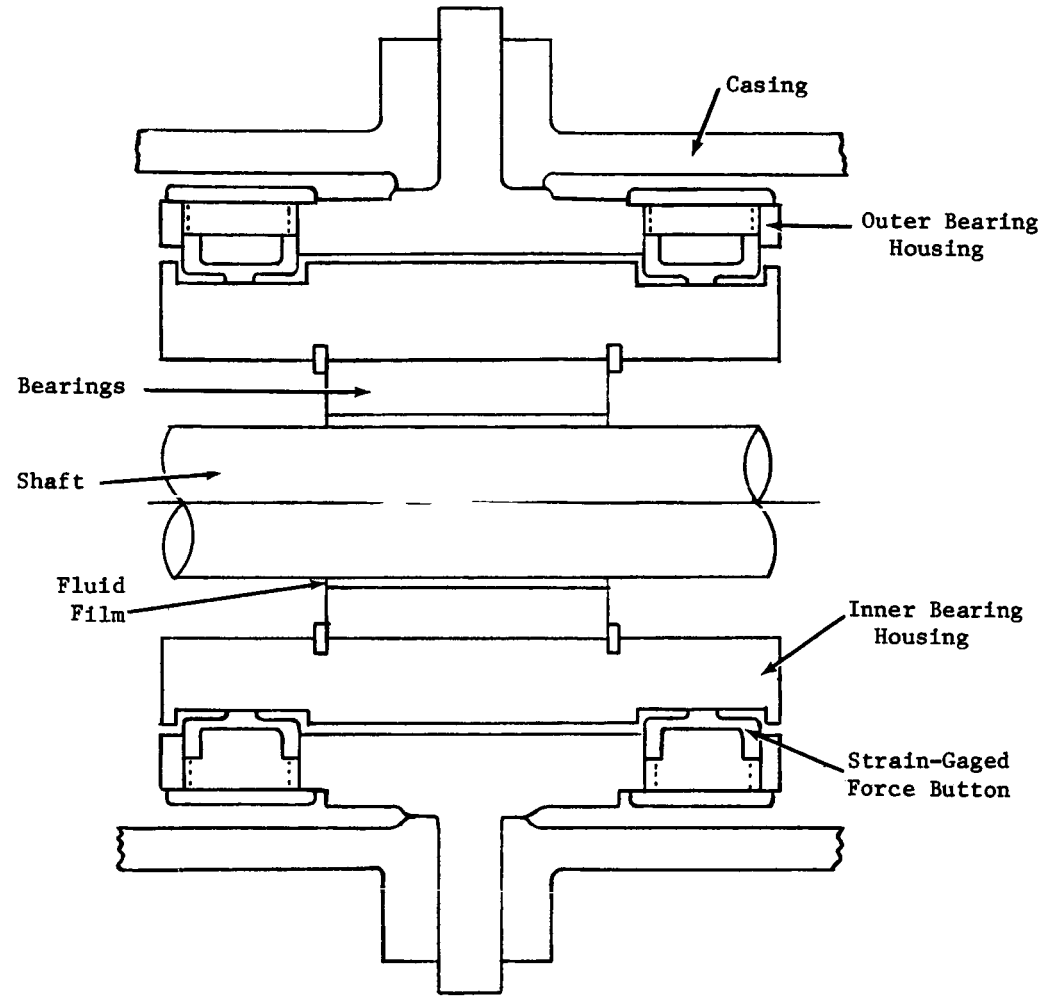

a. Inner Bearing Housing Supported By Force Buttons.

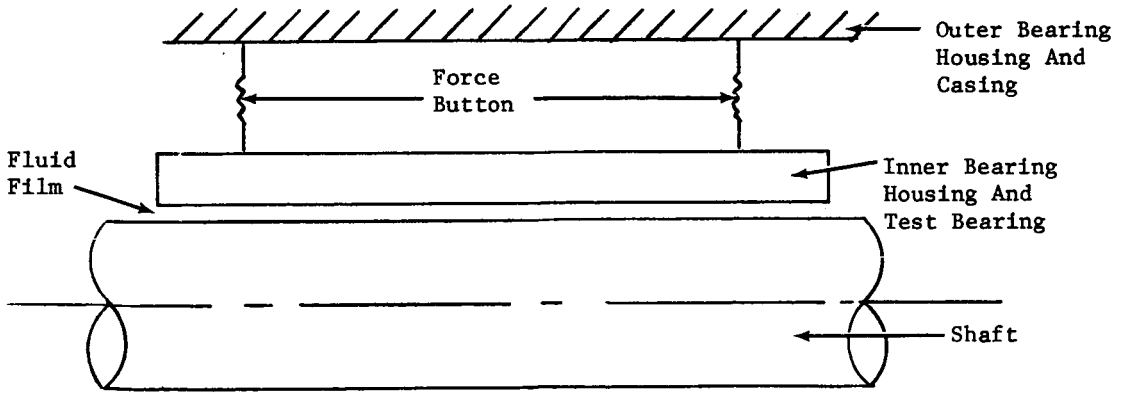

b. Equivalent Vibrational System.

J2000-38

Figure 39. Details of Inner Bearing Housing Supported by Strain-Gaged Force Button.

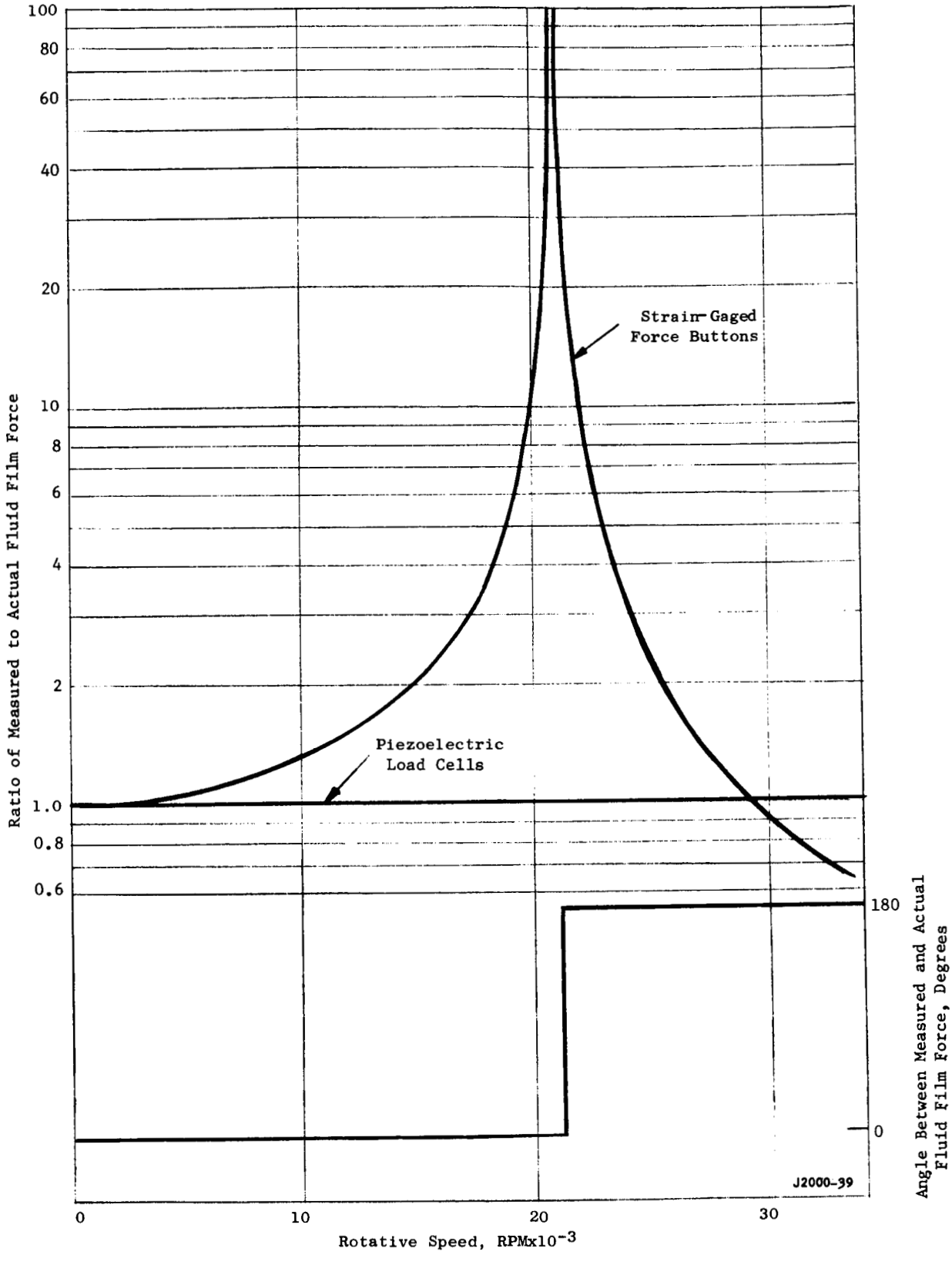

Figure 40. Effect of Force Sensor Selection on Force Measurement Errors.

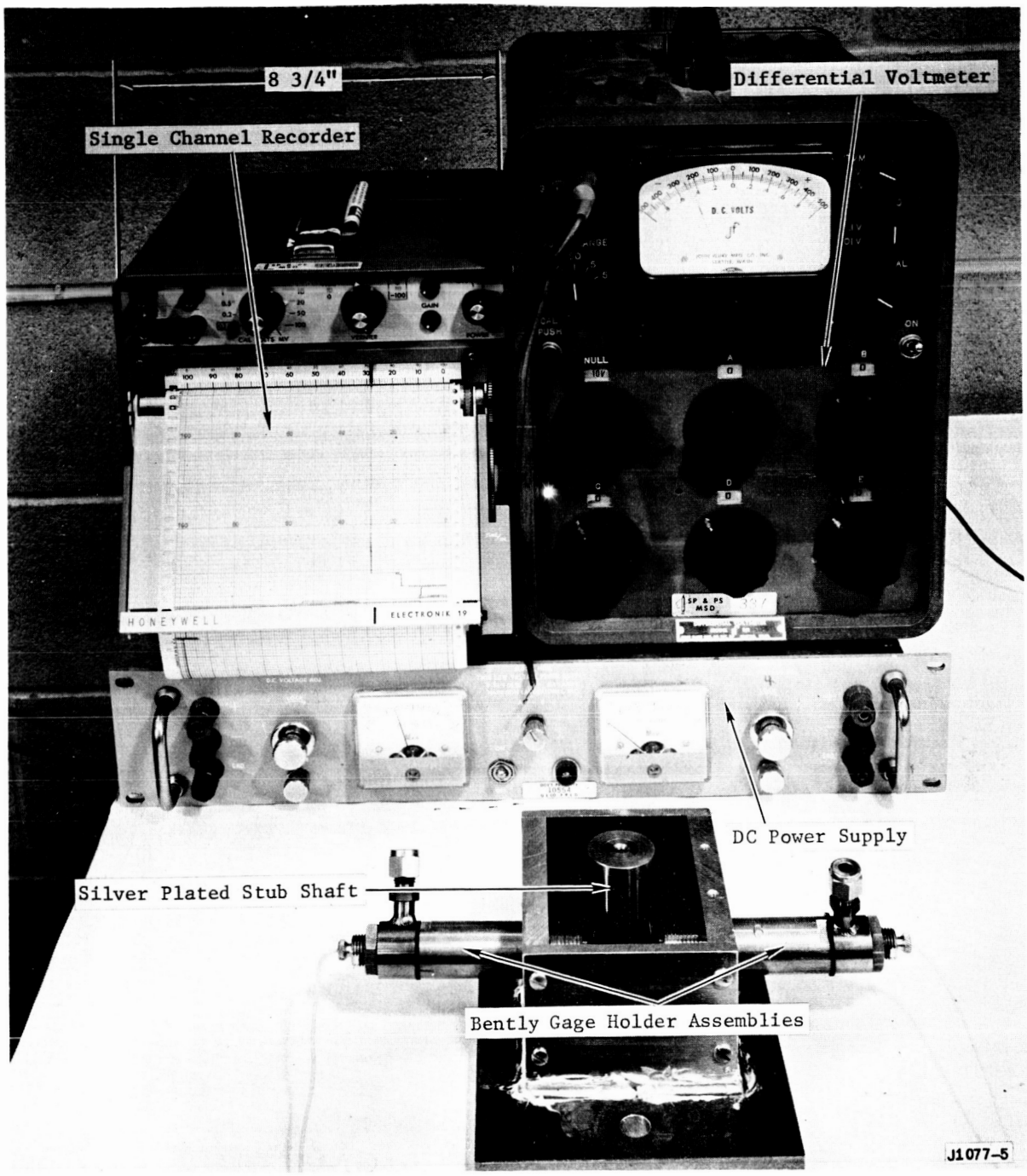

Figure 41. Proximity Probe Drift Test Rig.

APPENDIX

NOMENCLATURE

a	Distance between bearing center and center of radius of curvature of pad, mil
C	Fluid film damping coefficient, lb. sec./in.
c	Radial clearance, mils
d	Twice the radius of curvature of the pivot, in.
E	Young's modulus $\frac{\text{in.lb.}}{\text{in.}^3}$
F	Fluid film force, lb.
K_p	Pivot stiffness, lb./in.
K_{xx}, etc.	Fluid film stiffness, lb./in.
m	Preload coefficient
P	Force on pivot, lb.
R	Radius, in.
S	Sommerfeld Number
W	Steady unidirectional side load, lb.
X	Deflection in direction of side load, in.
Y	Deflection orthogonal to side load, in.
Z	general coordinate
$\dot{X}$, $\dot{Y}$	Time derivative of X, Y
β	Angular extent of pad, degrees
δ	Displacement of pivot surface, in.
θ_p	Angle from leading edge of pad to pivot location, degrees
ω	Angular speed of rotor, sec.^{-1}

NOMENCLATURE (Continued)

Subscripts

c	Cosine component
p	Refers to bearing pivot
s	Sine component
x	Refers to x coordinate
y	Refers to y coordinate
1	Refers to spherical pivot
2	Refers to Planar surface in contact with spherical pivot

DISTRIBUTION LIST FOR QUARTERLY REPORTS

CONTRACT NAS 3-6479

National Aeronautics and Space Administration
Washington, D.C. 20546
Attn: S. V. Manson - Code RNP

National Aeronautics and Space Administration
Washington, D.C. 20546
Attn: Dr. F. Schulman - Code RNP

National Aeronautics and Space Administration
Lewis Research Center
21000 Brookpark Road
Cleveland, Ohio 44135
Attn: Dr. B. Lubarsky - M.S. 500-201

National Aeronautics and Space Administration
Lewis Research Center
21000 Brookpark Road
Cleveland, Ohio 44135
Attn: Robert Cummings - M.S. 500-201

National Aeronautics and Space Administration
Lewis Research Center
21000 Brookpark Road
Cleveland, Ohio 44135
Attn: Ruth Weltmann - M.S. 500-309

National Aeronautics and Space Administration
Lewis Research Center
21000 Brookpark Road
Cleveland, Ohio 44135
Attn: John Weber - M.S. 3-19
Technical Utilization Office

National Aeronautics and Space Administration
Lewis Research Center
21000 Brookpark Road
Cleveland, Ohio 44135
Attn: Joseph Joyce - M.S. 500-309 (2)

National Aeronautics and Space Administration
Lewis Research Center
21000 Brookpark Road
Cleveland, Ohio 44135
Attn: James Dunn - M.S. 500-201

National Aeronautics and Space Administration
Lewis Research Center
21000 Brookpark Road
Cleveland, Ohio 44135
Attn: Report Control - M.S. 5-5

National Aeronautics and Space Administration
Lewis Research Center
21000 Brookpark Road
Cleveland, Ohio 44135
Attn: William J. Anderson - M.S. 6-1

National Aeronautics and Space Administration
Lewis Research Center
21000 Brookpark Road
Cleveland, Ohio 44135
Attn: Henry Slone - M.S. 500-201

National Aeronautics and Space Administration
Lewis Research Center
21000 Brookpark Road
Cleveland, Ohio 44135
Attn: Warner Stewart - M.S. 5-9

National Aeronautics and Space Administration
Lewis Research Center
21000 Brookpark Road
Cleveland, Ohio 44135
Attn: Edmond Bisson - M.S. 5-3

National Aeronautics and Space Administration
Lewis Research Center
21000 Brookpark Road
Cleveland, Ohio 44135
Attn: Dorothy Morris - M.S. 3-7

National Aeronautics and Space Administration
Lewis Research Center
21000 Brookpark Road
Cleveland, Ohio 44135
Attn: John Dilley - M.S. 500-309

Report Distribution List - NAS 3-6479 - Quarterly (Continued)

National Aeronautics and Space Administration
Jet Propulsion Laboratories
California Institute of Technology
4800 Oak Grove Drive
Pasadena, California 91103
Attn: John W. Stearns

National Aeronautics and Space Administration
Scientific & Technical Information Agency
P.O. Box 5700
Bethesda, Maryland 20014 (2 + Repro)

National Aeronautics and Space Administration
Western Operations Office
150 Pico Boulevard
Santa Monica, California 90406
Attn: John Keeler

Aeronautical Systems Division
Wright-Patterson Air Force Base
Dayton, Ohio 45433
Attn: George Sherman - API

Aeronautical Systems Division
Wright-Patterson Air Force Base
Dayton, Ohio 45433
Attn: Charles Armbruster - ASRMFP-1

Aeronautical Systems Division
Wright-Patterson Air Force Base
Dayton, Ohio 45433
Attn: John Morris - ASRCNL-2

U.S. Atomic Energy Commission
Germantown, Maryland 20545
Attn: Col. E. L. Douthett

U.S. Atomic Energy Commission
Germantown, Maryland 20545
Attn: Dr. Nicholas Grossman
Chief, Engineering Department

U.S. Atomic Energy Commission
Washington, D.C. 20546
Attn: Herbert D. Rochen RNP

Air University Library
Maxwell Air Force Base, Alabama
Attn: Director

U.S. Atomic Energy Commission
Technical Information Service Extension
P.O. Box 62
Oak Ridge, Tennessee

Oak Ridge National Laboratory
Post Office Box Y
Oak Ridge, Tennessee
Attn: H. W. Savage

Office of Naval Research
Washington, D.C. 20546
Attn: S. Doroff - Code 438

Armed Services Technical Information Agency
Arlington Hall Station
Arlington, Virginia 22212

Aerojet-General Corporation
Technical Library
Building 2015, Department 2410
P.O. Box 1947
Sacramento 9, California

Aerojet-General Corporation
Attn: Robert Gordon
SNAP-8 Program Director
Azusa, California 91703

Aerojet-General Corporation
Attn: John Marick
Azusa, California 91703

AiResearch Manufacturing Company
Sky Harbor Airport
402 South 35th Street
Phoenix, Arizona
Attn: Librarian

AiResearch Manufacturing Company
Sky Harbor Airport
402 South 35th Street
Phoenix, Arizona
Attn: Robert Gruntz

Report Distribution List - NAS 3-6479 - Quarterly (Continued)

AiResearch Manufacturing Company
Sky Harbor Airport
402 South 35th Street
Phoenix, Arizona
Attn: George Wheeler

Atomics International
Division of NAA
Canoga Park, California
Attn: L. M. Flower

The Barden Corporation
Research Precision Division
Danbury, Connecticut
Attn: Mrs. Bernice P. Tucos

The Barden Corporation
Research Precision Division
Danbury, Connecticut
Attn: Technical Library

Battelle Memorial Institute
505 King Avenue
Columbus, Ohio 43201
Attn: C. M. Allen

The Franklin Institute
Benjamin Franklin Parkway at 20th Street
Philadelphia, Pennsylvania 19103
Attn: William Shuggarts

General Electric Company
Missile & Space Vehicle Department
3198 Chestnut Street
Philadelphia 4, Pennsylvania
Attn: Edward Ray

Mechanical Technology, Inc.
968 Albany-Shaker Road
Latham, New York
Attn: Dr. Beno Sternlicht

Mechanical Technology, Inc.
9680 Albany-Shaker Road
Latham, New York
Attn: Eli Arwas

M.S.A. Research Foundation
Callery, Pennsylvania
Attn: G. E. Kennedy

Pratt & Whitney Aircraft Division
United Aircraft Corporation
East Hartford, Connecticut 06108
Attn: Dr. William Lueckel
Eng. Bldg. 2-H

Pratt & Whitney Aircraft Division
United Aircraft Corporation
East Hartford, Connecticut 06108
Attn: R. P. Shenchenko

Pratt & Whitney Aircraft Division
United Aircraft Corporation
East Hartford, Connecticut 06108
Attn: Karl A. Domeisen
Exp. Eng. Eng. 1-F

Rocketdyne
Division of North American Aviation, Inc.
6633 Canoga Avenue
Canoga, California 91303
Attn: Robert Spies

Sundstrand Aviation - Denver
A Division of Sundstrand Corporation
Denver, Colorado 80221
Attn: P. H. Stahlhuth

Southwest Research Institute
8500 Culebra Road
San Antonio, Texas 78206
Attn: Dr. R. A. Benton

The Franklin Institute
Benjamin Franklin Parkway
at 20th Street
Philadelphia, Pennsylvania 19103
Attn: Otto Decker

UAC Library
United Aircraft Research Laboratories
Gate 5R, Silver Lane
East Hartford, Connecticut 06108

Westinghouse Electric Corporation
Research Laboratories
Pittsburgh, Pennsylvania 15236
Attn: Mr. J. Boyd

Westinghouse Electric Corporation
Aerospace Division
Advanced Machine Systems Group
Lima, Ohio
Attn: Allen King

North American Aviation, Inc.
Atomics International
P.O. Box 309
Canoga Park, California 91304
Attn: Director, Liquid Metals Info. Center

National Aeronautics & Space Administration
Lewis Research Center
21000 Brookpark Road
Cleveland, Ohio 44135
Attn: Jack Heller - M.S. 500-201

Aeronautical Systems Division
Wright-Patterson Air Force Base
Dayton, Ohio 45433
Attn: John Zmurk APIP-1